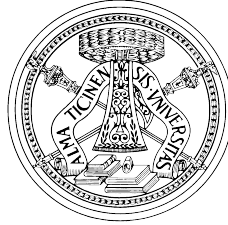


UNIVERSITÀ DEGLI STUDI DI PAVIA

Facoltà di Ingegneria

Dipartimento di Ingegneria Industriale e dell'Informazione



DOCTORAL THESIS IN MICROELECTRONICS

XXVII CYCLE

**Performance Limits, Design and
Implementation of LC harmonic
CMOS Oscillators**

Supervisor:

Chiar.mo Prof. Rinaldo CASTELLO

Coordinator:

Chiar.mo Prof. Franco MALOBERTI

Author:

Marco GARAMPAZZI

October 2014

UNIVERSITÀ DEGLI STUDI DI PAVIA

Abstract

Facoltà di Ingegneria

Dipartimento di Ingegneria Industriale e dell'Informazione

Doctor of Philosophy

Performance Limits, Design and Implementation of LC harmonic CMOS Oscillators

by Marco GARAMPAZZI

An intuitive yet sufficiently accurate analysis of oscillators topologies is presented and demonstrated with a dedicated test chip. An Impulse Sensitivity Function-based phase noise analysis for multi-resonators oscillators is presented. The analysis achieves good agreement between simulations and measurements and it is used in particular on class B with tail filter topology both N-only and p-n. The class B with tail filter oscillator is, indeed, one of the most promising topology to achieve good power efficiency while keeping low the phase noise. A high efficiency p-n class B with magnetically coupled tail filter is finally presented in order to answer the necessity of high efficiency, reliability and reducing the area occupation compared to classical implementations.

Contents

Abstract	iii
Contents	iv
List of Figures	vii
List of Tables	xi
Introduction	1
1 Oscillators and Phase Noise background	3
1.1 Introduction and Motivation	3
1.2 The Phase noise	5
1.3 Phase noise Models	11
1.3.1 Hajimiri’s model	12
1.3.2 Demir’s model	14
2 An Intuitive Analysis of Phase Noise Fundamental Limits Suitable for Benchmarking LC Oscillators	17
2.1 Introduction	17
2.2 Phase Noise in LC-Tank Oscillators	19
2.3 Different Oscillator Topologies	22
2.3.1 Class B oscillator	22
2.3.2 Class B oscillator with tail filter	25
2.3.3 Class C oscillator	27
Some class C evolutions	29
2.3.4 Class F oscillator	31
2.3.5 Transformer coupled oscillators	33
2.4 Comparison between topologies	34
2.4.1 A comment on other topologies	35
Clip and Restore	35
Class D	37
2.5 Experimental verification	38
3 Impulse Sensitivity Function based Phase Noise Analysis	43
3.1 Phase noise evaluation using Impulse Sensitivity Function	43

3.2	Class B with tail filter phase noise analysis	45
3.2.1	Class B with tail filter N-only	46
3.2.1.1	Main Tank	52
3.2.1.2	Switching transitions	53
3.2.1.3	Second Harmonic Tank	54
3.2.1.4	Active devices	58
3.2.2	A closed form expression of $1/f^2$ phase noise (N only)	62
3.2.3	Validation	63
3.2.4	Class B with tail filter p-n	66
3.2.4.1	Main tank	69
3.2.4.2	Second Harmonic Tanks	71
	Second Harmonic Tank (n)	71
	Second Harmonic Tank (p)	72
	Second Harmonic tank noise considerations	74
3.2.4.3	Active devices	75
	Transistors ISF (nMOS)	76
	Transistors ISF (pMOS)	79
3.2.5	Considerations of the $1/f^2$ phase noise (p-n)	81
3.3	Class F	86
3.3.1	Main tank	90
3.3.2	Active Devices	92
4	Efficient p-n class B oscillator with transformer based tail filtering	93
4.1	Introduction	93
4.2	Excess Noise Factor in LC-Tank Oscillators	96
4.3	Class-B with tail filter	97
4.4	Magnetically coupled resonator	100
4.5	Oscillators Implementation	102
4.6	Conclusion	107

List of Figures

1.1	Power consumption of a frequency synthesizers in transceivers . . .	4
1.2	Phasor representation of a) amplitude modulation b) phase modulation	6
1.3	Phase and voltage spectrum on a real oscillator	8
1.4	LC oscillator equivalent circuit	12
1.5	Impulse response of an oscillator voltage output waveform to a charge pulse injected a) at the peak of the sinusoidal voltage and b) at zero crossing	13
1.6	Oscillator trajectory	15
2.1	Generic LC oscillator	19
2.2	Benchmarking of different oscillator topologies using ENF	22
2.3	N-MOS, complementary MOS “class-B” LC oscillators and current, voltage waveforms	23
2.4	AC-biased class-B oscillator (NMOS only)	24
2.5	Oscillators with second-harmonic LC tail filter	25
2.6	Class-B oscillator with tail filter: calculated and simulated ENF and simulated power efficiency.	26
2.7	Class-C oscillator (NMOS only)	27
2.8	Class-C oscillator: calculated and simulated ENF and simulated power efficiency.	29
2.9	Schematic of two class C evolution	30
2.10	Class-F oscillator: a) circuit schematic and b) typical voltage waveform.	32
2.11	Comparison between Class-F and Class-B oscillators phase noise. Dots represent simulated data, lines are calculated	33
2.12	Chip photo and block diagram of the prototype.	38
2.13	Schematic of the prototype.	39
2.14	Oscillation amplitude vs bias current: measurements and simulations	39
2.15	Measured phase noise after frequency division by 2 of class-C and class-B oscillators at their respective maximum FoM bias point (12.5mA for Hybrid class-C/B and 21.6mA for class-B) when tuned at 7.6GHz. For comparison the simulated phase noise is also reported.	40
2.16	FoM vs output voltage for the class-B and Hybrid class-C/B oscillators: measurements and simulations.	40
2.17	ENF vs output voltage for the class-B and Hybrid class-C/B oscillators: measurements and simulations.	41
3.1	Class-B oscillators with $2\omega_0$ LC tail filter: N-only	46

3.2	Voltages waveforms of the approximated steady state oscillation . . .	48
3.3	Noise sources of a class-B oscillator with $2\omega_0$ LC tail filter	49
3.4	Idealized Class B with tail filter oscillator and its noise sources . . .	49
3.5	Numerical example of the ISF of a noise charge injected at z	51
3.6	Numerical example of the ISF of a noise charge injected across the switches	51
3.7	Main tank noise generator	53
3.8	Active devices working conditions	55
3.9	Working operation of switching transistors and the effect on the evaluation of the second harmonic tank noise	55
3.10	Numeric example of the evaluated perturbation over period on ΔV_1 (continuous line) and ΔV_2 (dashed line)	57
3.11	Impulse Sensitivity Function of the second harmonic tank: consider- ing the more complete analysis (continued) and approximated with just second harmonic (dashed)	57
3.12	Noise charge referred to MOSFETs	59
3.13	Noise charge referred to M_1 divided in differential and common mode components	59
3.14	ISFs obtained with a complete analysis (Γ_M), the one used in the evaluation ($\Gamma_{M,a}$) and the error ($\Gamma_{M,err}$)	61
3.15	Main Tank ISF simulated and evaluated	64
3.16	Second Harmonic Tank ISF simulated and evaluated	65
3.17	Active devices ISF simulated and evaluated	65
3.18	Output Noises of the different sources: simulated and calculated . .	66
3.19	Output Noises of the different sources: simulated and calculated . .	67
3.20	Class-B oscillators with $2\omega_0$ LC tail filter: p-n	67
3.21	Noise sources of a p-n class-B oscillator with $2\omega_0$ LC tail filter . . .	69
3.22	Main tank noise generator	70
3.23	Noise charge referred to the second harmonic tank (n)	72
3.24	Noise charge referred to the second harmonic tank (p)	73
3.25	a) Noise charge referred to M_2 b) The decomposition of the generator for the analysis	77
3.26	Interaction between noise charge generators (nMOS)	77
3.27	a) Noise charge referred to M_4 b) The decomposition of the generator for the analysis	79
3.28	Interaction between noise charge generators (pMOS)	79
3.29	Excess noise factor of N only (markers) and pn (lines)	83
3.30	Main Tank ISF simulated and evaluated	84
3.31	Second Harmonic Tank (n) ISF simulated and evaluated	85
3.32	Second Harmonic Tank (p) ISF simulated and evaluated	85
3.33	Active devices (nMOS, M_2) ISF simulated and evaluated	86
3.34	Active devices (pMOS, M_4) ISF simulated and evaluated	86
3.35	Output Noises of the different sources: simulated and calculated . .	87
3.36	Class-F oscillator: a) circuit schematic and b) typical voltage waveform.	87

3.37	Comparison between Class-F and Class-B oscillators phase noise. Dots represent simulated data, lines are calculated	89
3.38	Class-F oscillators total phase noise of the resonator (left scale) and percentage of the third harmonic tank (right scale). Dots are simulations, lines are calculations: a) $Q_3=3Q_1$, $C_3=C_1$; b) $Q_3=2Q_1$, $C_3=2/3C_1$; c) $Q_3=2Q_1$, $C_3=C_1$; d) $Q_3=Q_1$, $C_3=1/3C_1$; e) $Q_3=Q_1$, $C_3=C_1$	91
4.1	Characteristic behavior of N-only and p-n oscillators	94
4.2	Conceptual block diagram of a complete mobile system	95
4.3	Class-B oscillators with $2\omega_0$ LC tail filters: N-only and p-n	97
4.4	Complementary p-n class-B oscillator with a) dual and b) single $2\omega_0$ LC tanks at the tails	98
4.5	Simulated voltage waveforms	99
4.6	Phase Noise simulation mistuning the tail filter	100
4.7	From N only structure to complementary p-n class-B oscillator with magnetically coupled LC tanks at the tails	101
4.8	Simulated ISFs with and without transformer coupling	101
4.9	Layout of the magnetically coupled tail filter	102
4.10	Chip photo	103
4.11	Phase Noise measurements (after freq divider by 2) at the minimum and maximum frequency of oscillation (p-n)	103
4.12	Phase Noise measurements (after freq divider by 2) at the minimum and maximum frequency of oscillation (N only)	104
4.13	Measured (dots) phase noise after freq. divider by 2 and simulated (lines) phase noise with 6dB reduction as a function of power dissipation of p-n and N only oscillators	105
4.14	Measured Phase Noise and FoM over tuning range (p-n)	105
4.15	Measured Phase Noise and FoM over tuning range (N only)	106

List of Tables

2.1	Efficiency Comparison of NMOS VCOs	34
3.1	Noise contribution Fully differential vs. ground capacitors	64
4.1	Comparison table	106

Introduction

In recent years companies and universities prioritized their efforts on emerging services like mobility, cloud and analytics. Tablets and smartphones are more popular than desktop computers. Mobile devices have surpassed desktops in enabling people to do more on the internet and to be always connected, regardless of physical location. This scenario culminates to the necessity to integrate systems with multiple communications capabilities requiring ever increasing data transfer rates. Extending battery life, lowering power consumption and maximizing power efficiency are key features to lead the market especially when referred to mobile devices. Modern mobile smartphones have to support different cellular standards from the Global System for Mobile communication (GSM) to its Enhanced Data rates Evolution (EDGE), from the third generation (3G-UMTS), to the fourth generation Long Term Evolution (LTE) together with WiFi/WiMAX connectivity. In a radio frequency chip, to cover all these standards, different frequency synthesizers are used, which occupy significant amount of total area. Moreover, these different standards require very stringent specifications in terms of spectral purity for signal (de)modulation which are fulfilled with the use of LC harmonic oscillators, which are, for this reason, among the most power hungry building blocks in a transceiver.

Chapter 1 represents the introduction of this thesis. It describes briefly the scenario of LC oscillators, that it will be analyzed in the following chapters. It covers in a general and with just an introductory purpose the phase noise concept and representation together with models widely used in the analysis of phase perturbation in oscillators.

Chapter 2 is dedicated to an intuitive analysis of various commonly used oscillators in order to compare their fundamental limitations. A noise factor that represents the difference between the maximum achievable Figure of Merit and the actual

one is derived for all the topologies considered. A dedicated chip prototype has been realized and measured to verify the predictions.

Chapter 3 deals with a novel and rigorous analysis of phase noise using Impulse Sensitivity Function theory for different oscillators. In the first part class B with tail filter oscillator topology, both single switching pair and double switching pair, is analyzed. Class B with tail filter topology represents one of the most promising LC oscillators architecture. In the second part the same analysis is conducted for class F oscillator.

Chapter 4 presents a complementary p-n class B oscillator with two magnetically coupled second harmonic tail resonators. For the same oscillation amplitude (constrained by reliability concerns) and the same tank, the p-n oscillator achieves 3-4dB better Figure of Merit than an N-only reference. The transformer based tail filtering allows to save area occupation, respect to a classic implementation.

Chapter 1

Oscillators and Phase Noise background

1.1 Introduction and Motivation

The requirement of signal purity, in a continuously increasing range of frequencies, makes necessary the effort of both industry and university to reduce power consumption while preserving low the phase noise of frequency references. Due to a requirement of a wide frequency range, in an LTE transceiver, for example, different PLLs are used on chip, leading to the fact that RX/TX PLLs occupy 30% of the chip area in single carrier scenario and the count of PLL actually duplicates in carrier aggregation. Moreover, due to the stringent phase noise requirements, especially in mobile applications, LC oscillator are among the most power hungry building blocks in a transceiver. In GSM TX application, for example, phase noise must be less than $-162\text{dBc}/\text{Hz}$ at 20MHz offset frequency for 915MHz carrier [1] and these requirements are fulfilled consuming high amount of power of an RF frequency synthesizer [2, 3] and burning more than 30% of the cellular RX power [4, 5] (Fig. 1.1). High power efficiencies and low area occupation are clearly crucial, in such a scenario. Efficiency as well as the area trade off is determined by the oscillator topology while the needed frequency range by optimization of the resonator's components. Oscillator topology affects the conversion of circuit noise sources into phase noise changing the impulse sensitivity function (ISF) [6]. Moreover, it affects the power vs phase noise trade-off through the maximum achievable power conversion efficiency (η_P), i.e. the conversion of DC power (P_{DC})

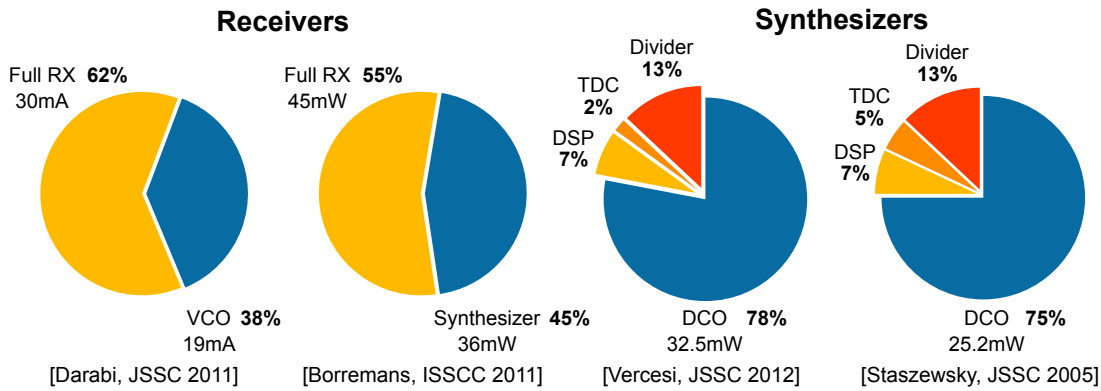


Figure 1.1: Power consumption of a frequency synthesizers in transceivers

into resonator RF power (P_{RF}), which directly affects the phase noise [7]. Thanks to its simplicity classic class B oscillator is widely used, however, it has different non idealities that degrade its phase noise performance like the current generator noise. Moreover its efficiency is limited in both current and voltage efficiency. It can not be maximized to avoid an increment of phase noise when the transistor enter the triode region. Class C oscillators achieve higher current efficiency, ideally 100%, but, for the same reasons as class B, voltage efficiency has to be limited. The use of voltage-biased topologies [8–10] eliminates a source of phase noise (i.e. the current generator) and improves power efficiency, but increases frequency pushing which has to be solved using for example dedicated LDO that reduces the overall efficiency. Large voltage swing (relative to the supply voltage) is desirable to achieve high power efficiency and to reduce phase sensitivity to device noise, as described by the ISF. However, as the active devices are driven by large signals, they can enter the triode region, thereby loading the tank, potentially degrading phase noise. This trade-off can be partially broken by adopting a low supply voltage, such that the active devices do not enter into triode even as the signal swing approaches (or exceeds) the supply rails. In practice, the use of a low supply voltage (e.g. 0.4V in [8]) makes the performances very sensitive to supply voltage variations and, when the oscillator is embedded in a complete transceiver, it necessitates a dedicated switch-mode voltage regulator to preserve power efficiency, thereby increasing cost. Other solutions include class-D oscillators [9], where the transistors are operated in deep triode to achieve good phase noise thanks to the low r_{ON} and the very fast switching, and clip-and-restore [10], where loading effects are compensated adopting step-up transformers to boost the gate voltage and reduce phase sensitivity to device noise. However, on-chip transformers typically have lower quality factors than simple inductors [11]. This is only partially compensated

by the fact that transformer-based resonators display a steeper phase response with respect to a simple LC-tank for the same quality factor [12]. Moreover, in both cases a low supply is required for reliability. Higher order resonators have also been proposed (class-F oscillators [13]) in order to increase the maximum slope of the output signal for a given peak-to-peak voltage swing. However, an accurate analysis [7] reveals that this approach is beneficial only when the Q of the resonator is higher at $3f_{OSC}$ than at f_{OSC} , which is typically not the case. For a standard nMOS Class-B oscillator, if an additional LC tank (resonating at $2\omega_0$) is inserted at the source of the active devices [14], the switching transistors can enter the triode region without loading the tank since they see a high impedance in series with them. This allows to preserve the ISF while increasing power efficiency. High η_P and low phase noise however correspond to excessive voltage swings (ideally up to π times the supply voltage for 100% η_P). A possible solution can be to lower the supply voltages used. However, in a system the voltage supply is not generally imposed by the oscillator and in most of the practical cases, in different applications, as well as of course for cellular transceivers [3, 15–22], supply voltages still higher than 1V are used for the analog circuitry. This means that for all these cases N only structure represents actually a sub-optimal solution. Adopting a complementary (push-pull) topology presented in Chapter 4, the peak efficiency is reached at lower (theoretically half) voltage swing compared to an N-type-only one, avoiding reliability concerns. The double switching pair class B with tail filter oscillator presented takes advantage of a transformer based tail resonator to more than halve the area occupation of tail resonator.

1.2 The Phase noise

In RF transceivers oscillators are key building blocks for frequency synthesis in both transmit and receive paths. In most systems one input of every mixer is driven by a periodic signal, hence the need for oscillators. Oscillators must satisfy specifications imposed by the system itself like frequency of operation and purity of the output signal. An ideal oscillator produces a perfectly periodic output of the form $v(t) = A_0 \cos(\omega_0 t + \phi_0)$, where A_0 , ω_0 and ϕ_0 are the oscillation amplitude, angular frequency and initial phase respectively, and they are constant over time. In this situation the zero crossings occur at exact integer multiples of $\tau_0 = 2\pi/\omega_0$. In an actual oscillator, however, due to unavoidable presence of noise sources,

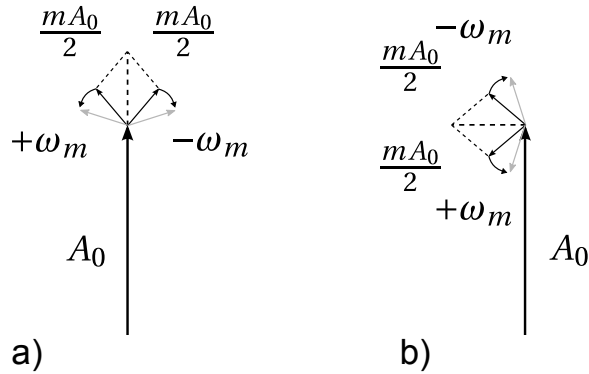


Figure 1.2: Phasor representation of a) amplitude modulation b) phase modulation

these quantities become modulated and thus time-dependent instead of remaining constant over time. Since a modulation of these different quantities occurs it is possible to divide, for sake of simplicity, the modulation between amplitude and frequency/phase modulation [23].

In case of amplitude modulation, the oscillator output voltage becomes:

$$v(t) = A_0[1 + m \cdot \cos(\omega_m t)] \cos(\omega_0 t + \phi_0) \quad (1.1)$$

where typically $m \ll 1$ and $\omega_m \ll \omega_0$. The output spectrum now consist of a Dirac Delta function at ω_0 which represents the pure sinusoidal signal and a couple of side-tones at angular frequencies $\omega_0 \pm \omega_m$. The resulting output voltage can be rewritten as:

$$v(t) = A_0 \sin(\omega_0 t) + \frac{mA_0}{2} \cos((\omega_0 - \omega_m)t) - \frac{mA_0}{2} \cos((\omega_0 + \omega_m)t) \quad (1.2)$$

Where $\frac{mA_0}{2} \cos((\omega_0 - \omega_m)t)$ is the lower side-band and $-\frac{mA_0}{2} \cos((\omega_0 + \omega_m)t)$ is the upper side-band [23]. A phasor representation of the amplitude-modulated carrier is shown in Fig. 1.2a.

In case of frequency modulation, on the other hand, the frequency can be written as: $\omega(t) = \omega_0 + \omega_m(t)$. Since the phase is the integral of the frequency, the output

signal can be written as:

$$v(t) = A_0 \cos \left(\omega_0 t + \phi_0 + \frac{\Delta\omega_0}{\omega_m} \sin(\omega_m t) \right) \quad (1.3)$$

A corresponding phase modulation also occurs in this case, with modulation index $m = \frac{\Delta\omega_0}{\omega_m}$. The resulting phase is:

$$\phi(t) = \Delta\phi \cdot \sin(\omega_m t) \quad (1.4)$$

Where $\Delta\phi = \Delta\omega_0/\omega_m$. If $\Delta\phi \ll 1$ rad holds, which is the case of small-angle modulation (*narrow band* frequency modulation), the signal $v(t)$ can be approximated as

$$\begin{aligned} v(t) &\cong A_0 \cos(\omega_0 t + \phi_0) - A_0 \sin(\omega_0 t + \phi_0) \cdot \frac{\Delta\omega_0}{\omega_m} \sin(\omega_m t) \\ &= A_0 \cos(\omega_0 t + \phi_0) - \frac{A_0}{2} \cdot \frac{\Delta\omega_0}{\omega_m} \cos((\omega_0 - \omega_m)t) + \\ &\quad - \frac{A_0}{2} \cdot \frac{\Delta\omega_0}{\omega_m} \cos((\omega_0 + \omega_m)t) \end{aligned} \quad (1.5)$$

As before a phasor representation of the two PM side-tones is visible in Fig. 1.2b. The ratio between the power of each side-tone and the power of the carrier is denoted as spurious-free dynamic range (SFDR) and is given by:

$$SFDR = \frac{\frac{1}{2} \left(\frac{A_0 \Delta\omega_0}{2 \omega_m} \right)^2}{\frac{A_0^2}{2}} = \frac{1}{4} \left(\frac{\Delta\omega_0}{\omega_m} \right)^2 = \left(\frac{\Delta\phi}{2} \right)^2 \quad (1.6)$$

It is interesting to note that the SFDR is equal to half the power of the modulated phase $\phi(t)$ with a spectrum S_ϕ (shown in Fig. 1.3a for a general case, not limited to a sinusoidal modulation). The SFDR is usually expressed in dBc, i.e. dB with respect to the carrier. An undesired phase modulation can also occur due to the presence of a noise source whose power spreads over a certain frequency interval. The noise perturbations induced by different noise sources are referred to as phase noise. Since S_ϕ is inversely proportional to the square of the frequency offset ω_m , it exhibits a $1/\omega_m^2$ tail (-20 dB/dec slope) in case of white noise source, while a $1/\omega_m^3$ dependence (-30 dB/dec) is present with $1/f$ noise sources.

The spectrum of output voltage is a scaled replica of S_ϕ folded around both sides of the carrier, as reported in Fig. 1.3b. This is valid if $\Delta\phi \ll 1$ rad holds. The power spectral density at $\omega_0 \pm \omega_m$ of the output voltage is given by $S_V(\omega_0 \pm \omega_m) \cong \frac{S_\phi(\omega_m) A_0^2}{2}$.

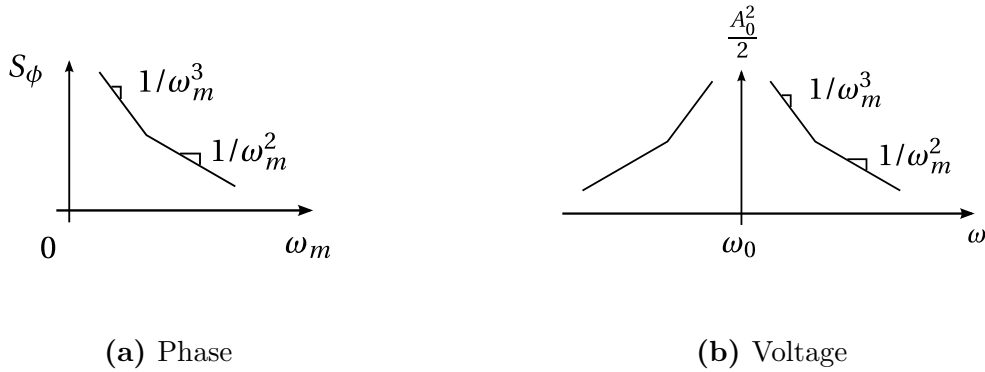


Figure 1.3: Phase and voltage spectrum on a real oscillator

The noise performance of an oscillator are quantitatively assessed, indeed, by defining a suitable signal to noise ratio. This figure is the ratio between the output noise power in a 1Hz bandwidth at the frequency offset from the carrier and the power of the carrier. This is defined as single side-band to carrier ratio (SSCR).

$$SSCR(\Delta_m) = \frac{S_V(\omega_0 \pm \omega_m)}{A_0^2/2} \cong \frac{S_\phi(\omega_m)}{2} [dBc/Hz] \quad (1.7)$$

There is an equivalence between SSCR and the SFDR once $\Delta\phi$ is expressed as

$$\Delta\phi = \sqrt{2S_\phi(\omega_m) \cdot 1Hz} \quad (1.8)$$

Hence the equivalence holds if the power of the sinusoid $\phi(t) = \Delta\phi \sin(\omega_m t)$ is equal to the noise power spectral density integrated over 1Hz bandwidth. When the offset frequency is equal to zero the S_ϕ diverges to ∞ . This is related to the small angle approximation that is no longer valid when ω_m approaches zero. This does not correspond to the real situation. Phase noise considering white noise has a Lorentzian spectrum that avoids any singularities at zero offset frequency and while maintaining the same asymptotic behavior. It also has the property that the total power integrated is equal to the power of the ideal carrier.

In some applications it is more useful to give a characterization of the phase/time deviation, the so called *jitter*, rather than the voltage spectrum. Jitter is a variation in the zero crossing times of a signal, or a variation in the period of the signal. There are actually different types of jitter that can be defined. Jitter is a statistical measure of a noisy oscillation process. the period of each cycle of the oscillator is different due to noise. Referring to τ_n as the period of cycle n . For a free running

oscillator with noise, the oscillation period will have a Gaussian distribution. This distribution has a mean value τ_{mean} whose inverse can be defined as the average frequency of oscillation. It has also a standard deviation.

The first type of jitter is *absolute jitter*. This type has the property that it is a function of time. It is given by the sum of each periods variation from the average.

$$\sigma_{abs}(t = N\tau_{mean}) = \sum_{n=1}^N \tau_n - \tau_{mean} \quad (1.9)$$

There is also the cycle to cycle jitter. It measures the variance of each period to the average period:

$$\sigma_c^2 = \lim_{N \rightarrow \infty} \left(\frac{1}{N} \sum_{n=1}^N (\tau_n - \tau_{mean})^2 \right) \quad (1.10)$$

The jitter expressed as time deviation is simply given by $\frac{\Delta\phi_{rms}}{\omega_0}$. Thus one of the possible solutions for jitter calculation, which is commonly used in practice, is excluding an interval of frequencies below a minimum value. This minimum value f_{min} is dictated by the duration of observation or by the speed of the phase correction algorithm.

Focusing now on a more practical case of LC oscillator, one of the simplest abstraction of the phase noise of an LC oscillator was presented by Lee and Hajimiri [24]. Considering a lossy resonator and an energy restoration element. The restorer is needed to compensate the tank loss to enable a constant amplitude oscillation. The only noise contributor is represented by the resonator and can be represented by the equivalent parallel resistance. The energy stored in the tank is

$$E_{stored} = \frac{1}{2} C V_{pk}^2 \quad (1.11)$$

where C is the capacitance of the resonator and V_{pk} is the peak value of the voltage signal. Thus the mean square signal voltage, assuming a sinusoidal waveform, which represent the carrier, is

$$\bar{V}_{sig}^2 = \frac{E_{stored}}{C} \quad (1.12)$$

Integrating the thermal noise density introduced by the resistor over the bandwidth of the RLC resonator determines the total mean square noise voltage.

$$\bar{V}_n^2 = 4k_B T R \int_0^\infty \left| \frac{Z(f)}{R} \right|^2 df = \frac{4k_B T R}{4RC} = \frac{k_B T}{C} \quad (1.13)$$

It is possible to combine (1.11) (1.13) to obtain a noise-to-signal ratio

$$\frac{N}{S} = \frac{k_B T}{E_{stored}} \quad (1.14)$$

Now taking explicitly into consideration the quality factor $Q = \omega E_{stored} / P_{diss}$ can be always written in terms of energy stored and energy dissipated. Therefore

$$\frac{N}{S} = \frac{\omega k T}{Q P_{diss}} \quad (1.15)$$

Remaining in this idealized case of an oscillator whose only losses and noise are due to the resonator, the mean square spectral density of the tank conductance is

$$\frac{\bar{i}_n^2}{\Delta f} = 4k_B T G \quad (1.16)$$

This current noise, once it is multiplied by the effective impedance, becomes voltage noise. It is now worth to recognize that in computing the impedance the restoring element offers in infinite impedance, thus hereafter ideally does not load the tank, the impedance seen is the one of a perfect LC network. As stated before phase noise is considered at a certain offset frequency from the carrier. Denoting $\Delta\omega$ the offset frequency from the carrier ω_0 , the impedance of an LC tank may be approximated by

$$Z(\omega_0 + \Delta\omega) \approx j \frac{\omega_0 L}{2\Delta\omega/\omega_0} \quad (1.17)$$

In general an unloaded tank quality factor can be written using the parallel impedance (conductance) $Q = R/\omega_0 L$ or equivalently $Q = 1/\omega_0 G L$. Using these expression into (1.17) yields

$$\|Z(\omega_0 + \Delta\omega)\| = \frac{1}{G} \frac{\omega_0}{2Q\Delta\omega} \quad (1.18)$$

Multiplying eventually the spectral of the mean square noise current by the squared magnitude of the tank impedance to obtain the voltage mean square noise spectral

density

$$\frac{\bar{v}_n^2}{\Delta f} = \frac{\bar{i}_n^2}{\Delta f} \cdot \|Z\|^2 = 4k_B T R \left(\frac{\omega_0}{2Q\Delta\omega} \right)^2 \quad (1.19)$$

The power spectral density of the output noise is frequency dependent because of the filtering action of the tank, that cause the $1/f^2$ behavior as well. Using now the equipartition theorem, in equilibrium, amplitude and phase noise power are equal. Therefore the always present amplitude limiting mechanism removes half the noise, remaining the other half into phase noise. Traditionally the mean square noise voltage density to the mean square carrier voltage. Performing the normalization leads to the expression for the single sideband noise spectral density:

$$L(\Delta\omega) = 10 \log \left(\frac{2k_B T}{P_{sig}} \left(\frac{\omega_0}{2Q\Delta\omega} \right)^2 \right) \quad (1.20)$$

This result that will be extensively used hereafter tells us that phase noise at a given offset improves as both the carrier power and Q increase. Of course this dependence makes sense since increasing the signal improves the signal to noise ratio, while increasing the quality factor improves quadratically because of the tank impedance.

1.3 Phase noise Models

To describe the phase noise phenomenon different models have been proposed in the last decades, far more complex than the Leeson's formulation [25]. In particular two models have been developed.

- The Hajimiri model which is based on the so called Impulse Sensitivity Function. A linear time variant model of the oscillator.
- Demir's model based on the decomposition of noise perturbation into phase and orbital deviation components.

The theoretical study of phase noise in electrical oscillator is a considerably more difficult task than traditional noise analysis. Here these two model will be briefly reviewed. Demir's model is more complete and gives more precise evaluation of the phenomenon. Hajimiri's model is more intuitive thanks to the ISF that describes the conversion noise to phase noise over time. However, usually some accuracy in

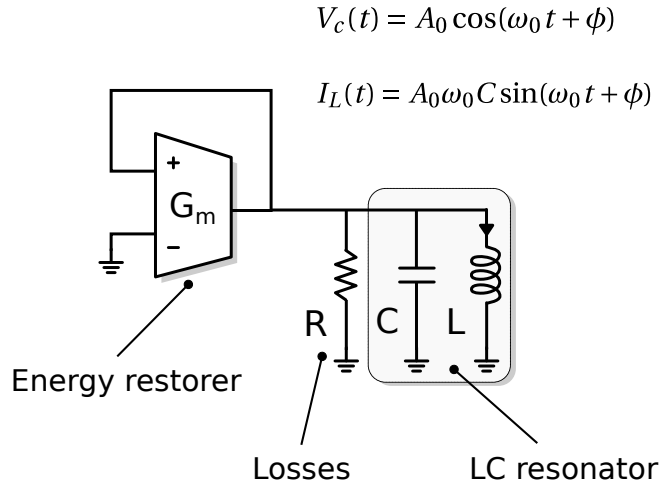


Figure 1.4: LC oscillator equivalent circuit

the prediction of a performance measure may be sacrificed if it is possible to obtain a simple analytical expression for the performance measure itself from which we can derive design insights.

1.3.1 Hajimiri's model

Hajimiri and Lee model was presented in [6] in the form of a general theory for phase noise in electrical oscillators. It is a linear time variant (LTV) model that describes the oscillating circuit as system with n inputs (each associated with one noise source) and two outputs that are the oscillation instantaneous amplitude $A_0(t)$ and the excess phase $\phi(t)$ of the oscillator. Noise inputs to this system are current sources injecting into circuit nodes and voltage sources in series with circuit branches. For each input source it is possible to consider a single input single output configuration. It is then possible to define two impulse response functions for each noise source, one for amplitude variations and one for excess phase. Injecting a current impulse $i(t)$ as shown in Fig. 1.5 the amplitude and the phase will have responses similar to that shown in Fig. 1.5. The instantaneous voltage change ΔV is given by (1.21).

$$\Delta V = \frac{\Delta q}{C_{tot}} \quad (1.21)$$

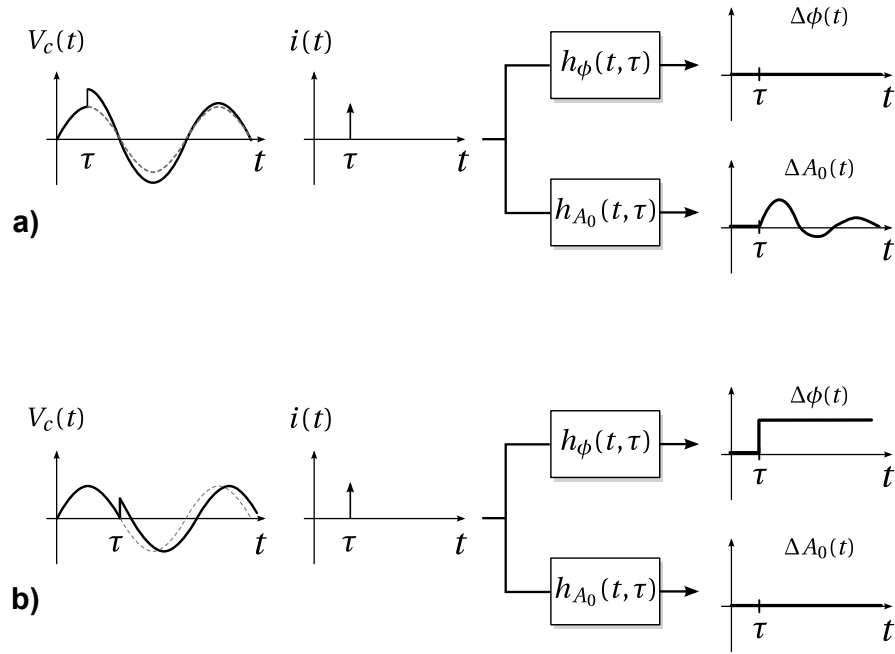


Figure 1.5: Impulse response of an oscillator voltage output waveform to a charge pulse injected a) at the peak of the sinusoidal voltage and b) at zero crossing

Where Δq is the total injected charge due to the current impulse and C_{tot} is the total capacitance at that node. It is worth to notice that the current impulse will change only the voltage across the capacitor and it will not affect the current through the inductor. The resultant impulse responses are time dependent. It can be seen that in particular if the impulse is applied at the peak of the voltage across the capacitor there will be no phase shift and only an amplitude change will result. On the other hand, if this impulse is applied at the zero crossing, it has the maximum effect on the excess phase and minimum effect on the amplitude. However there is an important difference between the phase and amplitude responses of any real oscillator, because some form of amplitude limiting mechanism is essential for stable oscillatory action. The system state will finally reach the trajectory called limit cycle. Both an explicit automatic gain control and the intrinsic non-linearity of the devices act similarly to produce a stable limit cycle. This means that the impulse response associated to A_0 is usually of a little interest, since it tends to asymptotically fade with time. On the contrary any fluctuation in the phase of the oscillation persists indefinitely. The unit impulse response for excess phase can be expressed as

$$h_\phi(t, \tau) = \frac{\Gamma(\omega_0 \tau)}{q_{max}} u(t - \tau) \quad (1.22)$$

Where q_{max} is the maximum charge displacement across the capacitor on the node and $u(t - \tau)$ is the unit step injected at time τ . $\Gamma(\omega_0 t)$ is the so called Impulse Sensitivity Function (ISF). It is dimensionless, frequency and amplitude independent periodic function with period 2π which describes how much phase shift results from applying a unit impulse at a time $t = \tau$. Given the ISF, the output excess phase $\phi(t)$ can be calculated by using (1.22) resulting in (1.23).

$$\Delta\phi(t) = \frac{1}{q_{max}} \int_{-\infty}^t \Gamma(\tau) i_n(\tau) d\tau \quad (1.23)$$

Where $i(t)$ represents the input noise current injected into the node of interest.

Hajimiri and Lee model can be applied to all classes of oscillators and it can be further extended to take into account the cyclostationary nature of noise process. It is possible to state that a noise to phase analysis is twice time-variant, since the transistor noise is generated in a cyclostationary fashion, and the noise to phase noise conversion is itself time-variant.

1.3.2 Demir's model

On the numerical side several works have been devoted to the implementation of fast and accurate predictions of the phase noise [26–29]. These methods are however not suitable to be used to derive a closed form analytical expression for the phase noise. The phase noise model proposed by Demir *et al.* uses a non linear perturbation analysis [27] that was first introduced by Kaertner [29]. Differently from Hajimiri's model, in the Demir's work the perturbation was not decomposed into phase and amplitude perturbation, like the intuition used in Kaertner work, but it was decomposed into phase-deviation component and an additive component that Demir calls orbital deviation. Maintaining the original notation, the unperturbed vector is denoted by $x_s(t)$ and it consists of the capacitor voltage and the inductor current. Then the intent of the Demir's model is to understand the response of the oscillator when an external perturbation $b(t)$ is applied. After major elaborations the unperturbed oscillator's periodic response $x_s(t)$ is modified to $x_s(t \pm \alpha(t)) \pm y(t)$ by the perturbation. Where $\alpha(t)$ is a changing time shift or phase deviation in the periodic output of the unperturbed oscillator and $y(t)$ is an additive component, the orbital deviation, to the phase shifted oscillator waveform. In particular $\alpha(t)$

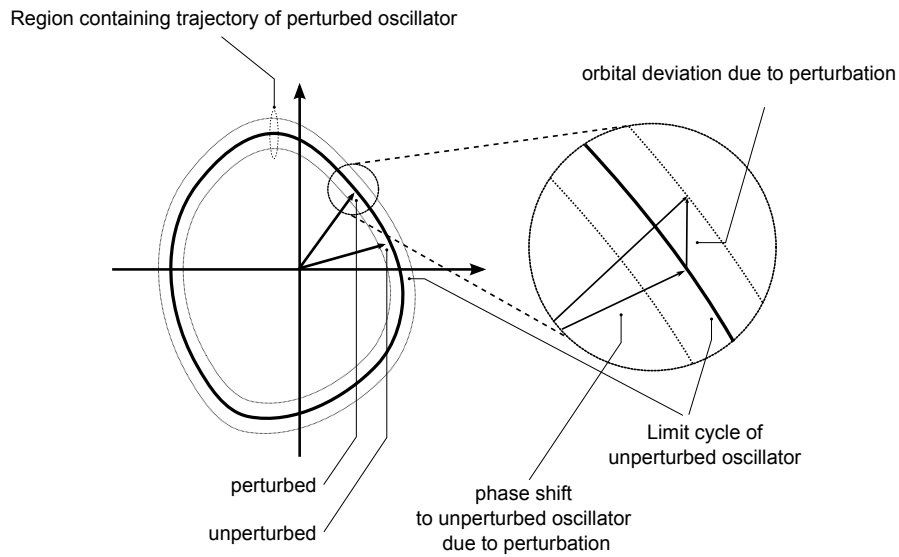


Figure 1.6: Oscillator trajectory

will in general keep increasing with time even if the perturbation $b(t)$ is always small, on the other hand the orbital deviation $y(t)$ will always remain small.

In [27] to give a more intuitive interpretation to the phase and orbital deviations, the oscillator response is viewed in the state-space or phase plane. Reporting in Fig 1.6 the voltage $v(t)$ across the capacitor against the current $i(t)$ through the inductor, the trace for the unperturbed oscillator forms a closed curve since this waveform is perfectly periodic. When the oscillator is then perturbed the periodicity is lost. For stable oscillator however the trajectory remains within a small band around the unperturbed trajectory. The closeness of the perturbed and unperturbed trajectories in the phase plane does not imply in general that the time domain waveforms are also close to each other. The point on the perturbed and unperturbed trajectory corresponding to a given time t will be, in general, far from each other. However, the waveform of the perturbed oscillator does remain close to the unperturbed waveform after it is time shifted by $\alpha(t)$. It is shown that $\alpha(t)$ grows very much like the integral of the perturbation. The analysis starts then from describing the oscillating system by means of a set of differential equations in the form (1.24):

$$\dot{x} = f(x) \tag{1.24}$$

Considering systems that have an asymptotically orbitally stable periodic solution $x_s(t)$, (1.24) is numerically solved to find the unperturbed solution. The interest is, however, in the response of such systems to a small state dependent perturbation of the form $B(x)b(t)$. For this reason the system is linearized around the steady state solution and then the perturbed component is added. The result of such analysis describes the behavior of the phase deviation α by means a differential equation (1.25).

$$\frac{d\alpha}{dt} = v_1^T [t + \alpha(t)] B[x_s(t + \alpha(t))] b(t) \quad (1.25)$$

Where v_1^T plays a similar role to Hajimiri's ISF and $B(\cdot)$ is a function mapping the effect of the circuit time-variance onto the perturbation vector $b(t)$ [30]. It is worth noting that (1.25) is a more refined version of (1.23) rewritten in a differential form.

Demir's model is the most generic and accurate model and can be applied to all classes of oscillators. A higher accuracy is achieved with respect to the ISF based method since the dependence of v_1^T and B in the induced phase shift α is taken into account. As a consequence it correctly predicts the Lorentzian shape of the output spectrum, since it does not collapse in case the frequency of the perturbation approaches the frequency of oscillation. On the other hand, the main drawback of this mathematical model is that it does not provide the designer a design insight into the phase noise generation mechanism.

Chapter 2

An Intuitive Analysis of Phase Noise Fundamental Limits Suitable for Benchmarking LC Oscillators

In this chapter an intuitive yet sufficiently accurate formulation of the phase noise of various commonly used oscillators, including most types of class-B (standard, AC-coupled and with tail filter) and class-C is derived and used to compare their fundamental limitation. A noise factor that represents the difference between the maximum achievable Figure of Merit and the actual one is derived for all topologies considered. Measurements on a dedicated chip prototype that integrates two of the most promising architectures allows to verify, in an unbiased way, the accuracy of the predictions. A very good agreement between the model and both simulation and measurement is obtained.

2.1 Introduction

Modern communication systems need clocks with very low phase noise and/or jitter. To minimize phase noise for a given power consumption, integrated oscillators often use as load a high-Q LC-tank. Through the years, integrated LC oscillators have improved as a result of technology and/or topologies evolution, however,

it is not always easy to ascertain the dominant reason of such improvements. Moreover, the growing request to extend battery life especially in modern smart phones has particularly encouraged an intense research to improve the design of fully integrated VCOs. The result is a deeper knowledge of phase noise mechanism and in the development of a large number of new solutions. In the past, following the pioneering work of Leeson [25], authors have analyzed oscillators either in a rigorous mathematical way or using a simpler yet accurate Linear Time Variant (LTV) approach [6, 27, 29, 31–33], but generally preferring rigor to intuitiveness. The goal is to determine the ultimate performance limit for some of the most used LC oscillator topologies, combining reasonable accuracy with intuitiveness. In addition, the theory is experimentally verified in a rigorous and objective way comparing the best two topologies in the exact same operating conditions i.e. technology, Q of the tank, dividers, etc. In the following LC oscillators are classified as it is done for Power Amplifiers considering negative resistance implemented with nMOS, pMOS or complementary pMOS-nMOS transistors, assuming an arbitrary gain between the tank and the active devices and that the bias current is supplied from the positive rail. No voltage biased oscillators are considered since in most of practical implementations the possibility to clearly control oscillator's power consumption is of great importance. It is worth mentioning that voltage biased topology, eliminating current generator noise source and permitting to achieve slightly higher efficiency, are becoming attractive for research. To compare different architectures we rely on a well-accepted Figure of Merit (FoM) [34]. Furthermore we normalize the phase noise to the ultimate limit through a very useful parameter called Excess Noise Factor (ENF) [35–37]. In the derivation of the FoM for the different topologies, $1/f$ noise is neglected only differential topologies are considered (for their many advantages e.g. exact 50% duty cycle, reduced cross talk, etc). Notice that a differential Colpitts oscillator is a special case of a negative resistance one and therefore is included in this analysis [38].

This chapter is organized as follows. Section 2.2 lists the oscillator considered i.e. those for which the tank is not loaded by the active devices, derives their phase noise and FoM, using some simplifying assumption, and introduces the concept of ENF. Section 2.4 compares the different topologies in term of ENF and defines the two most promising ones from fundamental arguments. Section 2.5 experimentally compares these topologies using a specially designed test bench.

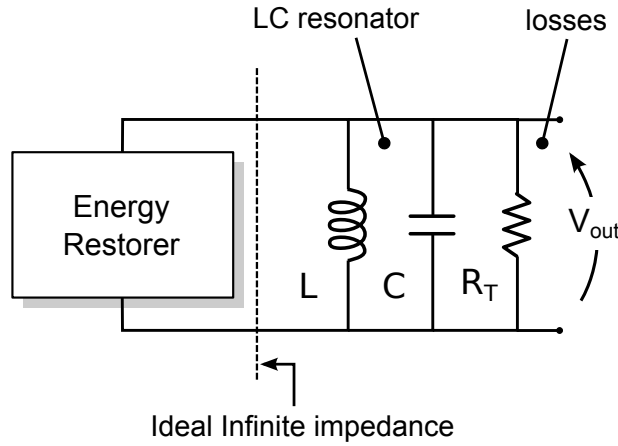


Figure 2.1: Generic LC oscillator

2.2 Phase Noise in LC-Tank Oscillators

The conceptual schematic of an LC-oscillators is shown in Fig. 2.1, where the LC-tank losses are represented by $R_T = Q/(\omega_0 C)$ and the active components by an energy-restoring block. According to the LTV theory of Hajimiri and Lee [6], the conversion of noise into phase noise is described by the Impulse Sensitivity Function (ISF) Γ . The ISF defines the effect of noise on the oscillation phase and is a function of the phase of the tank voltage. The general expression for the phase noise is given in (2.1).

$$L_T(\Delta\omega) = 10 \log \left(\frac{k_B T}{P_{RF}} \left(\frac{\omega_0}{Q \Delta\omega} \right)^2 (\Gamma_{T,rms}^2 + \alpha \Gamma_{M,rms}^2) \right) \quad (2.1)$$

Where k_B is the Boltzmann's constant, T the absolute temperature, $P_{RF} = A_0^2/2R_T$ is the power dissipated in the tank, α is a noise factor that includes in general γ_{mos} and attenuation between the tank and MOS gates, $\Gamma_{T,rms}^2$ and $\Gamma_{M,rms}^2$ are the *rms* ISF for R_T and the MOS transistors and no other noise source is here now considered. The ratio between RF power in the tank P_{RF} and the DC power P_{DC} , called power efficiency η_P , is expressed in terms of voltage and current efficiencies [39] η_I and η_V (2.2).

$$\eta_P = \frac{P_{RF}}{P_{DC}} = \frac{I_{RF} V_{RF}}{I_{DC} V_{DC}} = \eta_I \eta_V \quad (2.2)$$

Where I_{RF} and V_{RF} are the *rms* values of the fundamental components of current and voltage across R_T , V_{DC} and I_{DC} are the supply voltage and current. Using

(2.2) into (2.1), the oscillator's phase noise can be written as (2.3).

$$L_T(\Delta\omega) = 10 \log \left(\frac{k_B T}{P_{DC}} \left(\frac{\omega_0}{Q\Delta\omega} \right)^2 \frac{(\Gamma_{T,rms}^2 + \alpha\Gamma_{M,rms}^2)}{\eta_P} \right) \quad (2.3)$$

Different oscillators are compared in terms of a Figure of Merit (2.4) [34] that normalizes the phase noise to the oscillation frequency ω_0 , the offset frequency $\Delta\omega$ and the power dissipation (expressed in *mW* or *dBm*).

$$FoM = -10 \log \left(L(\Delta\omega) P_{DC,mW} \left(\frac{\Delta\omega}{\omega_0} \right)^2 \right) \quad (2.4)$$

Using (2.3) into (2.4) leads to the handy expression (2.5).

$$\begin{aligned} FoM &= -10 \log \left(\frac{k_B T (\Gamma_{T,rms}^2 + \alpha\Gamma_{M,rms}^2)}{10^{-3} Q^2 \eta_P} \right) \\ &= 173.8 \text{dBc/Hz} + 10 \log \left(\frac{\eta_P Q^2}{(\Gamma_{T,rms}^2 + \alpha\Gamma_{M,rms}^2)} \right) \end{aligned} \quad (2.5)$$

Assuming that the oscillation voltage is nearly sinusoidal and that the energy restoring element drives the tank from a high impedance, the ISF for R_T is a sinusoid in quadrature with the tank voltage giving $\Gamma_{T,rms}^2 = 1/2$ [6]. To improve the *FoM* we can act on three fronts. First the tank Q , getting *6dB* for every doubling of it. Second, on the power efficiency, getting only *3dB* for every doubling of it. Third, on the ISF and excess noise factor of the transistors. Assuming 100% power efficiency, noiseless transistors and no other noise contribution, the *FoM* can be denoted as FoM_{max} (2.6).

$$\begin{aligned} FoM_{max} &= -10 \log \left(\frac{k_B T}{2 \cdot 10^{-3}} Q^2 \right) \\ &= 173.8 \text{dBc/Hz} + 10 \log (2Q^2) \end{aligned} \quad (2.6)$$

FoM_{max} is a thermodynamic limit associated with the noise and power dissipation of the unloaded tank. Expressing the actual *FoM* in terms of FoM_{max} gives what we call Excess Noise Factor (2.7) ENF [36].

$$ENF = FoM_{max} - FoM = 10 \log \left(\frac{2(\Gamma_{T,rms}^2 + \alpha\Gamma_{M,rms}^2)}{\eta_P} \right) \quad (2.7)$$

The ENF defines the distance from the ultimate limit. The same concept was proposed by van der Tang and Kasperkovitz [36] putting $F = 1$ into Leeson expression and assuming 100% efficiency, rigorously derived by Bank [35] using an ISF approach and by Murphy *et al.* using a phasor approach [33]. If the transistor current noise power spectral density is proportional to the derivative of the drain current with respect to the gate voltage $\Gamma_{M,rms}^2 = 1/2$ [35, 38] and for a direct coupling between tank and transistors, the excess noise factor α is just γ_{mos} . Using this result into (2.5) and (2.7) gives (2.8) and (2.9).

$$\begin{aligned} FoM &= -10 \log \left(\frac{2k_B T (1 + \gamma_{mos})}{10^{-3} Q^2 \eta_P} \right) \\ &= 173.8 \text{dBc/Hz} + 10 \log \left(\frac{2\eta_P Q^2}{(1 + \gamma_{mos})} \right) \end{aligned} \quad (2.8)$$

$$ENF = 10 \log \left(\frac{(1 + \gamma_{mos})}{\eta_P} \right) \quad (2.9)$$

More generally, α is proportional to the inverse of the voltage gain between tank and active devices. In Colpitts oscillators this factor is larger than one due to capacitance partition from drain to gate, while when using transformer coupling the factor can be either larger or smaller than one. VCO topologies mimic those of RF Power Amplifiers (PA). We analyze VCOs (PAs) for which the load is naturally represented by a parallel resonator and the active device by a Norton equivalent [40]. This includes class B, C and F. These topologies are the most commonly used, although some recently proposed ones cannot be, directly, included in the model e.g. “Clip and Restore” and class-D [41, 42]. These oscillators will be discussed, and it is worth to underline that, even if they can not be modeled by the simple ENF expression, the ENF can be still used in general to assess the improvements of the oscillator topology. The ENF of published oscillators [8, 9, 13, 14, 32, 42–58] grouped by topology, is plotted in Fig. 2.2 versus tank Q. This data indicate no clear winner and a very large spread within the same architecture, although class-B with tail filter and class-C are the closest to the limit (also Colpitts which can be however assimilated to a class-C [38]). Second order effects often dominate and the reported tank Q can be inaccurate (e.g. in [43] FoM and Q are inconsistent as pointed out in [36] and this data is not reported in Fig. 2.2). The difficulty to extract the tank Q, together with the high sensitivity of phase noise to Q, limits the ability to assess the potential of a new topology. Because of this we have built a test chip to compare different topologies in the exact same operating conditions. In the following for the oscillators satisfying (2.8) we determine the

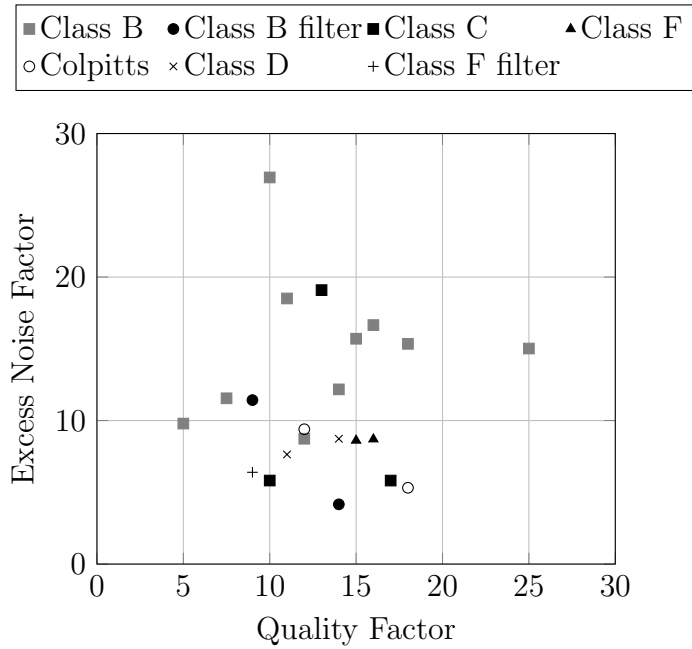


Figure 2.2: Benchmarking of different oscillator topologies using ENF

minimum achievable ENF showing that the only differentiator is efficiency which is maximized maximizing η_I and voltage swing. However, the following three aspects should be considered. First, the voltage drop across the bias current source, V_B , degrades efficiency by $1 - V_B/V_{dd}$. Second, the bias transistors contribute to phase noise in a topology dependent way. Third, in some cases there is a maximum voltage swing beyond which the active devices load the tank causing $\Gamma_{M,rms}^2$ to increase.

2.3 Different Oscillator Topologies

2.3.1 Class B oscillator

For the class-B oscillator the shape of the tank current can be usually approximated as a square wave (Fig. 2.3b), assuming negligible parasitic capacitance at the tail current generator. The *rms* fundamental component of the RF current is $\sqrt{2}/\pi I_{DC}$ and η_I is $\sqrt{2}/\pi$. Due to the tail current source, the active devices do not load the tank even when they enter the triode region. Therefore the maximum η_V occurs at the maximum achievable swing and is equal to $\sqrt{2}V_B/V_{dd}$. This gives an η_P of $2/\pi(1 - V_B/V_{dd})$. For the complementary class-B oscillator of Fig. 2.3a the shape of the tank current is shown in Fig. 2.3b. In this case the fundamental

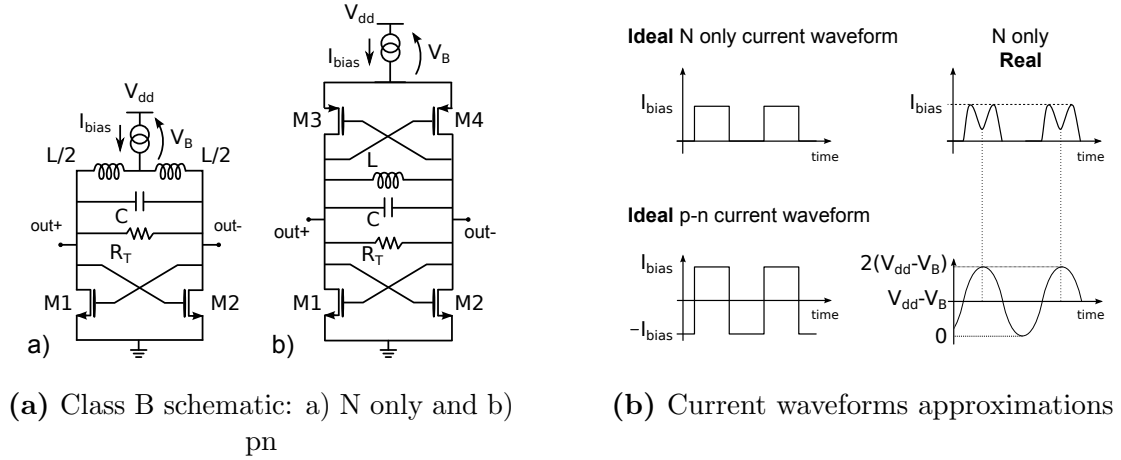


Figure 2.3: N-MOS, complementary MOS “class-B” LC oscillators and current, voltage waveforms

component of the RF current is $2\sqrt{2}/\pi I_{DC}$, and η_I is $2\sqrt{2}/\pi$. On the other hand, since the voltage cannot exceed the supply, the maximum η_V is equal to $(1 - V_B/V_{dd})/\sqrt{2}$. This gives an η_P of $2/\pi(1 - V_B/V_{dd})$. We conclude that for N-only and p-n implementations, η_V is twice for the former and η_I is twice for the latter giving the same η_P . Andreani, Fard [59] and Murphy *et al.* [33] have shown that for a p-n oscillator (2.8) and (2.9) are valid only if the tank is floating otherwise the phase noise is degraded. In practice, however, it is possible to make such a degradation reasonably small by proper designing of the tank (e.g. differential tuning), acting on the relative size of the pMOS and nMOS devices and using a p-type bias.

Let us compare the real and ideal performances of a class-B VCO, focusing on the drain current flowing through a transistor and its drain voltage output. Let us now consider that the current generator is not contributing any noise and that it works properly even with a vanishing saturation voltage between drain and source. In this way we are able to maximize the voltage output swing giving maximum voltage efficiency. Moreover, if the transistor are ideal switches the current at their drain is a perfect square wave and its fundamental harmonic component is $2/\pi$ times the DC current I_{DC} , thus giving a current efficiency of $\sqrt{2}/\pi$. However, in a real class-B VCO the voltage output must be significantly lower to guarantee the current functionality of the current generator and most important when transistor enter triode region loading effects occurs. For this reason the oscillator works with a limited voltage efficiency, typically around 60%. Another reason of reduction of efficiency is the parasitic capacitors at the common source of the switching couple.

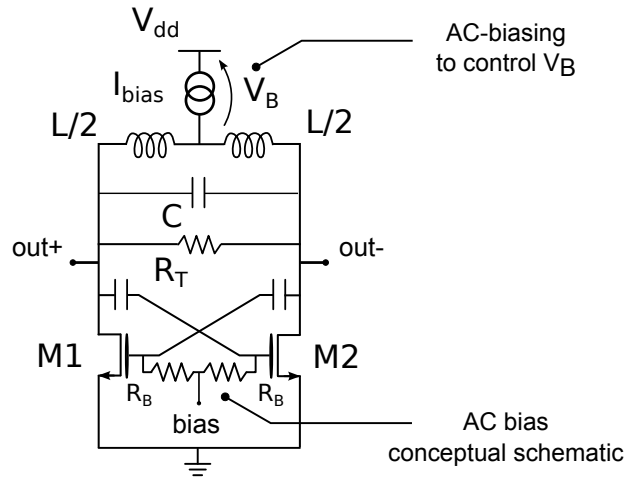


Figure 2.4: AC-biased class-B oscillator (NMOS only)

This tends to reduce current efficiency when the transistors work in triode region due to a shape of the current reported in Fig. 2.3b. This leads to the fact that the current shape is no more a pure square wave but rather it presents a drop at the peak of the voltage oscillation. Having this current shape reduce the current efficiency to about 55-50%.

To summarize, the ENF of an ideal class-B oscillator is $10 \log[\pi V_{dd}/2V_{sw}(1 + \gamma_{mos})]$, where V_{sw} is the peak swing, and is uniquely defined by η_V . Two important non-idealities however exist. First, the current source contributes phase noise proportionally to its g_m , suggesting to increase V_B . This represents a trade-off with η_V and an optimum FoM versus V_B should exist. However, for a given supply voltage and DC current, the value of V_B is defined by the size of the switching devices, leaving no room for further optimization. Second, due to the tail parasitic capacitance, when the switching transistors are in the triode region they load the tank, contributing extra noise. Therefore, as the swing increases, there is a trade-off between efficiency and noise that limits the FoM, making it much smaller than FoM_{max} i.e. ENF much larger than $3dB$.

Consider as an example the circuit N only of Fig. 2.3a with a tank Q of 15 and $V_{dd} = 1.5V$. Simulations give a minimum ENF above 10 dB, due to an η_P of 29% (5.4 dB loss), a tail transistor noise 5% of the total (0.2 dB loss), and a switching MOS noise, enhanced by the tail parasitic capacitance, 61% of the total (4.6 dB loss). One way to improve efficiency is to use AC coupling to control V_B by forcing a DC voltage drop on the capacitor connected between the drain and gate of the

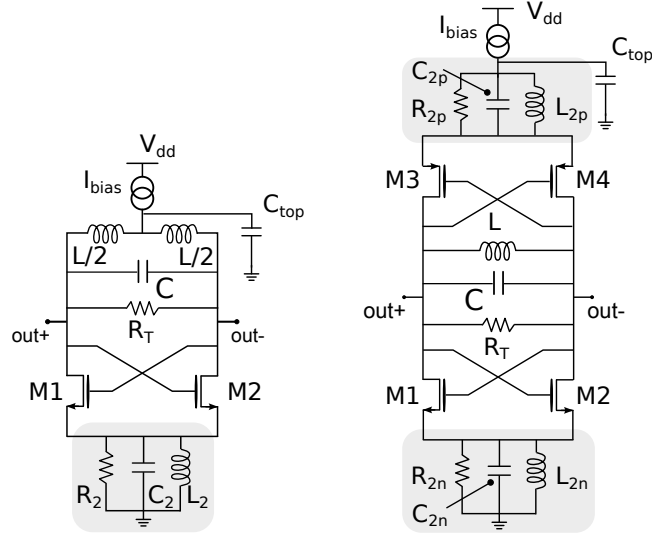


Figure 2.5: Oscillators with second-harmonic LC tail filter

switching transistors as shown in Fig. 2.4 (for simplicity Fig. 2.4 and the followings with AC coupling represent only conceptual schematics where the circuit that set the DC bias is not shown). While η_I is not improved the extra degree of freedom allows to improve η_V and therefore ENF (e.g. for the previous example by about $1.5dB$).

2.3.2 Class B oscillator with tail filter

Most of the above limitations can be overcome placing an additional LC-tank, resonating at $2\omega_0$, at the tail of a class-B oscillator [14]. Three advantages are obtained. First, the common source node can swing below ground, increasing the maximum η_V . Second, the switching transistors can enter the triode region without loading the tank since they see a high impedance in series with them. Third, the noise of the current source around $2\omega_0$ can be filtered with a large capacitance C_{top} . The presence of an extra tank within the circuit creates an additional state variable and the ISF needs to be computed with a more complex approach [29]. The demonstration of the model and the calculation of the ISF is presented in Chapter 3. As simple message to the designer, simulation shows that if the impedance of the tank is sufficiently high, (2.9) still describes the new topology in a sufficiently accurate way. The best ENF can be reached with both the AC coupled topology and the classic DC coupling (Fig. 2.5). AC coupling helps, as mentioned, in having control on V_B , and in particular it helps for low current consumption. Towards

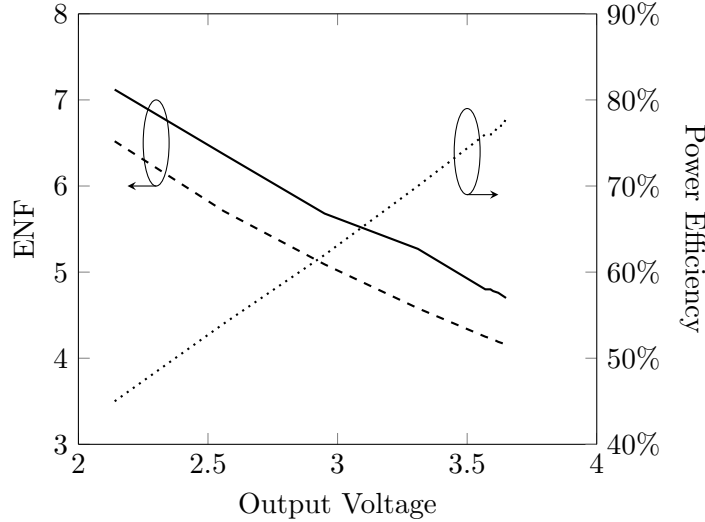


Figure 2.6: Class-B oscillator with tail filter: calculated and simulated ENF and simulated power efficiency.

the minimum ENF the improvement offered by AC coupling is marginal or even null, when in fact the current generator is in triode. In this case, although the shape of the tank current is no longer a square wave (due to the presence of C_{top} that allows large spikes of current from the supply), η_I is still remarkably close to $\sqrt{2}/\pi$ up to the maximum achievable voltage swing. Ideally η_P would reach 100% for a differential swing of πV_{dd} peak ($V_B = 0$), giving a minimum ENF of 3dB (if $\gamma_{mos} = 1$). In reality, simulation results (Fig. 2.6) give a maximum η_P close to 80%. Extrapolating the efficiency curve of Fig. 2.6 for even higher swings (assuming not to break the transistors) it may seem that more than 100% η_P could be reached. In reality at some point a decrease of η_I would nullify the slight increase of η_V , making η_P to saturate to a value close, but still below, 100%. We compare ENF from the model (assuming a $\Gamma_{T,rms}^2 = 1/2$, $\Gamma_{M,rms}^2 = 1/2$ and $\gamma_{mos} = 1$) and from simulations as a function of the output voltage swing. As shown in Fig. 2.6 simulations confirm the model within an error of 0.8 dB over a large range of swings. This error is due to excess transistors noise and is probably explained by an increase in γ_{mos} for high swing. A practical limit of the class-B oscillator with tail filter is the large voltage that the active device must endure. For a 1.5V supply simulation shows that the maximum V_{GS} is close to 4V. It might seem that the solution is to reduce the voltage supply. However, the reader should be considered that once the oscillator is inserted in a system it does not impose the voltage supply. Moreover, even with the technology scaling in most of the practical cases the voltage supply for analog circuitry is still higher than 1V. Reliability concerns are greatly reduced using the

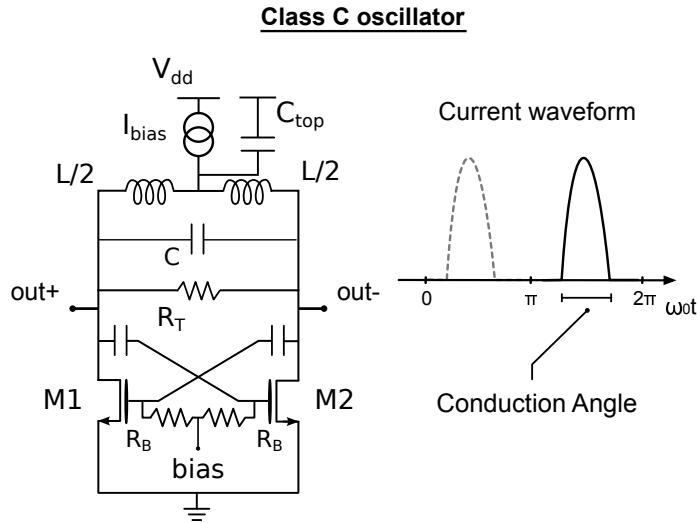


Figure 2.7: Class-C oscillator (NMOS only)

p-n topology shown in Fig. 2.5b. In this case, 100% η_P is reached with half the voltage swing of the n-only topology i.e. $\pi/4V_{dd}$ peak. Simulation for the same operating condition as above (using a fully-differential tank capacitance) shows that the best ENF is close to that of the n-only case with a maximum V_{GS} of 1.9V, i.e. compatible with thick oxide device almost always available in any deep scaled CMOS technology.

2.3.3 Class C oscillator

Another way to improve ENF is by improving η_I . The tail current shaping technique was introduced by Soltanian and Kinget [60], observing that shaping the tail current was a method to obtain a higher output swing and thus a better phase noise. The tail current was made large when the oscillator output voltage reaches its maximum or minimum and was made small (ideally zero) during the zero crossing. The result was, in fact, to have improved the current conversion between DC and RF. This leads to a preliminary, and actually not optimized, version of the class-C oscillator. We had to wait Mazzanti and Andreani [38] to push the class C to its optimum with a deeper understanding and further optimization of the oscillator circuit. The resulting class C schematic is the same as the AC coupled class B (Fig. 2.4) with the addition of a large capacitance in parallel to the current source (Fig. 2.7). Despite their apparent similarity, the two topologies behave very differently. First, since the DC drop on the coupling capacitors is much larger for the former, the

switching transistors are off when balanced. Second, the large capacitor shunting the current source allows to deliver sharp current spikes at the peak of the voltage swing. Combining these two effects drastically reduces the conduction angle for the tank current, as shown in Fig. 2.7. In the limit the tank current becomes a series of pulses giving an η_I of $1/\sqrt{2}$ and an η_P $(V_{sw}/V_{dd})(1 - V_B/V_{dd})$, where V_{sw} is the peak voltage swing. For the same bias current this could give $3.9dB$ increase in the ENF compared with a class-B oscillator ($1.95dB$ due to better η_I , $1.95dB$ due to better η_V), as indicated in the literature [38]. However, to get such an improvement the class-B oscillator should have been operated at small oscillation amplitudes, very far from the optimum ENF (i.e. in current limited mode). For the same oscillation amplitude only η_I increases, giving a $1.95dB$ ENF improvement. If the noise of the current source is negligible, the ENF of a class-C oscillator is given by $10 \log(V_{dd}/V_{sw})(1 + \gamma_{mos})$ where V_{sw} is the peak swing. This shows that also a class-C oscillator has an ENF uniquely defined by its voltage swing and, for the same V_{dd} , it has the same ENF of a class-B with a voltage swing $2/\pi$ times smaller. Ideally, with $V_B = 0$, 100% η_P can be reached with a differential voltage swing of $2V_{dd}$ peak (compared with πV_{dd} in the class-B oscillator with tail filter). The large shunt capacitance of the class-C oscillator filters out the noise of the bias allowing a smaller V_B further improving η_P . The class-C oscillator has a drawback that severely limits its phase noise at large oscillation amplitudes efficiency. Due to the shunt capacitor, when the switching transistors are in the triode region they load the tank, increasing noise. The maximum swing that ensures saturation is $V_{dd} - V_B$ (assuming that the switching transistors are biased just one threshold above ground). In this condition, even assuming $V_B = 0$, η_P is 50% with a loss of $3dB$ in the ENF. In practice the optimum FoM is achieved when the device just enters the triode region at the oscillation peak with a slightly higher noise but a sufficiently higher η_P to give a better ENF [38]. We compare ENF from the model (assuming a $\Gamma_{T,rms}^2 = 1/2$, $\Gamma_{M,rms}^2 = 1/2$ and $\gamma_{mos} = 1$) and from simulations as a function of the output voltage swing in the same operating conditions as above. Such a comparison is shown in Fig. 2.8, which also plots η_P . As expected, initially η_P increases and ENF decreases almost linearly with the swing. In this region the model error stays below $1dB$ and is caused by the transistors noise (γ_{mos} is larger than 1). At large voltage swings, where the switching transistors enter into the linear region, the model cannot be used since the circuit loads the tank. The difference between model and simulation increases due to two effects. First, noise from tank, switching pair and current source increase. Second η_I decreases,

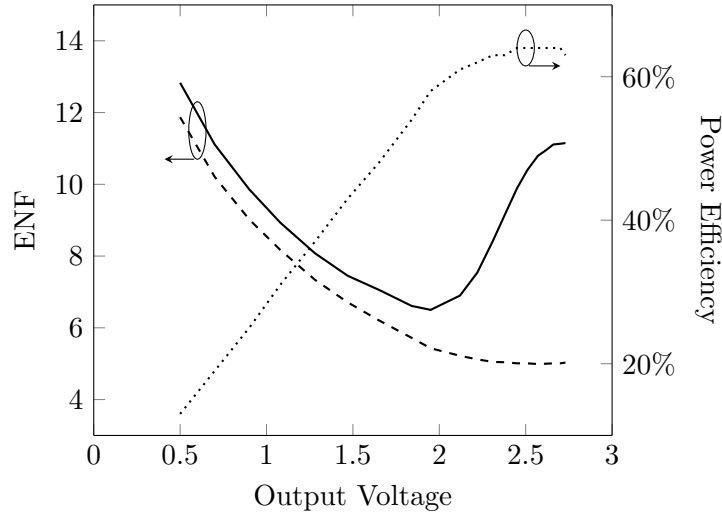


Figure 2.8: Class-C oscillator: calculated and simulated ENF and simulated power efficiency.

canceling the corresponding increase in η_V as shown in the η_P plot. Simulation predicts a minimum of the ENF of 6.5dB for a differential peak swing of $1.3V_{dd}$, which is close to the ENF of the model at the edge of its range of validity.

Some class C evolutions Class C topology suffers from a trade-off between a robust start-up and the maximum oscillation amplitude in steady state operation. In fact, there are two different optimal values: one that guarantees the start up, when the voltage bias at the gates is high enough to allow the oscillation to build up with a safe margin, and a second one in steady state, when, thanks to the action of C_{top} , it is possible to reduce the gate bias. The trade off between the two bias points determines the maximum oscillation amplitude consequently the phase noise and ENF performances. Okada *et al.* [61] improves this trade off using a hybrid topology where a parallel of two core switching pair was used. A switching pair used to guarantee start up, when the other pair used to have a class C operation, with lower gate bias applied. This approach was demonstrated in [62] for a cellular transmitter VCO in which an hybrid class B/class C oscillator is proposed (shown in Fig. 2.9a). It uses a degenerated class B core switches to control the current flowing through the class B path while the maximum of the bias current flows through the class C counterpart. It should be noted, as pointed out in [62], that due to the lack of source feedback the transistors of the class C core are pushed slightly out of the saturation region. This yields to the fact that the low frequency noise of the bias resistances find a straightforward path to the tank where it is converted into phase noise. For this reason their noise should be pushed at very low

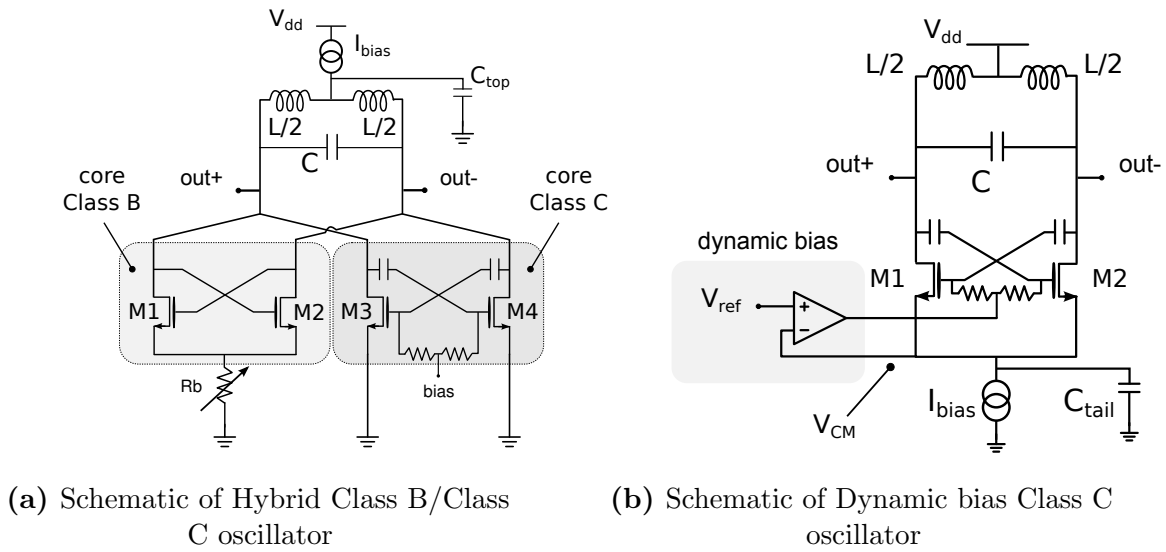


Figure 2.9: Schematic of two class C evolution

frequency acting on the values of the resistance and capacitors to be filtered out by the Phase Locked Loop where the VCO is going to work. The hybrid class B/class C represents an important step towards finding a solution of the start up and oscillation amplitude trade off and so it increases the robustness of the oscillator. It implies, however, a slightly lower efficiency compared to a pure class C topology, but it still achieved about 25% better current efficiency compared to a pure class B oscillator with identical performance. While the hybrid class C VCO solutions have strengthened the start up condition paying with a lower current efficiency, more recently a dynamic bias class C VCO (shown in Fig. 2.9b) was proposed [39]. The bottom biased topology proposed uses a negative feedback to sense the common mode voltage at the transistors source to adjust consequently V_{bias} at their gates. Settling time, stability and steady state error between the operational amplifier reference and the common mode voltage depend on the bandwidth and the DC gain of the operational amplifier itself. Moreover, as long as the transistors are working in class C the high impedance seen at the drain of the current generator at low frequencies suppresses the contribution of the op-amp noise to phase noise (in general the op-amp contributes via AM-to-PM conversion). The dynamic bias of the core transistor is thus another suitable solution to try to break the trade off presents in the original class C topology.

2.3.4 Class F oscillator

Another way to improve efficiency in a PA is by acting on the resonator. The goal is to create an output waveform with sharper transitions (ideally a square wave) so that the active devices dissipate power for a smaller percentage of time. The same concept should give a better FoM since efficiency and FoM are directly related. In addition the new resonator has a different ISF, with potentially an even larger effect on the ENF. A possible class-F oscillator (shown in Fig. 2.10a) uses two series-connected LC tanks, resonating respectively at the fundamental frequency (ω_0) and at the third harmonic. Assuming a square wave current and sufficiently high Q , the voltage across the first tank is a sinusoid at ω_0 and the voltage across the second tank a sinusoid at $3\omega_0$, with opposite phase. If the tank impedances at $3\omega_0$ and at ω_0 are comparable, the voltage resemble the one of Fig. 2.10b. At the switching instants the waveform has a higher slope than a sinusoid with the same peak amplitude, potentially improving phase noise. This oscillator is analyzed using the ISF approach in Chapter 3. Here the major results as well as the conclusions will be reported. Based on the ISFs theory [6] deriving the perturbation vector to the steady state trajectory, the phase noise this type of class F can be expressed as (2.10).

$$L_{tot}(\Delta\omega) = 10 \log \left(\frac{k_B T}{2P_{sig}} \left(\frac{\omega_0}{\Delta\omega Q_{\omega_0}} \right)^2 f_{res} (1 + \gamma_{mos}) \right) \quad (2.10)$$

Where, P_{RF} is the signal power, Q_{ω_0} is the Q of the tank at ω_0 , and f_{res} is the resonator noise factor, given in (2.11), which is a function of the ratio between the resonator impedances and the quality factors of the two resonators.

$$f_{res} = \frac{\left(1 + 9 \frac{C_3}{C_1} \frac{A_3^2}{A_1^2} \frac{3Q_{\omega_0}}{Q_{3\omega}} \right) \left(1 + \frac{3Q_{\omega_0}}{Q_{3\omega}} \frac{C_3}{C_1} \frac{A_3^2}{A_1^2} \right)}{\left(1 + 9 \frac{C_3}{C_1} \frac{A_3^2}{A_1^2} \right)} \quad (2.11)$$

Assuming transistor current noise is γ_{mos} times the derivative of the drain current with respect to the gate voltage, the transistors phase noise is γ_{mos} times the tank phase noise i.e. the result derived in [35] [38] for harmonic oscillators is true also for class-F. To minimize ENF we need to minimize f_{res} and to maximize efficiency. Observing (2.11) and considering the more rigorous analysis in Chapter 3 it can be seen that f_{res} decreases as $Q_{3\omega_0}$ is increased. Moreover, if $Q_{3\omega_0}$ is greater than $5/3Q_{\omega_0}$, f_{res} is smaller than 1 and is proportional to C_3 . The minimum C_3 is when

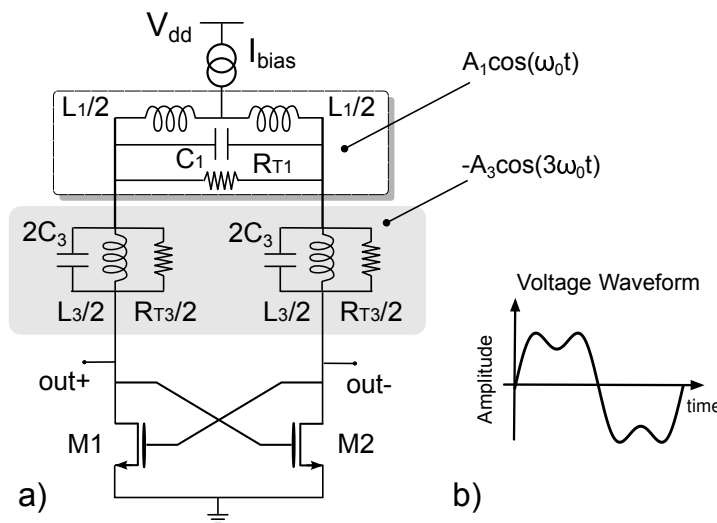


Figure 2.10: Class-F oscillator: a) circuit schematic and b) typical voltage waveform.

the impedances at $3\omega_0$ and at ω_0 are equal (to prevent oscillation at $3\omega_0$). If $Q_{3\omega_0}$ is too small f_{res} becomes actually larger than 1, nullifying any potential advantage in using a class F topology. In Chapter 3, and here reported, to verify the analysis, two class-F and a class-B oscillators have been simulated for the same operating conditions. In one class-F $Q_{3\omega_0}$ is equal to Q_{ω_0} , while in the other $Q_{3\omega_0}$ is equal to $3Q_{\omega_0}$. In both cases the resonator impedance at ω_0 and at $3\omega_0$ is nearly equal. Fig. 2.11 reports the simulated and calculated phase noise as a function of the DC power dissipation. As expected, increasing $Q_{3\omega_0}$ gives a better phase noise. When the Q_{ω_0} and $Q_{3\omega_0}$ are equal class-F and the class-B oscillators show the same phase noise since conversion efficiency and resonator noise compensate each other.

The analysis considers a possible implementation of class F oscillator. Recently the harmonic tuned LC tank [52] is represented with the use of a transformer by Babaie and Staszewsky [13]. It is worth to point out that the improvement in terms of ISF and, as a consequence, the overall possible improvement in terms of ENF here analyzed, remains true only if transistors are working in saturation region. They, in fact, would cause otherwise loading the tank, which is highlighted by the analysis in Chapter 3. Moreover the use of transformer increases the complexity of the tank design and usually on chip transformer have indeed lower quality factors than simple inductors. This partially is compensated by the fact that thanks to the multi-resonance a transformer based resonators displays a steeper phase response with respect to a simple LC tank for the same quality factor [12].

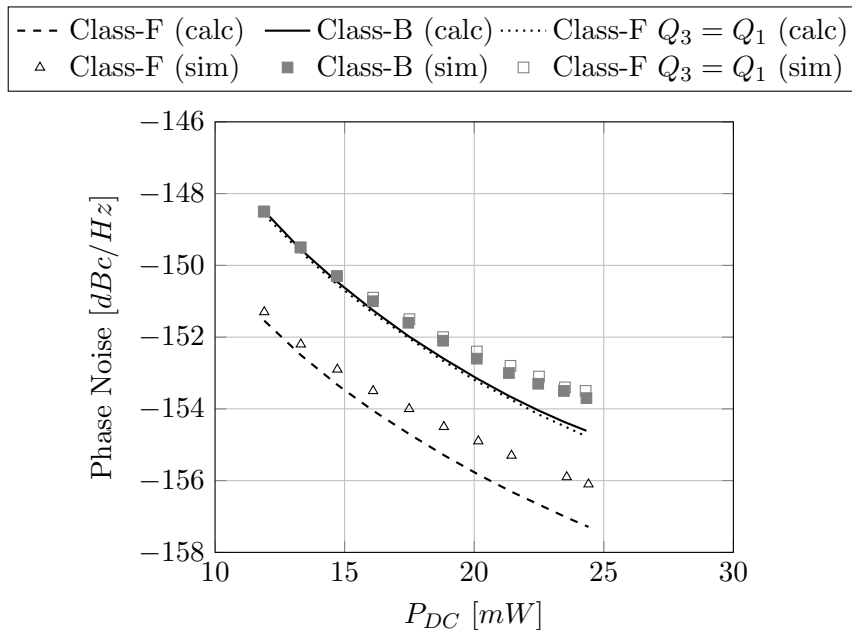


Figure 2.11: Comparison between Class-F and Class-B oscillators phase noise. Dots represent simulated data, lines are calculated

2.3.5 Transformer coupled oscillators

Transformer based oscillators are often used to improve tuning range ([57, 63–66]) thanks to different resonant modes at different frequencies. In fact, as analyzed in [63], high order LC tanks have potential advantages in wideband or multiband applications. However, with the increase of resonator order, frequency stability becomes an issue and more design parameters have to be optimized simultaneously (including inductance ratio, capacitance ratio and coupling factor). As an example Goel *et al.* [66] obtained a good peak FoM of $192\text{dBc}/\text{Hz}$, however, since the impedance and quality factor can change significantly from mode to mode, the FoM varies more than 5dB over the tuning range ([63–66]). On the other hand, the transformer-coupled technique can be used also to reduce the noise of the active devices, i.e. to improve ENF. In fact, introducing a gain between the tank and the active devices, reduces α in (2.7). This was done via a step-up transformer by Mazzanti and Andreani [38] for a class-C oscillator, which obtained one of the highest FoM published. Experimental verification, however, shows nearly the same ENF as with direct coupling. This is because in a transformer coupled oscillator the active devices contribute less noise but enter earlier in the linear region due the larger swing. Since for class-C the optimum FoM is achieved with the active devices just reaching the edge of the linear region at maximum swing, transformer coupling reduces both noise and efficiency. Transformer coupling can be used in

Table 2.1: Efficiency Comparison of NMOS VCOs

Osc. type	$\eta_{I,max}$	$\eta_{V,max}$	$\eta_{P,max}$	ENF_{min}
Class B	$\sqrt{2}/\pi$	$\sqrt{2} \left(1 - \frac{V_B}{V_{dd}}\right)$	$\frac{2}{\pi} \left(1 - \frac{V_B}{V_{dd}}\right)$	10dB
Class B AC-bias	$\sqrt{2}/\pi$	$\sqrt{2} \left(1 - \frac{V_B}{V_{dd}}\right)$	$\frac{2}{\pi} \left(1 - \frac{V_B}{V_{dd}}\right)$	8.5dB
Class B AC-bias LC-filter	$\sqrt{2}/\pi$	$\frac{\pi}{\sqrt{2}} \left(1 - \frac{V_B}{V_{dd}}\right)$	$\left(1 - \frac{V_B}{V_{dd}}\right)$	4.5dB
Class C	$1/\sqrt{2}$	$1/\sqrt{2}$	1/2	6dB
Class F	$\sqrt{2}/\pi$	$\frac{4\sqrt{2}}{\pi} \left(1 - \frac{V_B}{V_{dd}}\right)$	$\frac{8}{\pi^2} \left(1 - \frac{V_B}{V_{dd}}\right)$	8.5dB

class B with LC tail filter topology with potential benefits since the active devices can enter the linear region without loading the tank. Even if simulation and theory indeed show a potential transistor noise reduction, the step-up transformer-coupled [38] oscillator suffers from several drawbacks. The quality factor of the secondary is usually less than the primary, which means its noise is no more negligible. Second, the absolute quality factor obtainable is less than the one of a single inductor. Finally, a step-up transformer generally occupies more area than its equivalent inductor. Another key problem is device reliability due to high swing at the gate. A way to mitigate the latter problem is to use p-n topology and/or to reduce the voltage supply. The need of a very low voltage supply, which may help from a reliability point of view, poses a challenge in the design of the voltage regulator, always needed in industrial applications.

2.4 Comparison between topologies

Table 2.1 summarizes the maximum power efficiency and the minimum ENF for the oscillators considered. The most promising topologies are the class-B with tail filter and the class-C. Notice, that further benefits could potentially be achieved using

transformer coupling, but we have not inserted this possibility in the table due to its many practical limitations. Table 2.1 looks only at fundamental noise limits and doesn't reflect other important design considerations and practical aspects, such as tuning range, start-up issues and area occupation. From an industrial point of view class-B with tail filter and class-C are the most feasible structures. Therefore these are the two topologies we have chosen for the prototype circuit implementation. Class-B with tail filter is one of the most interesting architectures thanks its advantages, obtained with a relatively simple design and a small additional area. On the other hand class-C oscillators suffer from a trade-off between oscillation amplitude and start-up conditions that could reduce its advantages with respect to a class-B. To improve efficiency the gate bias voltage should be as low as possible, while meeting the Barkhausen criteria in a reliable way. To overcome this limitation in the last years solutions like dynamic bias [39] and hybrid class C/B [62] were presented. As a consequence we have decided to implement the hybrid class C/B oscillator for its greater robustness even if it has a higher ENF compared with a simple class-C.

2.4.1 A comment on other topologies

In the previous analysis we have considered explicitly only oscillators that don't load the tank. As a consequence topologies like the "clip and restore" [41] as well as class D [42] weren't taken into account. Due to what we simply call loading effect these type of oscillators can not be described directly with (2.9). The scope of this section is to describe their peculiar characteristic trying in any way to compare them with the more classical topologies, and then to use the ENF where possible to compare their performances.

Clip and Restore The clip and restore technique was used to reduce phase noise for base-station applications. This technique implies hard limiting and subsequently restoring the resonating waveform [41]. The key idea is that thanks to hard limiting the transistors drain voltage it is possible to desensitize the oscillation phase to the circuit noise. The oscillator perform the clipping and the restoring process using a step up transformer in the feedback path. This path restores the fundamental frequency component with a sufficient gain to overdrive the transistors forming the oscillator core. Since the theory of Impulse sensitivity function of Hajimiri

and Lee defines the sensitivity of the oscillating waveform to perturbations at different time instances within one cycle, a designer is motivated to consider that waveshape can be used to expand the trade off between phase noise and power consumption as we already discussed in Section 2.2. Of course this observation is the same that motivates the class F oscillator analyzed in Section 2.3.4. In a class F oscillator, however, to not to degrade the phase noise performances, the transistors have to work in saturation region and we have demonstrated that there can be no advantages in the use of such a topology depending on the quality factor of the resonators involved. On the other hand the clip and restore technique deliberately pushes the transistors to work in triode having as a matter of fact a low impedance that load the tank, increasing the noise.

By design the time during which the tank is loaded can be made small and potentially, it should be able to eliminate, if perfect switching is involved, the phase noise contribution of the active device. Intuitively this is of easy understanding. If a good switch is involved it offers when *ON* a short circuit and the noise completely recirculates, during the opposite switching phase it is *OFF* and as a consequence it doesn't contribute to noise. However this simple explanation does not take into account that in fact during this period the tank is loaded by the low impedance offered in series when the transistor is fully *ON*, incrementing de facto the phase noise. The design concept analysis in [41] shows that in any case the noise could be reduced if the times between the two switching phase is made small. However in practice the noise-to-phase conversion of the transistor can't be zero and, at the same time, this means the loading effect begins to be relevant and the advantage is in practice limited.

Let us now comment the efficiency of the oscillator. We have seen that, even if the noise sources that affect the phase noise can't be described the same way as we did for the oscillators that can be analyzed like the Norton equivalent, the other important parameter that has to be maximized in order to get a good ENF is the efficiency. It is interesting to notice that the experienced oscillation amplitude is about $3V_{dd}$. This recall what it is obtained simulating the class B with tail filter. If reasonable good switches are used this translates in a current efficiency that is about 60% (of course considering that it is impossible to reach 100% power efficiency). Slightly lower than a square wave conversion factor, but still close to that value. In fact there's no reason to exclude a square wave like behavior of the transistors current, leading to simple but strong way to analyze an oscillator.

Once again this simply confirms that using good switches yields to a better power efficiency (observation that explained a class F analysis). The problem, as a general rule, might be to obtain such efficiency without paying in higher overall phase noise due to other effects.

Class D Class D oscillator uses the concept of class D power amplifier. First of all the observation is to eliminate the current generator which is a limitation of the maximum oscillation amplitude for example in a classic class B oscillator. This, as well as the research efforts to continuously reducing the supply voltage, well explains the interest of voltage biased oscillator structures. However, eliminating the current biasing yields to a higher sensitivity to supply voltage variations and it makes more difficult to control the oscillator consumption. Class D can be used with very low V_{dd} , actually it is possible to say that it even requires low supply, but the supply pushing is much higher than in either class B or class C VCOs. This poses a challenge in the design of the class D VCO in particular together with the voltage regulator always needed in real life applications.

Let us start considering once again the efficiency and then to report the analysis of this type of oscillator that has some unique characteristics. Class D operation leads to the use of good switches. Again, at least ideally, if a perfect switch is used no power is dissipated on the active devices, resulting in a higher power efficiency and thus a better ENF (FoM). As a direct consequence, if the current efficiency doesn't degrade, the use of good switches maximizes the oscillation amplitude, which in fact also in class D oscillator reaches a peak of approximately $3V_{dd}$. Moreover the power efficiency can be pushed to be 90% because the product of drain voltage and channel current in MOS transistors is close to zero.

A key difference between the class D and other classic topologies is the time variant behavior of the LC tank compared to the time invariant class B, class C and class F LC tank. In the class D the switches short each oscillator output to ground for half of the oscillation period during which the respective inductor and capacitor are decoupled from each other. Due to this time variant nature it exhibits a different oscillation frequency which is also dependent on whether the tank capacitance is floating or single ended. Moreover, it actually prevents the very convenient use of a single parallel tank resistance subsuming all losses in a classic time invariant resonator.

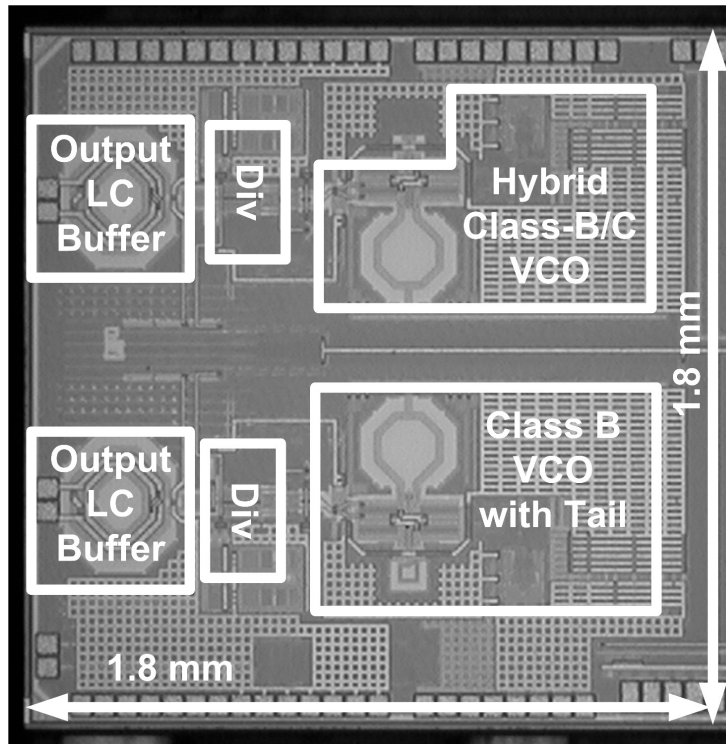


Figure 2.12: Chip photo and block diagram of the prototype.

In practice an equivalent tank quality factor has been derived in [42] and it was used to compare the class D oscillator with other topologies in Fig. 2.2 resulting actually in noisy implementation, but surely capable of good efficiency. This is due to the loading effect and to this time variant nature. As a consequence what is obtained from a efficiency point of view is partially lost in terms of noise having at the end something worse than a class C VCOs referring to ENF. In [42] the increasing of the noise was recognized due to a loading effect and for this reason they added a tail filter at twice the frequency. With this architecture the time variant nature is considered vanished, as a proof it gives back the expected frequency of oscillation (the classic $1/\sqrt{LC}$).

2.5 Experimental verification

A key challenge to compare different oscillators is the strong noise sensitivity to tank Q . It is necessary to know Q with a few percent accuracy to ascertain improvements of the order of 1 dB. This difficulty has resulted in reported numbers inconsistent or even unfeasible. To verify our model a test chip was implemented in TSMC 55nm CMOS (shown in Fig. 2.12) that includes a class-B oscillator with tail filter,

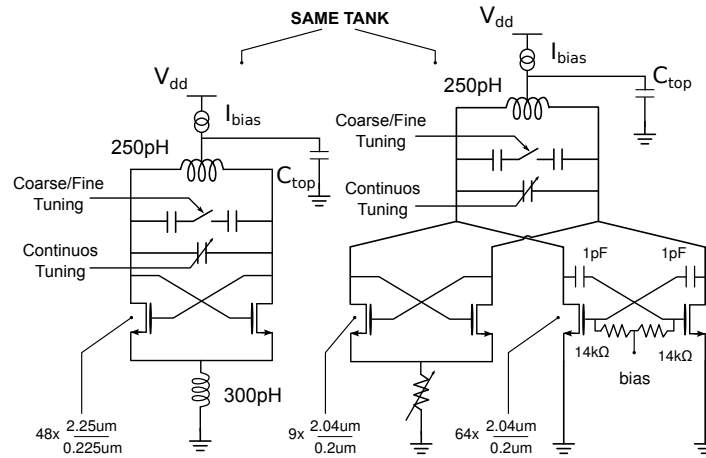


Figure 2.13: Schematic of the prototype.

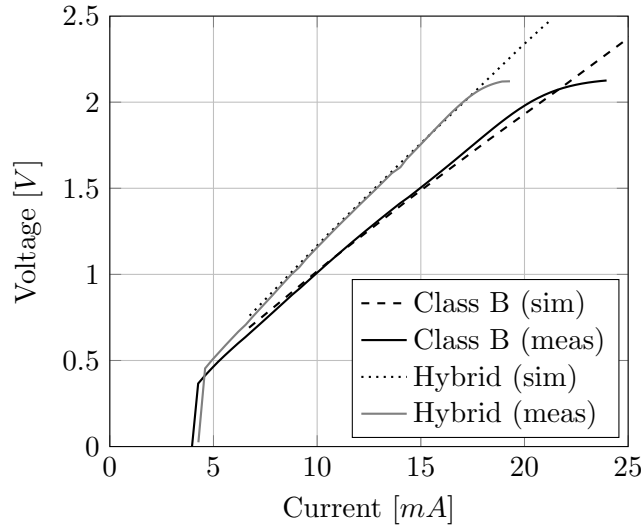


Figure 2.14: Oscillation amplitude vs bias current: measurements and simulations

and an hybrid class-C/class-B oscillator (shown in Fig. 2.13) oscillating around $7.5GHz$ two dividers by 2 and two peak detectors to sense the oscillation amplitude. In both cases n-type transistors implement the negative resistance and a p-type transistor provides the bias current. The gate voltage bias for the core transistors in the hybrid oscillator is provided by an external voltage generator through a passive on-board low-pass RC filter with very low cut-off frequency. Great care was taken to eliminate spurious effects. First of all the same tank (including tuning) was used for both topologies. To see the effect of the divider the class-B oscillator was stepped twice followed by two different dividers. Almost identical phase noise is obtained after division up to about $20MHz$ offset demonstrating that the phase

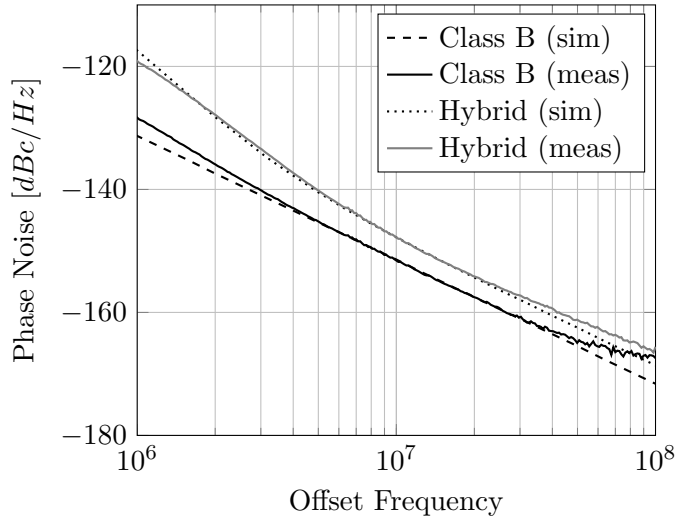


Figure 2.15: Measured phase noise after frequency division by 2 of class-C and class-B oscillators at their respective maximum FoM bias point (12.5mA for Hybrid class-C/B and 21.6mA for class-B) when tuned at 7.6GHz. For comparison the simulated phase noise is also reported.

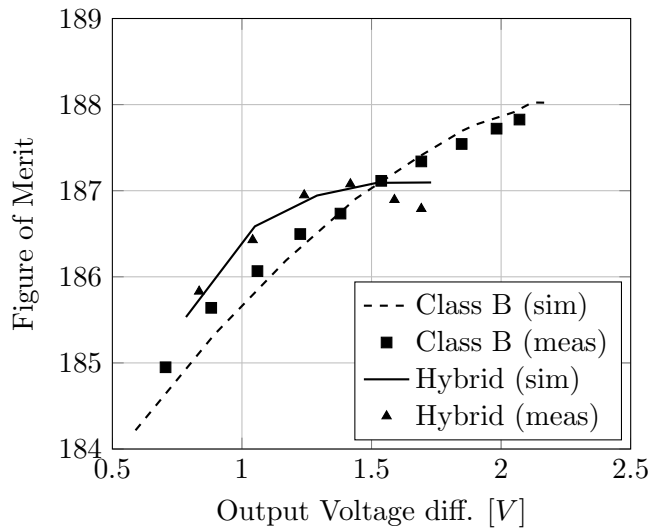


Figure 2.16: FoM vs output voltage for the class-B and Hybrid class-C/B oscillators: measurements and simulations.

noise of the dividers is negligible in the frequency of interest. Both VCOs are tunable from about 6.1GHz to 8.7GHz through two MOM capacitor bank (a 7 bit coarse and a 4 bits fine) and a continuous tuning varactor. For the class B oscillator a small tail inductor resonates the tail capacitance at $2\omega_0$. Due to its low Q (about 3) is not tuned as ω_0 varies. Figure 2.15 shows the simulated and measured phase noise for both oscillators with a 1.5V supply. The bias currents at maximum FoM are 12.5mA for the hybrid and 21.6mA for class-B.

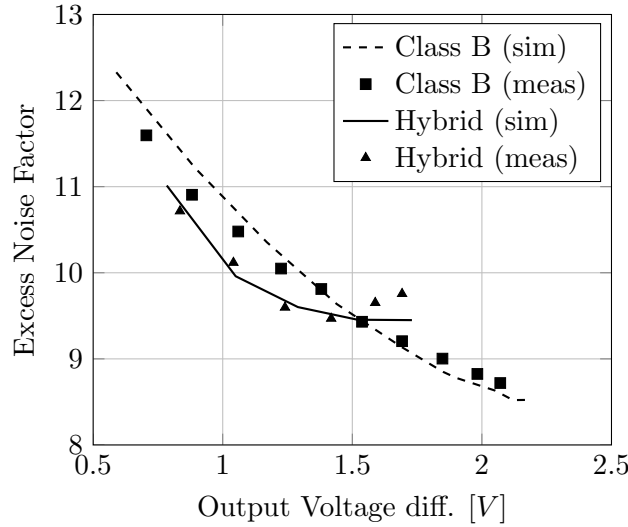


Figure 2.17: ENF vs output voltage for the class-B and Hybrid class-C/B oscillators: measurements and simulations.

Both oscillators exceed the GSM requirement [1, 55] of $-150\text{dBc}/\text{Hz}$ at 20MHz offset with 3.6GHz carrier over the entire tuning range. The hybrid oscillator shows an extra noise term below 10MHz offset associated with the resistors at the gate of the switching transistors in the class-C portion which are relatively small. They should be of higher value to push their noise contribution to lower frequency and being able to filter it out with the PLL in which the oscillator will be naturally inserted. Figure 2.14 shows oscillation amplitude vs. bias current for the two cases, the two different slopes show an η_I about 25% better for the hybrid. This is significantly less than what is expected for ideal class-B vs class-C. Simulations partially explain the lower efficiency of the hybrid class-C/class-B structure [62]. The peak detector maximum voltage range limits the validity of the data at high swing. From the measured oscillation amplitude vs. bias current and simulated η_I a tank Q about 9.7 at 7.6 GHz is obtained. This relatively low value is due to the large tuning range and very low target phase noise that increases sensitivity to non idealities [57]. Peak FoM is 187.1 and 187.9dB with an η_P of 36% and 42% for the hybrid and class-B respectively (Fig. 2.16). These results agree well with simulations and are consistent with the model prediction that at the peak FoM should depend only on efficiency. Measured and simulated FoM and ENF versus output voltage for both topologies are plotted in Fig. 2.16 and Fig. 2.17 respectively. At low bias, the superior η_I of the hybrid gives (see Fig. 2.16) better η_P , leading to a better FoM. For the hybrid, however, as the amplitude increases and the transistors enter triode region, ISF increases and the FoM reaches

a peak around $1.4V$ p-t-p swing. On the other hand, for the class-B the tail filter avoids loading the tank even if the transistors enter the triode region. As a result transistor ISF change only slightly up to $2.1V$ p-t-p giving a higher peak FoM. Notice that the class-B oscillator could achieve an even higher FoM if pushed to higher oscillation amplitudes (ideally $4.7V$ p-t-p gives 100% η_P). The oscillation amplitude was limited to $2.1V$ p-t-p for reliability reasons.

Chapter 3

Impulse Sensitivity Function based Phase Noise Analysis

3.1 Phase noise evaluation using Impulse Sensitivity Function

The theoretical study of phase noise in electrical oscillator is a more difficult task compared to traditional analysis mainly due to two reasons. First, the conversion of the noise into phase noise is not constant across the oscillation period [6]. Second, any real oscillator generates large signals, which means that a small-signal circuit that has linearized components values around the constant bias point is no longer able to describe the nature of the oscillator and of the active noise sources. The large signal analysis may yield to unexpected results, compared to the small signal one. In fact, notable result in the works [32, 38] is that the phase noise caused by the MOS switches is independent of the switch transconductance, which appears to be separate with the familiar notion that transistors noise is a linear function of the transistor transconductance (at least ideally). As a direct consequence, for example, doubling the bias current does not change the noise generated by the oscillator core (if the switches are still working in the same operating region).

The nontrivial noise-to-phase-noise conversion has been explicitly recognized by Hajimiri and Lee [6], whose Impulse Sensitivity Function theory is based to the fact that noise-to-phase-noise conversion is a linear, time-variant (LTV) process. According to the Linear Time Variant theory of Hajimiri and Lee [6], the conversion

of noise into phase noise is described by a dimensionless, frequency and amplitude independent periodic function which describes how much phase shift results from applying a unit charge impulse at a certain time. The Impulse Sensitivity Function (ISF, with the symbol Γ) defines the effect of noise on the oscillation phase and is a function of the phase of the tank voltage. The general expression for the phase noise using ISFs is given in (3.1).

$$L(\Delta\omega) = 10 \log \left[\frac{4k_B T}{P_{RF}} (\Gamma_T^2 + \Gamma_M^2 \alpha) \left(\frac{\omega_0}{2Q\Delta\omega} \right)^2 \right] \quad (3.1)$$

Where $P_{RF} = A_1^2/2R_T$ is the power dissipated in the tank, α is the noise factor that includes, in general, γ_{MOS} and attenuation between tank and MOS gates, Γ_T^2 and Γ_M^2 are the rms ISF for the tank and the MOS transistors and no other noise source is considered, k_B is the Boltzmann's constant and T the absolute temperature. The problem to evaluate the noise conversion into phase noise is related to the evaluation of the ISFs for the different noise sources. The evaluation starts considering the state vector \vec{X} of the system, then the deviation $\Delta\vec{X}$ to the steady state trajectory will be computed. In general it is obtained when a charge pulse Δq is applied across one of the capacitors and a steady state phase error is produced in the oscillator. The phase error is a function of the time instant (within the oscillation period) when the charge pulse is injected, according to the ISF theory. In particular, the phase error $\Delta\phi_i$ produced is proportional to the Impulse Sensitivity Function by (3.2).

$$\Delta\phi_i = \frac{\Gamma(\omega_0 t)}{q_{max}} \Delta q \quad (3.2)$$

The ISF in terms of state-space vectors is given in (3.3) [6, 30]. It is worth mentioning [30] that the particular form of $\Delta\phi_i$ only played a minor role in Hajimiri's theory. In that work, in fact, the phase error was primarily determined by applying a series of time shifted transient simulations. This type of evaluation is numerical by its nature and lacks of the universality possessed by a symbolic closed-form expression.

$$\Gamma_i = \omega_0 \frac{q_{max}}{\Delta q} \frac{\Delta\vec{X}_i \cdot \dot{\vec{X}}}{|\dot{\vec{X}}|^2} \quad (3.3)$$

In (3.2) and (3.3) q_{max} is just a normalizing factor, being the maximum charge across the capacitor placed between the nodes of interest. For this reason in the following q_{max} will not be evaluated and in particular when the ISF will be plotted

over the oscillation period, for simplicity, it will be denoted as its scaled replica (3.4).

$$h(\omega_0 t) = \frac{\Gamma(\omega_0 t)}{q_{max}} \quad (3.4)$$

This permits, in fact, to not determine the value of q_{max} and to directly compare the phase responses associated to current sources located in different points of the circuit.

Once the ISF has been evaluated and thus the phase responses of the noise sources have been investigated, the phase noise $L(\Delta\omega)$ caused by a white current noise source $\overline{i_{n,i}^2}$ in an LC-tank oscillator can be obtained using (3.5).

$$L(\Delta\omega) = 10 \log \left[\frac{\Gamma_{i_{n,rms}}^2 \overline{i_{n,i}^2} / \Delta f}{2q_{max}^2 \Delta\omega^2} \right] \quad (3.5)$$

The phase noise expression (3.5) based on Γ_i reported in (3.3) is, however, not correct in general. This assumes that the noise perpendicular to the steady state-space trajectory of the oscillation does not generate any contribution to phase noise. For this reason (3.3) can be considered if the orthogonal components to the trajectory has been neglected [30]. Andreani and Wang [30], based on the more accurate phase noise evaluation proposed by Demir *et al.* [27] and Kaertner [29], have demonstrated that the error made without considering this component, using appropriate normalization factor of the state variables, is in fact negligible. Their considerations, that were made referring to a simple LC tank with losses, can be actually extended to the more general case of having more tanks.

3.2 Class B with tail filter phase noise analysis

The Class B with tail filter has demonstrated to be one of the most promising architectures in terms of Excess Noise Factor (or equivalently Figure of Merit) thanks to the possibility to obtain very good efficiencies without increasing the noise. This architecture was presented as a solution to reduce the noise contribution of the current generator [14], but a more accurate analysis can demonstrate the intuitive view regarding the fact that the tail filter helps in avoiding loading effects and thus permits to push the oscillator towards a high efficiency operation without being limited by phase noise degradation. In fact, adding a second harmonic resonator, three advantages are actually obtained. First, as said, the common source node

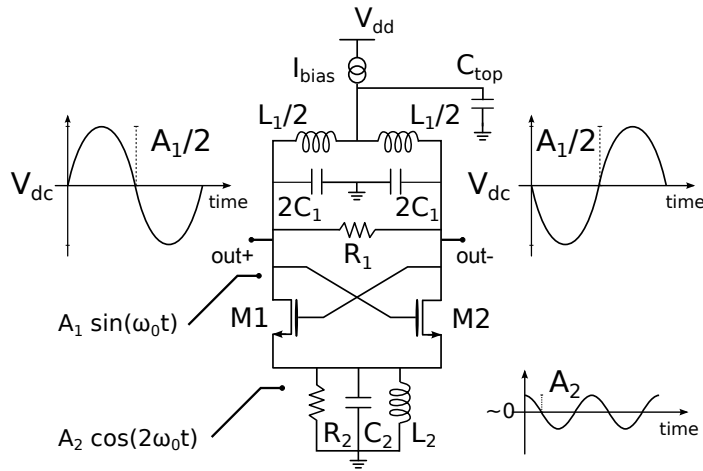


Figure 3.1: Class-B oscillators with $2\omega_0$ LC tail filter: N-only

can swing below ground, increasing the maximum voltage efficiency. Second, the switching transistors can enter the triode region without loading the tank since intuitively it sees a high impedance in series. Third, the noise of the current source around $2\omega_0$ can be filtered with a large capacitance. In the following analysis the scope is to demonstrate the intuitiveness behind the loading effects (somehow associated to the pipe effect [67], but extended to LTV oscillating systems), and to give, according with simulations, some insights to the design of this type of oscillators obtaining a closed form expression even in the case of transistor working in triode. At first the N-only topology will be studied and then the analysis will be extended to the p-n topology.

3.2.1 Class B with tail filter N-only

The analysis will refer to the oscillator in Fig. 3.1 in which a general Class B with tail filter N only is reported. The main tank is represented considering, more generally, the capacitors to ground because, when the tuning capabilities are added, this is the actual situation and for this reason it gives a more complete analysis. Moreover, without loss of generality, a top biased topology is here considered, but the same considerations can be done for a bottom biased architecture. It is characterized by a LC tank that resonates at the fundamental frequency (ω_0) and by a second one which resonates at twice the frequency. The peculiar characteristic of this type of oscillator is, indeed, the second harmonic LC tank at the bottom of

the active devices (in Fig. 3.1 the MOSFETs M_1 and M_2), which allows the source to swing below ground and it offers a high impedance to the main tank during MOSFETs switching. The ISF for each noise source is calculated starting from the state vector \vec{X} defined in (3.6) [6, 29, 30].

$$\vec{X} = [V_{C_1} \quad \sqrt{\frac{L_1}{C_1}} I_{L_1} \quad \sqrt{\frac{C_2}{C_1}} V_{C_2} \quad \sqrt{\frac{L_2}{C_1}} I_{L_2}] \quad (3.6)$$

The four state variables are the voltages on the capacitors and the currents flowing through inductors. Each state variable is scaled in such a way that the squared sum of the state variables is proportional to the stored energy. This kind of normalization is the one we've used in [7]. The steady state oscillation is approximated by a sinusoid at ω_0 across the main tank, whose amplitude is here indicated as A_1 and a cosinusoid at $2\omega_0$ across the second tank at the sources of the transistors with amplitude A_2 . The reason of their $\pi/4$ phase difference can be understood thanks to Fig. 3.2, in which an example of the wave-forms at the drains (and/or gates) of the active devices as well as the voltage waveform at their source are reported as a function of the oscillation phase. The simulation is made pushing the transistors to work almost like good switches (the W/L ratio could be even further increased and so reducing V_{ds} , at the cost of more parasitic). It is worth noticing that in general the voltage at the transistors source is not only composed by the second harmonic component, and that it is a function of MOS sizing. Regarding the main tank $Q_1 = 20$ with an inductance $L_1 = 600pH$ and, on the other hand, for the second harmonic tank $Q_2 = 20$ and $L_2 = 400pH$. The losses of the main tank as well as the one of the tail LC resonator were represented for simplicity by a parallel resistance.

The system can be represented as the steady-state vector \vec{X}_0 in (3.7) to which a random perturbation vector ΔX will be added.

$$\vec{X}_0 = [A_1 \sin(\omega_0 t) \quad A_1 \cos(\omega_0 t) \quad A_2 \sqrt{\frac{C_2}{C_1}} \cos(2\omega_0 t) \quad A_2 \sqrt{\frac{C_2}{C_1}} \sin(2\omega_0 t)] \quad (3.7)$$

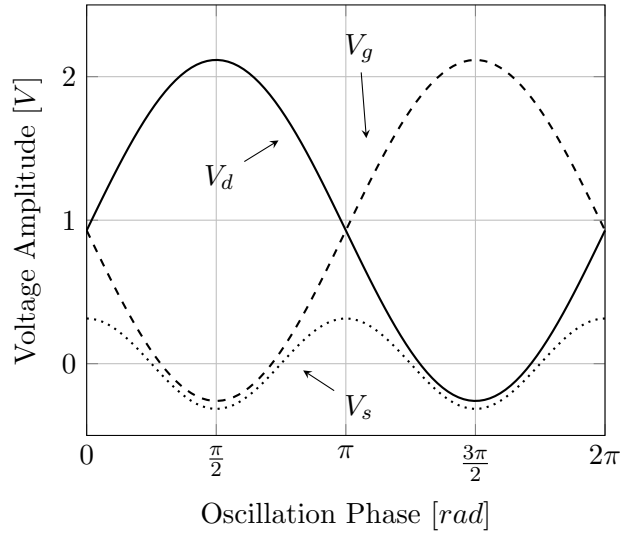


Figure 3.2: Voltages waveforms of the approximated steady state oscillation

Eventually, neglecting the component of ΔX orthogonal to the trajectory, the phase perturbation $\Delta\phi$ can be derived from the state variables derivatives $\dot{\vec{X}}$ [6, 30].

$$\begin{aligned} \dot{\vec{X}}^t = & [\omega_0 A_1 \cos(\omega_0 t) \quad -\omega_0 A_1 \sin(\omega_0 t) \\ & -2\omega_0 A_2 \sqrt{\frac{C_2}{C_1}} \sin(2\omega_0 t) \quad 2\omega_0 A_2 \sqrt{\frac{C_2}{C_1}} \cos(2\omega_0 t)] \end{aligned} \quad (3.8)$$

To evaluate the perturbation ΔX a noise charge for each noise source is injected at the node of interest and the effect of the noise charge on other nodes is computed. To compute the Impulse Sensitivity Function, at last, from (3.8) we can write $|\dot{\vec{X}}|^2$ reported in (3.9).

$$|\dot{\vec{X}}|^2 = A_1^2 \omega_0^2 \left(1 + 4 \frac{C_2}{C_1} \frac{A_2^2}{A_1^2} \right) \quad (3.9)$$

This normalization factor depends on the choice made to represent the state vector variables and it is, in fact, proportional to the stored energy.

The main noise sources are the resonators losses and the transistors noise, neglecting the noise due to the current source. Indeed, the noise due to the current source is negligible thanks the large capacitor C_{top} that has the purpose to filter its noise.

Since a more rigorous analysis of this type of oscillator has been never made, to give a more insight view of consequences of adding a second harmonic tank at the source at first an idealized case will be considered and then a more practical situation will be targeted.

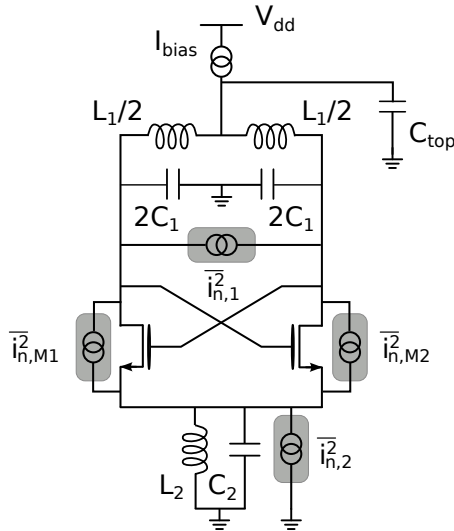


Figure 3.3: Noise sources of a class-B oscillator with $2\omega_0$ LC tail filter

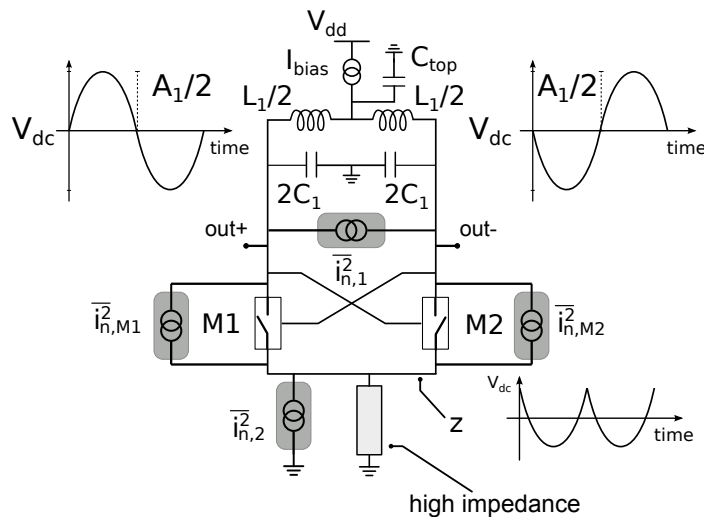


Figure 3.4: Idealized Class B with tail filter oscillator and its noise sources

Idealized Intuitive analysis

Since the Class B with tail filter has demonstrated to be able to reach very good efficiencies its idealized condition considers to have perfect switches and thus no power losses on the active devices. Moreover, we do not consider to have strictly a second harmonic LC tank at the source, but to have a generic network able to give a high impedance when needed and thus that permits the source to swing following perfectly the output voltage. Of course no other assumptions on the noise sources will be made, and for this reason every possible noise source (active devices as well as the main tank noise and the potential general network noise)

will be discussed. In such a situation, to consider perfect switches means that the shape of voltage at z is a negative rectified sine (Fig. 3.4). In this situation in fact the node z is able to follow exactly and instantaneously the nodes *out+* and *out-* when the corresponding switch is closed. In the following paragraphs no rigorous mathematical derivation will be made since this situation is unpractical, but only a qualitative and intuitive understanding of the ISFs in this idealized scenario. In the oscillator of Fig. 3.4 the noise sources are the tanks losses and the active device and to evaluate the effect of these on the phase noise it is possible to determine their Impulse Sensitivity Function.

Main tank The noise of the main tank is due to the unavoidable losses of the LC tank. These losses can be represented with good approximation with an equivalent parallel resistance, whose value depends on the the values of either L or C and the quality factor ($R = Q/\omega_0 C$, for a tank oscillating at ω_0). In this way the noise is injected differentially and we might consider that there are no effects due to the presence of the additional tank at the bottom. Thus the ISF of the main tank is in quadrature with the sinusoidal signal across the tank according with the Hajimiri's ISF theory (3.10).

$$\Gamma_1 \approx \frac{\cos(\omega_0 t)}{C_1} \quad (3.10)$$

High impedance network The noise of the here called *high impedance network* can be modeled the same as it has been done with the main tank, considering an equivalent noisy parallel resistance. The impulse noise charge is injected at node z and because of the switching behavior it is injected into the parallel of $2C_1$ and C_2 alternatively referred to *out+* and *out-*. Since any noise charge injected into the main tank translates to phase noise by a cosine, the result is a cosine multiplied by a square wave, obtaining a resulting waveform reported in Fig. 3.5. The ISF has a strong component at the second harmonic as expected. The absolute value is not here strictly important, but it depends on the voltage amplitudes and capacitance considered. It is worth to notice that the ISF recalls the one that can be evaluated for the current generator in a classic LC tank CMOS oscillator [32].

Active Devices For what concerns the active devices it is possible to determine qualitatively the ISF of a noise charge injected in parallel to the switch, for example M_1 (Fig. 3.4). Under ideal switching operation when the switch is *ON*, because

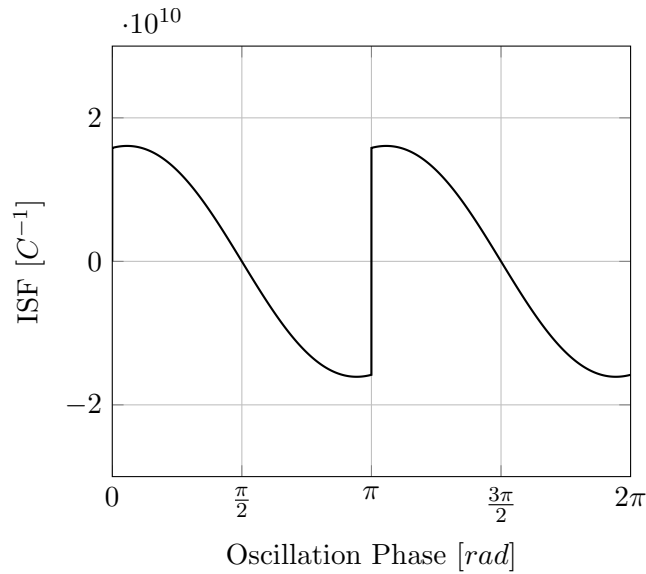


Figure 3.5: Numerical example of the ISF of a noise charge injected at z

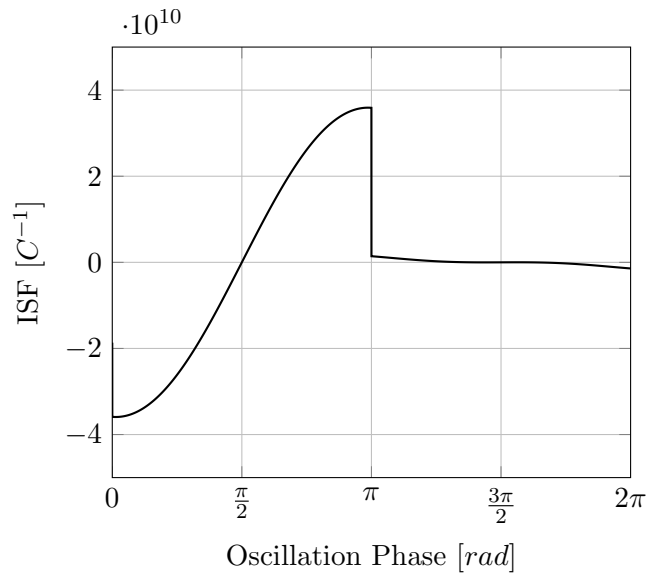


Figure 3.6: Numerical example of the ISF of a noise charge injected across the switches

the noise generator sees a short circuit and high impedance on the other sides, its effect is null. When the switch is *OFF* however there is an equivalent noise generator across the main tank and as a consequence the ISF during this phase is a cosinusoide. Eventually it gives the ISF reported in Fig. 3.6. What it's interesting of this very simple analysis is that in a perfect switching scenario, no power is dissipated and no phase noise is added by the active devices. This gives an easy rule of thumb in the design of this type of oscillators. Because is desirable to have good switches, the designer should increase the W/L of the MOS transistors at

the limit it affects too much the tuning range. It permits to increase the efficiency of the oscillator itself, and thus to work at its minimum ENF.

Another very important observation subsequent to this simple analysis is the importance of a good assumptions when referred to transistors switching. If an hard switching hypothesis is made the error in phase noise evaluation is very high since it will lead, as seen, in zero phase perturbation caused by the active devices.

3.2.1.1 Main Tank

We want to estimate the phase noise of the oscillator starting with the main tank noise. If a charge is injected differentially at the resonator, it is across the capacitor C_1 (Fig. 3.7). The perturbation occurs only at the nodes across the main resonator and in particular $\Delta X_1 = \Delta q/C_1$. The perturbation vector in (3.11) represents the perturbation on the nodes across the main tank.

$$\Delta \vec{X} = \begin{bmatrix} \frac{\Delta q}{C_1} & 0 & 0 & 0 \end{bmatrix} \quad (3.11)$$

The corresponding phase error is obtained multiplying for the first element of the derivative of the steady state vector normalized by its module squared (3.12).

$$\Delta \phi_1 = \omega_0 \frac{\Delta q}{C_1} \frac{\dot{X}_1}{|\dot{X}|^2} \quad (3.12)$$

Using (3.8), (3.9) and (3.11) in (3.3) the ISF of the main tank can be computed. The main tank ISF is reported in (3.13).

$$\Gamma_1 = \frac{q_{max}}{A_1 C_1} \frac{\cos(\omega_0 t)}{\left(1 + 4 \frac{C_2}{C_1} \frac{A_2^2}{A_1^2}\right)} \quad (3.13)$$

Considering the noise spectral density of the main tank, which is $\overline{i_{n,1}^2}/\Delta f = 4k_B T \omega_0 C_1 / Q_1$, together with (3.13), we can rewrite (3.5) in (3.15) to obtain its contribution to phase noise. Where $\Gamma_{1,rms}^2$ is given in (3.14).

$$\Gamma_{1,rms}^2 = \frac{1}{2} \frac{q_{max}^2}{A_1^2 C_1^2 \left(1 + 4 \frac{C_2}{C_1} \frac{A_2^2}{A_1^2}\right)^2} \quad (3.14)$$

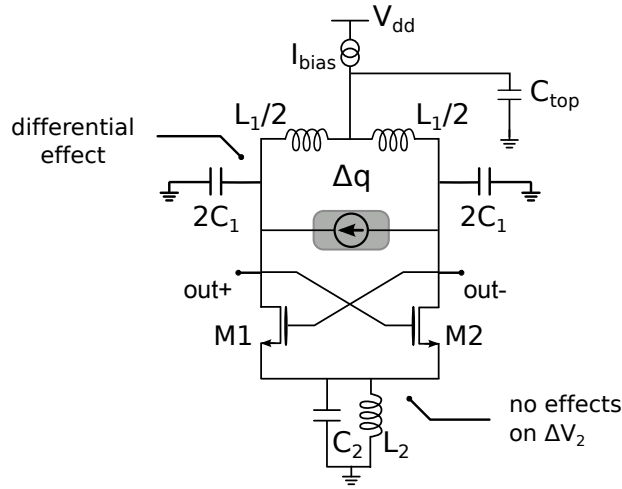


Figure 3.7: Main tank noise generator

$$L_{T_1}(\Delta\omega) = 10 \log \left(\frac{4k_B T \omega_0 C_1}{2\Delta\omega^2 Q_1} \frac{1/2}{A_1^2 C_1^2 \left(1 + 4\frac{C_2}{C_1} \frac{A_2^2}{A_1^2}\right)^2} \right) \quad (3.15)$$

Considering $P_{sig} = A_1^2 \omega_0 C_1 / 2Q_1$ (3.15) becomes (3.16).

$$L_{T_1}(\Delta\omega) = 10 \log \left(\frac{k_B T}{2P_{sig}} \left(\frac{\omega_0}{\Delta\omega Q_1} \right)^2 \frac{1}{\left(1 + 4\frac{C_2}{C_1} \frac{A_2^2}{A_1^2}\right)^2} \right) \quad (3.16)$$

The phase noise contribution of the main tank differs to a classic oscillator with only one LC resonator for the normalization factor which in classical case is equal to 1. This may suggest the designer to maximize the ratio A_2/A_1 and the ratio C_2/C_1 . However it must be taken into account that A_2 is inversely proportional to C_2 because it determines the impedance at $2\omega_0$. for this reason the only way to obtain an advantage in increasing the capacitance C_2 is to increase also the quality factor in order to maintained at the first order (at least ideally) the same A_2 . The possible advantage suggested by (3.16) is however in practice very limited, having eventually a normalization factor very close to 1.

3.2.1.2 Switching transitions

One of the major problems of oscillators and thus of the phase noise analysis is related to the oscillators large signal behaving. Any usual small signal approximation, may yield in general to a misleading result. For example, the contribution of the

thermal noise of the core transistors to phase noise in a generic harmonic oscillator does not, to the first order, depend on the transconductance of the core transistor [38]. Result that is opposite to the classical small signal analysis. In literature, to analyze noise to phase noise conversion, more then often the transistors square law is used to determine the conduction angle under particular conditions like fixing the current flowing in the transistor [32, 58–60] and using verilogA models for simulations. Even if these approximations permit to well describe the conversion noise to phase noise often they miss in the possibility to be actually used for future analysis on different topologies. On the other hand, some other analysis use a simulated ISF and then, to describe the oscillator behavior, a fitting ISF is found to determine the noise conversion into phase noise. This method leads to a good estimation of the conversion principle and it can be used for different topologies, but this result has a strong numerical nature and it may lack therefore the kind of generality that characterized a symbolic closed form expression of the ISF. Here we suppose only to know the oscillator's steady state, which usually is well predictable taking into account the current efficiency conversion, and we want to use only the steady state to determine the working regions of the active devices. The point is to find a way to describe the switching behavior and, if possible, a way to determine if the transistors are actually working as good switches. For this reason we rely on the MOSFETs V_{ds} . In particular the difference between the active devices' V_{ds} normalized by their sum. This gives $f(\varphi)$ (3.17), where $\varphi = \omega_0 t$ which is, in fact, based on the steady state oscillation.

$$f(\varphi) = \frac{A_1 \sin(\varphi)}{2(A_2 \cos(2\varphi) - V_{dc})} \quad (3.17)$$

Where V_{dc} is the DC voltage at transistors gate/drain. $f(\varphi)$ is reported as an example in Fig. 3.8a. In Fig. 3.8a $f(\varphi)$ doesn't reach 1 (or -1) because it is obtained using the waveforms previously reported in Fig. 3.2 in which a small V_{ds} drop when the transistor is *ON* can be noted. For simplicity to determine the time during which the active devices are *ON* we rely to the absolute value of $f(\varphi)$ denoted as $g(\varphi)$ (shown in Fig. 3.8b).

3.2.1.3 Second Harmonic Tank

The noise referred to the second harmonic tank can be identified with an equivalent parallel noisy resistance. Its noise spectral density is $\overline{i_{n,2}^2}/\Delta f = 8k_B T \omega_0 C_2/Q_2$ and

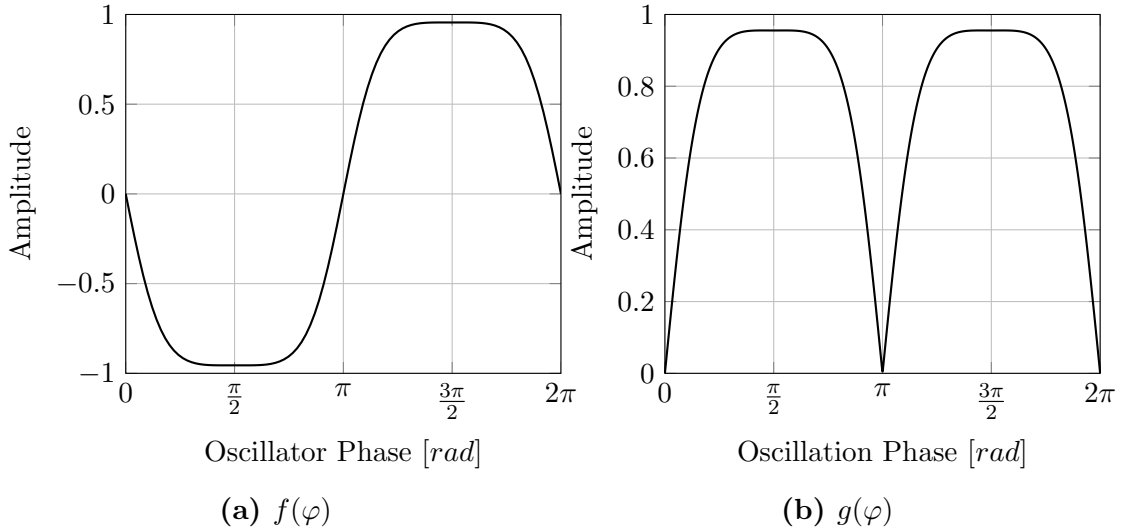


Figure 3.8: Active devices working conditions

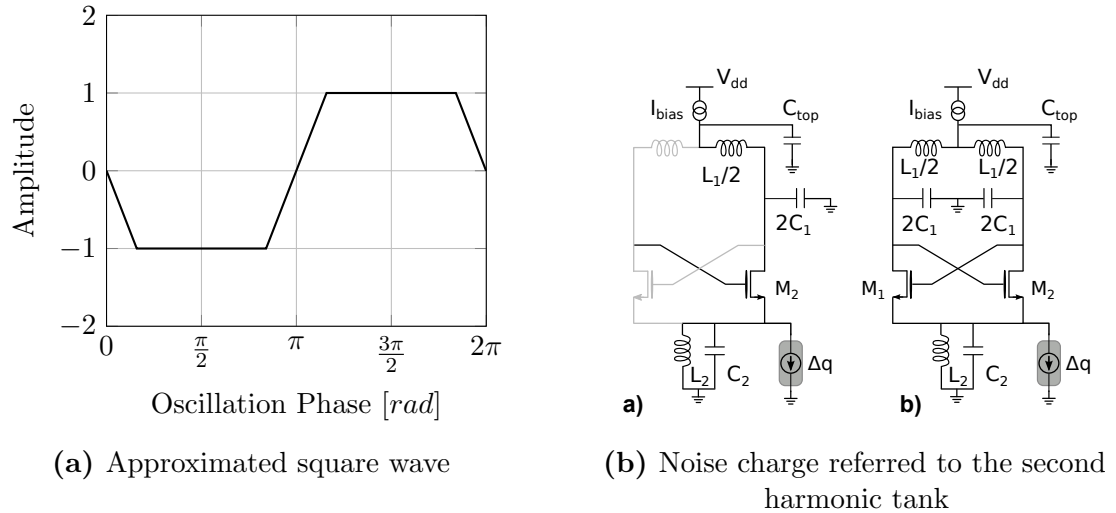


Figure 3.9: Working operation of switching transistors and the effect on the evaluation of the second harmonic tank noise

to compute the ISF the related charge is injected at the source as shown in Fig. 3.9b. The effects on different nodes of the oscillator due to the charge injection will be affected by the transistors switching. During the oscillation it is possible to distinguish two cases. First, when one transistor is *ON* and the other one is *OFF*. Second, during transitions, when both transistors are *ON*. This ends up having a "square wave like" behavior (e.g. Fig. 3.9a, the sign depends only if it's intended either M_1 or M_2 to be *ON*) which actually represents the operating condition of the oscillator. In the following to take into account the effects of the interaction between the two tanks, when the MOS transistor is completely *ON* it will be considered as an ideal switch and so with zero impedance. This assumption

leads to the natural consequence of being more accurate at higher amplitudes of operation, which actually represents the optimum operation of the oscillator. As a consequence, when one transistor in *ON* the charge injected at the source will be instantaneously divided between both capacitors C_1 and C_2 , of course regardless of which MOSFETs is *ON*. In particular the noise charge will be seen at the output (ΔV_1) multiplied by a square-wave. Then, because the charge is injected at the source, there is an effect on V_2 as well. When one transistor is *ON* and the other is *OFF* the charge is always redistributed between C_1 and C_2 and in particular ΔV_2 and ΔV_1 are equal in module, but during transitions the capacitance seen at V_2 is only C_2 and there is no effect on ΔV_1 . Using $f(\varphi)$ we can automatically define the time during which the transistor is either *ON* or *OFF* as well as the transition time as reported in Fig. 3.8b using its absolute value. These functions are here used to determine when the charge is injected in either the sum of $2C_1$ and C_2 or only C_2 .

With these considerations and using $f(\varphi)$ and $g(\varphi)$ we can write ΔV_1 and ΔV_2 (3.18).

$$\Delta V_1 = -\frac{f(\varphi)\Delta q}{2C_1 + C_2} \quad \Delta V_2 = -\frac{g(\varphi)\Delta q}{2C_1 + C_2} - \frac{1}{C_2}(1 - g(\varphi)) \quad (3.18)$$

From (3.18) we can write the perturbation vector related to the second harmonic tank noise source reported in (3.19).

$$\Delta \vec{X} = \left[-\frac{f(\varphi)\Delta q}{2C_1 + C_2} \quad 0 \quad -\sqrt{\frac{C_2}{C_1}} \left(\frac{g(\varphi)\Delta q}{2C_1 + C_2} + \frac{1}{C_2}(1 - g(\varphi)) \right) \quad 0 \right] \quad (3.19)$$

In Fig. 3.10 are reported the contributors of ΔV_1 and ΔV_2 and so the effects of the injected charge at the output and at the source. It is possible to recognize that during a complete switching ΔV_1 and ΔV_2 are almost equal in module, while during the commutations ΔV_2 increases in module because the generator sees only C_2 and ΔV_1 crosses zero because there's no effect on it. The plot of second harmonic ISF is shown in Fig. 3.11 which has, as expected, a strong component at twice of the oscillation frequency. $\Gamma_{2,rms}$ of this more complete analysis will be, however, computed numerically. Unfortunately this does not give a simple design insight of the conversion of the noise into phase noise. For this reason to have a more intuitive view and thus, to obtain a closed expression, it's possible to consider an approximation which considers only the second harmonic component for $\Gamma_{2,simple}$ (3.20). This approximation does not work in general, but it's enough accurate

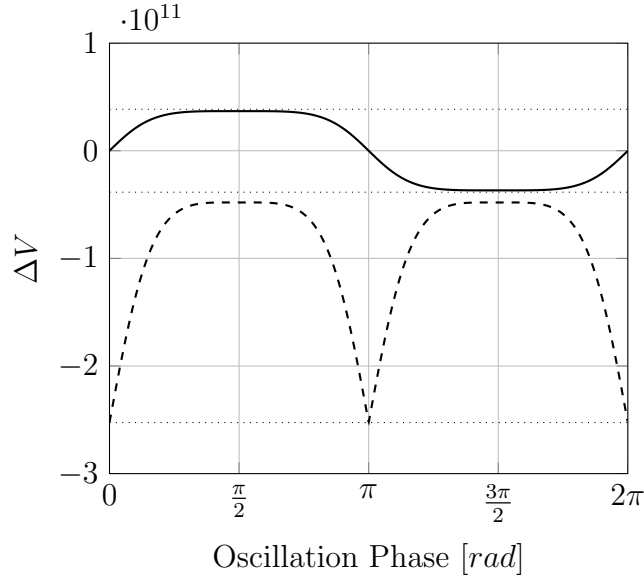


Figure 3.10: Numeric example of the evaluated perturbation over period on ΔV_1 (continuous line) and ΔV_2 (dashed line)

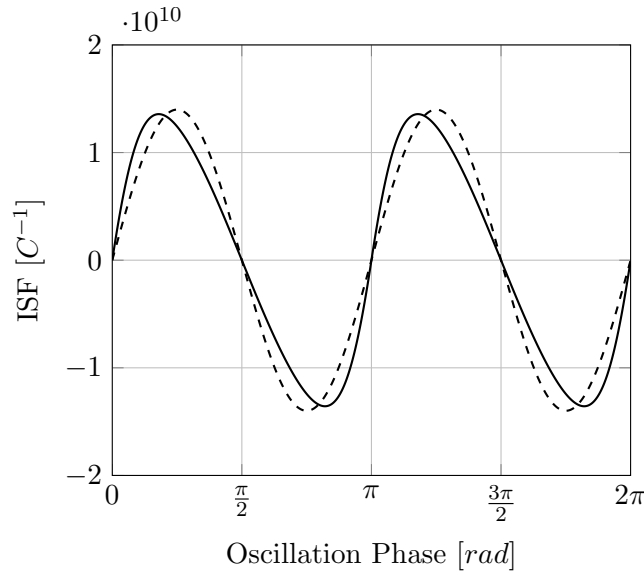


Figure 3.11: Impulse Sensitivity Function of the second harmonic tank: considering the more complete analysis (continued) and approximated with just second harmonic (dashed)

under the assumptions considered of good switches with low V_{ds} .

$$\Gamma_{2, \text{simple}} = \frac{q_{max}}{C_1 A_1 \left(1 + 4 \frac{C_2 A_2^2}{C_1 A_1^2}\right)} \left(2\sqrt{2} \frac{A_2}{A_1} \sin(2\varphi)\right) \quad (3.20)$$

In Fig. 3.11 the result of this simple approximation analysis is reported compared to a more accurate analysis.

In general with good designs the noise contribution of the second harmonic tank is about 5% of the total, leading to a negligible error in phase noise calculation.

3.2.1.4 Active devices

Now we want to evaluate the noise of the active devices. Class B with tail filter topology attracts for the possibility to push the transistors in triode region without occurring in loading the tank and thereby increasing the phase noise.

$$\overline{i_{nMOS}^2} = 4k_B T \gamma g_0(\omega_0 t) = 4k_B T \gamma \frac{\partial I_{out}(\omega_0 t)}{\partial V_{in}(\omega_0 t)} \quad (3.21)$$

We consider the oscillation across the tanks defined in (3.22), and we represent the current by its Fourier expansion (3.22).

$$\begin{aligned} V_{tank} &= A_1 \sin(\omega_0 t) \\ V_{tank2} &= A_2 \cos(2\omega_0 t) \\ I_{out}(\omega_0 t) &= \sum_{k=0}^{\infty} I_{k,out} \sin(k\omega_0 t + \phi_k) \end{aligned} \quad (3.22)$$

Now substituting (3.21) in (3.22) we can write (3.23).

$$\begin{aligned} g_{ds}(\omega_0 t) &= \frac{\partial I_{out}(\omega_0 t)}{\partial V_{in}(\omega_0 t)} \\ &= \frac{\partial I_{out}(\omega_0 t)/\partial t}{\partial V_{in}(\omega_0 t)/\partial t} \\ &= \frac{\sum_{k=0}^{\infty} k I_{k,out} \cos(k\omega_0 t + \phi_k)}{\frac{A_1}{2} \cos(\omega_0 t) + 2A_2 \sin(2\omega_0 t)} \end{aligned} \quad (3.23)$$

In which the voltages of the MOS that is taken into account are used.

It's necessary now to determine the effects of an injected noise charge impulse across the capacitors. Referring to Fig. 3.12b we can divide the noise charge equivalent generator between a charge injected at the source of the MOSFET and one injected at the main tank. Furthermore the noise generator at the main tank can be divided in a differential component and in a common mode component both with half the value (Fig. 3.13). We can recognize that the differential part is easily manageable since it produces a $\Delta V_1 = -\Delta q/2C_1$ and $\Delta V_2 = 0$. Its analysis is in

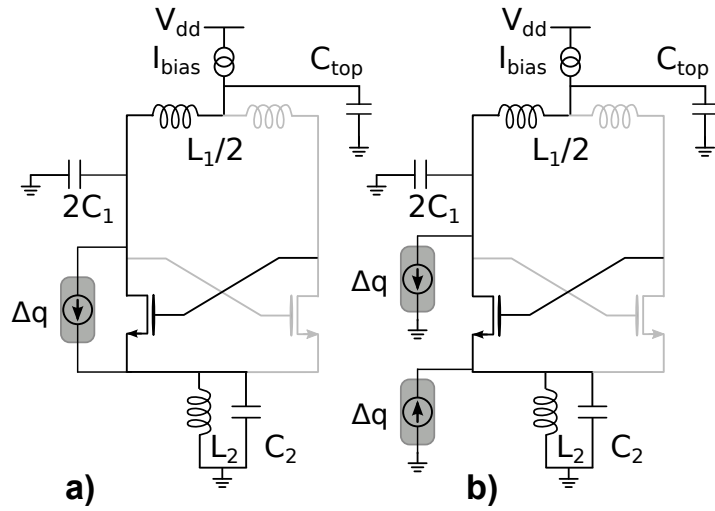


Figure 3.12: Noise charge referred to MOSFETs

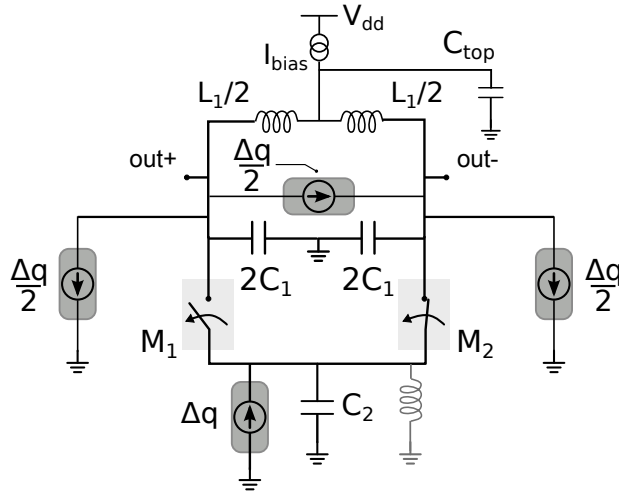


Figure 3.13: Noise charge referred to M_1 divided in differential and common mode components

fact equivalent to the one done for the noise of the main tank. Now we have to take into account the interactions between the common mode component and the charge injected at the source. Let us start considering when M_2 is *ON*. Once again the approximation of good switches with zero impedance is made to simplify the analysis. As consequence we have an effect on both ΔV_1 and ΔV_2 (3.24).

$$\begin{aligned}\Delta V_1 &= -\frac{\Delta q}{2(2C_1 + C_2)} - \frac{\Delta q}{4C_1} \\ \Delta V_2 &= \frac{\Delta q}{2(2C_1 + C_2)}\end{aligned}\tag{3.24}$$

The opposite situation is when M_2 is now *OFF* and M_1 is *ON*. Now the effect is similar as before with a sign changed on V_1 (3.25), but unchanged for V_2 .

$$\begin{aligned}\Delta V_1 &= \frac{\Delta q}{2(2C_1 + C_2)} + \frac{\Delta q}{4C_1} \\ \Delta V_2 &= \frac{\Delta q}{2(2C_1 + C_2)}\end{aligned}\quad (3.25)$$

Then, during the switching time, we consider to not have effects on ΔV_1 since the signal is taken differentially, but it's injected as common mode. On the contrary on V_2 we have a charge injected on C_2 giving (3.26).

$$\begin{aligned}\Delta V_1 &= 0 \\ \Delta V_2 &= \frac{\Delta q}{C_2}\end{aligned}\quad (3.26)$$

Thus, it is now possible to rewrite the previous (3.24), (3.25) and (3.26) using $f(\varphi)$ and $g(\varphi)$ defined in 3.2.1.3 obtaining (3.27).

$$\begin{aligned}\Delta V_1 &= -\frac{\Delta q}{2C_1} + f(\varphi) \left(\frac{\Delta q}{2(2C_1 + C_2)} + \frac{\Delta q}{4C_1} \right) \\ \Delta V_2 &= \frac{\Delta q \cdot g(\varphi)}{2(2C_1 + C_2)} + (1 - g(\varphi)) \frac{\Delta q}{C_2}\end{aligned}\quad (3.27)$$

Using (3.27) it is possible to derive the correspondent ΔX_1 and ΔX_2 and thus Γ_M (3.28).

$$\begin{aligned}\Gamma_M &= \frac{q_{max}}{C_1 A_1^2 \left(1 + 4 \frac{C_2 A_2^2}{C_1 A_1^2} \right)} \left(-\frac{A_1}{2} \cos(\varphi) - 2A_2 \sin(2\varphi) + \right. \\ &\quad \left. \frac{(4C_1 + C_2) \cos(\varphi) (A_1 f(\varphi) + 8A_2 g(\varphi) \sin(\varphi))}{4(2C_1 + C_2)} \right)\end{aligned}\quad (3.28)$$

The phase noise contribution due to the active device becomes (3.29) using (3.5), (3.28), (3.23), substituting $\varphi = \omega_0 t$ and integrating over the period T .

$$L_m(\Delta\omega) = 10 \log \left(\frac{2}{T} \int_0^T \frac{4k_B T \gamma}{2q_{max}^2 \Delta\omega^2} \Gamma_M^2(\omega_0 t) \frac{\sum_{k=0}^{\infty} k I_{k,out} \cos(k\omega_0 t + \phi_k)}{\frac{A_1}{2} \cos(\omega_0 t) + 2A_2 \sin(2\omega_0 t)} dt \right)\quad (3.29)$$

In general to evaluate (3.29) each current harmonic should be considered. However, since the denominator has 2 components: 1 at the fundamental and 1 at twice the frequency, and observing that Γ_M in the expression (3.28) has the same components $A_1/2 \cos(\varphi) + 2A_2 \sin(2\varphi)$, we could divide Γ_M in this first part, denoted as $\Gamma_{M,a}$,

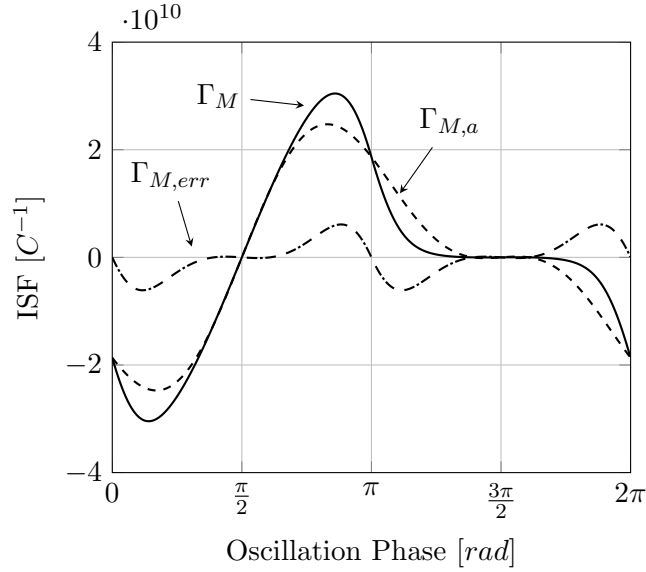


Figure 3.14: ISFs obtained with a complete analysis (Γ_M), the one used in the evaluation ($\Gamma_{M,a}$) and the error ($\Gamma_{M,err}$)

and the other component denoted as $\Gamma_{M,err}$ (Fig. 3.14).

$$\Gamma_{M,a} = \frac{q_{max}}{C_1 A_1^2 \left(1 + 4 \frac{C_2 A_2^2}{C_1 A_1^2}\right)} \left(-\frac{A_1}{2} \cos(\varphi) - 2A_2 \sin(2\varphi)\right) \quad (3.30)$$

To obtain a closed form for the transistor noise $\Gamma_{M,a}$ will be, indeed, considered, knowing that the error between the two ISFs is limited to the transitions and no error is made during complete switching. Using only the first and second harmonics allows us to simplify and consider only the same harmonics components in the current. Considering the $\Gamma_{M,a}$ we can write the expression of the phase noise related to the active elements (3.31) because it's now natural to consider also for the current the components at ω_0 , with the same phase as the signal, and the component at $2\omega_0$ with a phase shift of $\pi/4$. Moreover in (3.31) $I_1 = A_1(\omega_0 C_1/Q_1)$ and $I_2 = A_2(2\omega_0 C_2/Q_2)$.

$$L_m(\Delta\omega) = 10 \log \left(\frac{2}{2\pi} \int_0^{2\pi} \frac{4k_B T \gamma I_1}{2\Delta\omega^2 A_1} \frac{1}{A_1^2 C_1^2 \left(1 + 4 \frac{C_2 A_2^2}{C_1 A_1^2}\right)^2} \right. \\ \left. \left(\frac{1}{2} \cos(\varphi) + 2 \frac{A_2}{A_1} \sin(2\varphi) \right) \left(\cos(\varphi) + 2 \frac{I_2}{I_1} \sin(2\varphi) \right) d\varphi \right) \quad (3.31)$$

Solving (3.31) we can write the phase noise due to the transistors (3.32).

$$L_m(\Delta\omega) = 10 \log \left(\frac{4k_B T \gamma I_1}{2\Delta\omega^2 A_1} \frac{\left(\frac{1}{2} + \frac{8A_2^2 C_2 Q_1}{A_1^2 C_1 Q_2}\right)}{A_1^2 C_1^2 \left(1 + 4\frac{C_2}{C_1} \frac{A_2^2}{A_1^2}\right)^2} \right) \quad (3.32)$$

Where the ratio I_1/A_1 is equal to the equivalent parallel resistance of the main tank. Moreover, this means that the transistors noise is proportional to the one of the main tank by γ and a factor that depends on the design of the oscillator.

3.2.2 A closed form expression of $1/f^2$ phase noise (N only)

Let us now derive a closed form for the phase noise to compare it with classic oscillators that don't load the tank. In the previous sections every contribution to the phase noise has been computed by means of its Impulse Sensitivity Function and starting from (3.5) is possible to derive the expression of the phase noise caused by each white current noise source in LC oscillator. The phase noise formula of the major contributors are reported in (3.33), (3.34) and (3.35).

$$L_{T_1}(\Delta\omega) = 10 \log \left(\frac{4k_B T \omega_0 C_1}{2\Delta\omega^2 Q_1} \frac{1/2}{A_1^2 C_1^2 \left(1 + 4\frac{C_2}{C_1} \frac{A_2^2}{A_1^2}\right)^2} \right) \quad (3.33)$$

$$L_{T_2}(\Delta\omega) = 10 \log \left(\frac{4k_B T 2\omega_0 C_2}{2\Delta\omega^2 Q_2} \frac{\frac{1}{2}(8\frac{A_2^2}{A_1^2})}{A_1^2 C_1^2 \left(1 + 4\frac{C_2}{C_1} \frac{A_2^2}{A_1^2}\right)^2} \right) \quad (3.34)$$

$$L_m(\Delta\omega) = 10 \log \left(\frac{4k_B T \gamma \omega_0 C_1}{2\Delta\omega^2 Q_1} \frac{\left(\frac{1}{2} + \frac{8A_2^2 C_2 Q_1}{A_1^2 C_1 Q_2}\right)}{A_1^2 C_1^2 \left(1 + 4\frac{C_2}{C_1} \frac{A_2^2}{A_1^2}\right)^2} \right) \quad (3.35)$$

Summing each contributors and considering $P_{sig} = A_1^2 \omega_0 C_1 / (2Q_1)$ it is possible to write a closed expression for the phase noise of the Class B with tail filter oscillator.

$$L_{tot}(\Delta\omega) = 10 \log \left(\frac{k_B T}{2P_{sig}} \left(\frac{\omega_0}{\Delta\omega Q_1} \right)^2 \frac{\left(1 + 16\frac{A_2^2}{A_1^2} \frac{C_2}{C_1} \frac{Q_1}{Q_2} + \gamma \cdot \left(1 + 16\frac{A_2^2}{A_1^2} \frac{C_2}{C_1} \frac{Q_1}{Q_2}\right)\right)}{\left(1 + 4\frac{C_2}{C_1} \frac{A_2^2}{A_1^2}\right)^2} \right) \quad (3.36)$$

As (3.36) suggests, as a general rule, the quality factor of the second harmonic tank should be maximized. In this way three effects would be achieved. First, the

absolute noise of the tail resonator is reduced. Second it increases the impedance seen during the switching, avoiding loading effect. This translates into a reducing of the factor that multiplies γ . Third, it helps increasing the efficiency affecting the amplitudes value here considered given by the system. The second element that should be taken into account in the design is about C_2 . It might seem that since C_2 appears squared at the denominator and instead it is linear at the numerator, it should be increased. However, this observation doesn't take into account the fact that it is multiplied by A_2 , which is inversely proportional to C_2 . This means that, for a given Q_2 , if C_2 increases, A_2 decreases, leading to a higher phase noise. This yields to the fact that C_2 should be in general reduced, even if also the simulations have shown that the optimum is not for $C_2 = 0$. For relatively small values of C_2 can be seen an optimum of C_2 which depends also on the quality factor Q_2 .

Trying to further simplify the phase noise expression, because the phase noise due to the second harmonic tank is usually limited to about 5% of the total in usual design, it can be considered in general negligible. Noticing that the factor which multiplies the MOS contributor is very similar to one of the negligible second harmonic tank noise and that the denominator is only slightly higher than 1 in most of the practical cases, (3.36) can be written in a more elegant and widely used way (3.37).

$$L_{tot}(\Delta\omega) \approx \frac{k_B T}{2P_{sig}} \left(\frac{\omega_0}{\Delta\omega Q_1} \right)^2 (1 + \gamma) \quad (3.37)$$

This powerful result demonstrates that adding the second harmonic tank gives the possibility to increase significantly the efficiency of about a factor of 2 compared to a classic class B without increasing sensibly the noise.

3.2.3 Validation

In the following the evaluation previously made is verified with simulations. The analysis assumes the knowledge of the steady state and so we suppose to know the voltage amplitudes as well as the circuits parameters. Simulations are done considering the oscillator circuit shown in Fig. 3.1, with *bsim 4.5* models of 65nm CMOS process.. As said for the evaluation were considered explicitly capacitors referred to ground representing a more general case. In any case in Table 3.1 as an example are reported the noise contribution in case of capacitors fully differential and entirely to ground. The difference is relatively small between the two cases. The

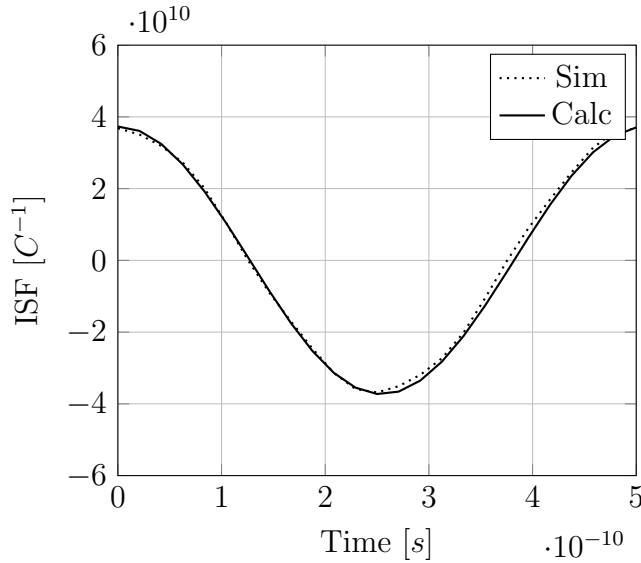


Figure 3.15: Main Tank ISF simulated and evaluated

Table 3.1: Noise contribution Fully differential vs. ground capacitors

	Fully Differential		Capacitors to ground	
	Noise Contrib.	% of the Total	Noise Contrib.	% of the Total
Main Tank	$2.64 \cdot 10^{-17}$	40%	$2.68 \cdot 10^{-17}$	46.7%
Transistors	$3.1 \cdot 10^{-17}$	47.78%	$2.6 \cdot 10^{-17}$	45.4%
Tail Tank	$3.61 \cdot 10^{-18}$	5.54%	$3.36 \cdot 10^{-18}$	5%

oscillator has a main tank quality factor $Q_1 = 20$ and $Q_2 = 20$ for second harmonic tank. The inductors have a value of $L_1 = 600pH$ and the oscillation frequency is set to $2GHz$ and the offset frequency considered is $10MHz$ because only thermal noise is of our interest for this analysis. Flicker noise upconversion is in general due to different mechanisms that were not considered in the previous analysis. It is worth to comment that second harmonic tank helps also in reducing some of these mechanisms: like the Groszkowski effect due to the current modulation. In current biased oscillator mainly the flicker upconversion is due to non linear parasitic capacitance modulation and the modulation of the tail capacitance at the transistors tail. Resonating them at the second harmonic reduces their impact. However, simulations have shown a higher sensitivity of the $1/f^3$ phase noise to a mis-tuning of the second harmonic filter. To have a verification of the analysis made, relatively the Impulse Sensitivity Function, it's possible to evaluate it with a simulation. In particular the method proposed by Pepe *et al.* [68] has been used. This method, based on the linear-time variant analysis of oscillators, computes

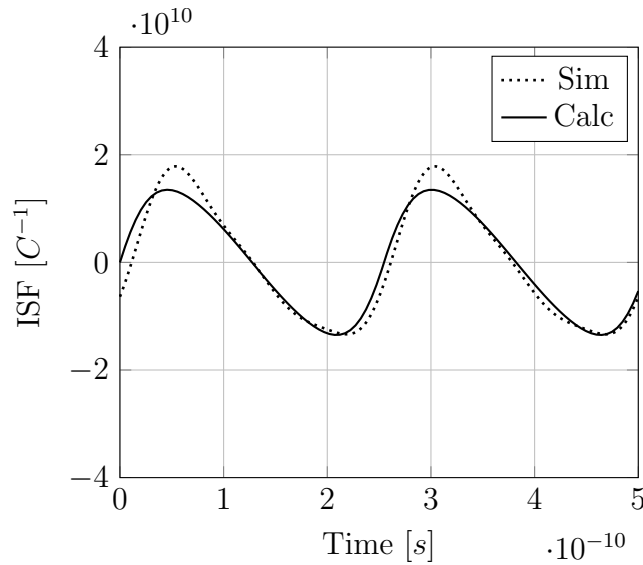


Figure 3.16: Second Harmonic Tank ISF simulated and evaluated

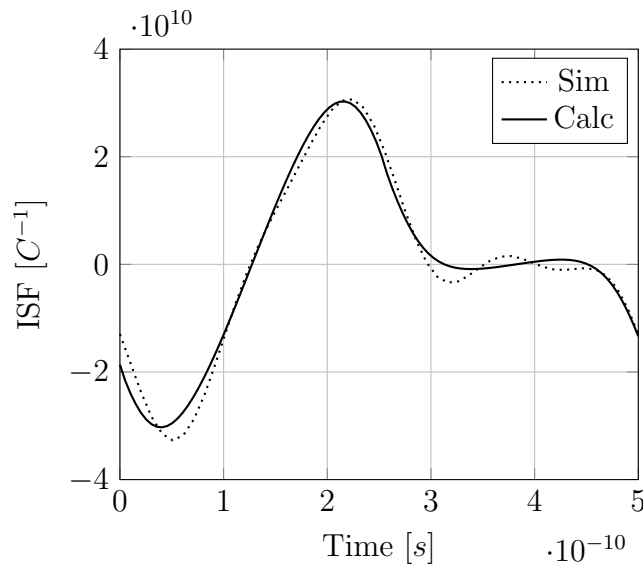


Figure 3.17: Active devices ISF simulated and evaluated

the impulse phase response by mean of periodic steady-state (PSS) and periodic transfer function (PXF) simulations. It permits to obtain the ISF in the frequency domain allowing a faster computation than the transient analysis and injection of charge pulses along the oscillator period. The evaluated phase noise and the simulations rely on the same operating condition. In the simulation in the frequency domain 6 harmonics are considered. The simulated ISFs and the calculated one have a good agreement (Fig. 3.15,3.16,3.17). Now let us extend the verification of the analysis considering different values of quality factors and different ratios C_2/C_1 . At first, in Fig. 3.18 are reported the noise contributors, expressed in $dB10$,

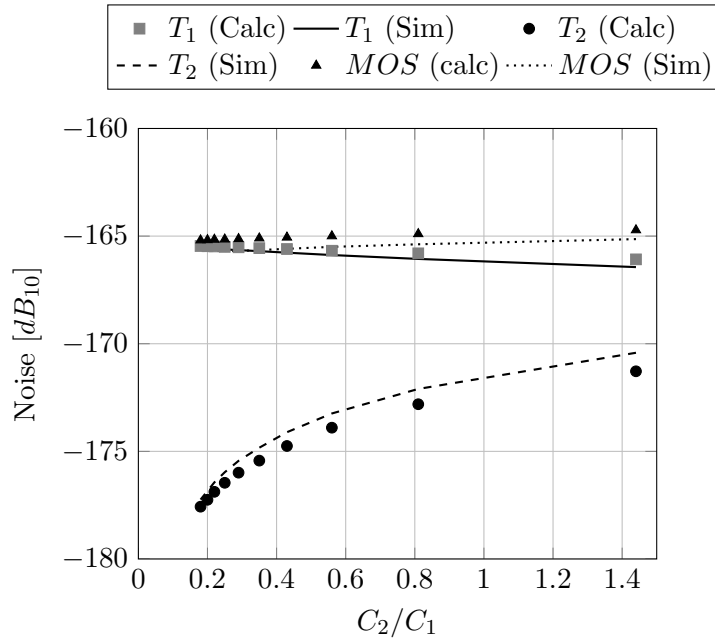


Figure 3.18: Output Noises of the different sources: simulated and calculated

of the oscillator, with $Q_2 = 20$. There is a very good agreement between the theory and the simulations. This also underlines the correct choice of the normalization of the steady state vector, giving an error always less than $1dB$ due to the neglected orthogonal component, thus giving to the designer an insight view to the phase noise conversion mechanism. Let us now evaluate the Excess Noise Factor of this oscillator. For sake of generality it is reported in Fig. 3.19 considering different values of Q_2 and once again different ratios C_2/C_1

3.2.4 Class B with tail filter p-n

The LC-tank oscillator with a p-n architecture, sometimes called *double switch pair oscillator* or *differential pair oscillator*, offers for the same current consumption twice the voltage swing compared to N-only architectures. It permits to be efficient maintaining the voltage swing within the breakdown voltage and as a consequence it may avoid reliability issues for practical implementation in which the voltage supply is higher than 1V. Even if the same topology of oscillator has been used in general p-n and N-only may be different due to the different behavior between nMOS and pMOS. Here an analysis of the class B with tail filter p-n is presented trying to clarify why and when single and double switching pair are similar and try to give an insight to the phase noise conversion in order to help the designer. Let us now consider a general p-n Class B oscillator with $2\omega_0$ tail filter of Fig. 3.20. Without

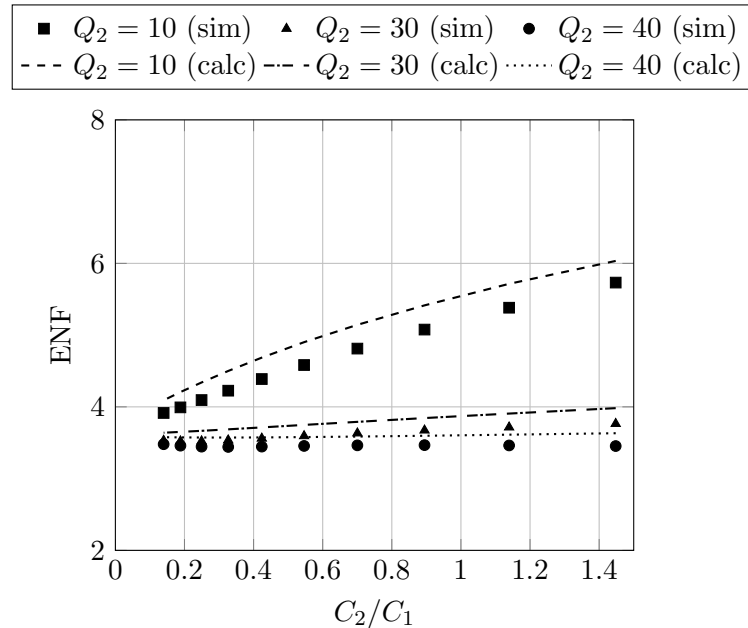


Figure 3.19: Output Noises of the different sources: simulated and calculated

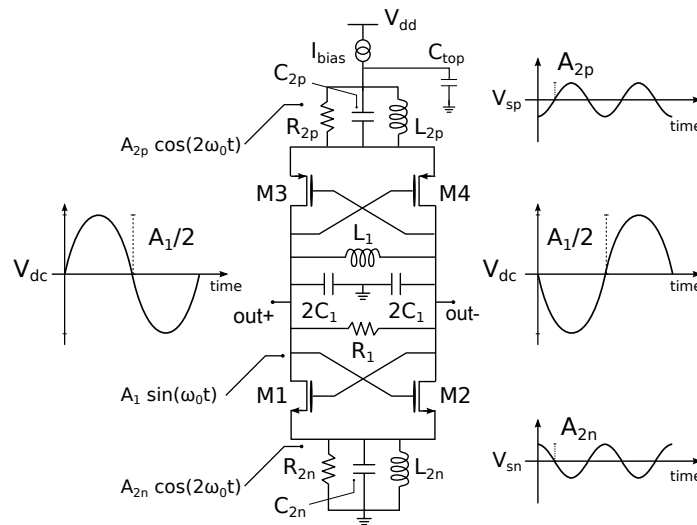


Figure 3.20: Class-B oscillators with $2\omega_0$ LC tail filter: p-n

loss of generality a top biased architecture is considered. The major difference compared to the N only structure is the fact that there are two $2\omega_0$ resonators, one at the nMOS source and the other at the pMOS source. The necessity will be clearer later during the analysis, but it's already possible to mention that they are required when a main tank with capacitors to ground is present. The absence on one side, without a not perfectly differential main resonator, would create otherwise a low impedance path yielding to loading effects. The presence of capacitors to ground, however, represents a general, sometimes worse and often

real situation because when the tuning capabilities are added the main tank is no more fully differential within the entire frequency range, and also because MOS parasitics, whose effects become more dominant for high frequencies, are always present. In designing the circuit, n-channel MOS and p-channel MOS transistors have been sized to set the output nodes to about half the supply voltage. This choice is the best to maximize the oscillation output swing. By assuming the same threshold voltage for both types of transistors this condition leads to set the same transconductance for both nMOS and pMOS, which translates in keeping the W/L ratio of pMOS transistors (W_P/L_P) about twice the W/L of nMOS transistors (W_N/L_N).

To compute the ISF for each noise source the starting point is the definition of the state vector (3.38).

$$\vec{X} = [V_{C_1} \quad \sqrt{\frac{L_1}{C_1}} I_{L_1} \quad \sqrt{\frac{C_{2n}}{C_1}} V_{C_{2n}} \quad \sqrt{\frac{L_{2n}}{C_1}} I_{L_{2n}} \quad \sqrt{\frac{C_{p2}}{C_1}} V_{C_{2p}} \quad \sqrt{\frac{L_{2p}}{C_1}} I_{L_{2p}}] \quad (3.38)$$

The presence of an additional tank resonating at $2\omega_0$ increases the dimension of the state vector if compared to N-only structure previously analyzed. In fact now the system can be modeled with a sixth order system. The six state variables are always the voltages on the capacitors and the currents through the inductors. Each state variable is scaled, once again, in such a way that the squared sum of the state variables is proportional to the stored energy. Now referring to Fig. 3.20 the steady state is approximated considering a sinusoid at ω_0 across the main tank, a cosinusoid at $2\omega_0$ across the tank at the nMOS sources and a cosinusoid always at $2\omega_0$, but with opposite sign, across the pMOS sources. Thus the system can be represented by its steady state vector \vec{X}_0 in (3.39).

$$\vec{X}_0 = [A_1 \sin(\omega_0 t) \quad A_1 \cos(\omega_0 t) \quad A_{2n} \sqrt{\frac{C_{2n}}{C_1}} \cos(2\omega_0 t) \\ A_{2n} \sqrt{\frac{C_{2n}}{C_1}} \sin(2\omega_0 t) \quad -A_{2p} \sqrt{\frac{C_{2p}}{C_1}} \cos(2\omega_0 t) \quad -A_{2p} \sqrt{\frac{C_{2p}}{C_1}} \sin(2\omega_0 t)] \quad (3.39)$$

Then the perturbation to the steady state will be evaluated to compute the phase noise contribution for each noise source (Fig. 3.21). From (3.39) it's straightforward to obtain its derivative (3.40) and then the normalization factor $|\dot{\vec{X}}|^2$ is evaluated

The phase noise contribution of the main tank in (3.45) differs to a classic oscillator with only one LC resonator for the normalization factor which in classical case is equal to 1, characteristic that was already pointed out in the N-only architecture. This, like in the N-only, may suggest the designer to maximize the ratio A_{2n}/A_1 , A_{2p}/A_1 and the ratio C_{2n}/C_1 and C_{2p}/C_1 or to unbalance the structure trying to prioritize only one ratio. However it must be taken into account that A_{2n} as well as A_{2p} are inversely proportional to the respective C_2 because it determines the impedance at $2\omega_0$. for this reason the only way to obtain an advantage in increasing the capacitance C_2 is to increase also the quality factor in order to maintain at the first order (at least ideally) the same A_2 . It is worth to underline here again the relationship between the N only structure and the p-n. As mentioned before and now remarked, it can be noted that for the same main tank, if $|A_{2n}| = |A_{2p}| = |A_{2,N-only}|$, $|A_{1,N-only}| = |A_1|$ and $C_{2n} = C_{2p} = 1/2C_{2,N-only}$ the single pair and differential pair are equivalent.

3.2.4.2 Second Harmonic Tanks

Second Harmonic Tank (n) To determine the noise of the second harmonic tank we define the function $f_n(\varphi)$ (3.46) to divide the oscillation period between the *ON/OFF* states and the switching transition. The difference with the $f(\varphi)$ that has been defined in Section 3.2.1.2 is only that here will be distinguished from the nMOS side and the pMOS side. In particular the nMOS side, which is denoted as $f_n(\varphi)$ refers to the amplitude of the oscillation at $2\omega_0$ at the n-channel transistors .

$$f_n(\varphi) = \frac{A_1 \sin(\varphi)}{2(A_{2n} \cos(2\varphi) - V_{dc})} \quad (3.46)$$

In (3.46) V_{dc} is the DC voltage at the output and $\varphi = \omega_0 t$. As already said value V_{dc} is about half the supply voltage and in general the designer should prefer to put it at almost half the supply voltage to maximize the swing. Assuming now that the transistors M_2 and M_3 are *ON*, referring to Fig. 3.23 and making the assumption here that the transistors are working like good switches, we can write the voltage perturbation across the capacitors (3.47)

$$\Delta V_1 = \frac{\Delta q}{2C_1 + C_{2n}} \quad \Delta V_{2,n} = -\frac{\Delta q}{2C_1 + C_{2n}} \quad \Delta V_{2p} = 0 \quad (3.47)$$

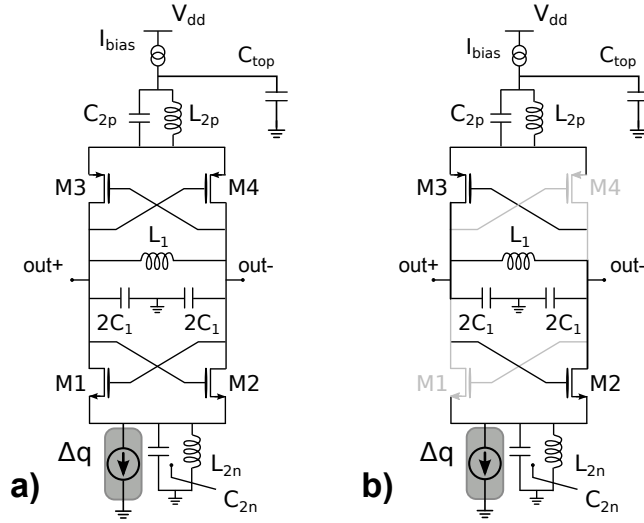


Figure 3.23: Noise charge referred to the second harmonic tank (n)

during the other half of the oscillation period when M_1 and M_4 are *ON* (3.48).

$$\Delta V_1 = -\frac{\Delta q}{2C_1 + C_{2n}} \quad \Delta V_{2,n} = -\frac{\Delta q}{2C_1 + C_{2n}} \quad \Delta V_{2,p} = 0 \quad (3.48)$$

At last during the switching transition the only effect will be on $\Delta V_{2,n}$ (3.49).

$$\Delta V_1 = 0 \quad \Delta V_{2,n} = -\frac{\Delta q}{C_{2n}} \quad \Delta V_{2,p} = 0 \quad (3.49)$$

When the transistors are completely *ON* the perturbations ΔV_1 and $\Delta V_{2,n}$ are equal in module, thus these considerations yields to the perturbation vector (3.50).

$$\Delta \vec{X} = \left[-\frac{f_n(\varphi)\Delta q}{2C_1 + C_{2n}} \quad 0 \quad -\sqrt{\frac{C_{2n}}{C_1}} \left(\frac{g_n(\varphi)\Delta q}{2C_1 + C_{2n}} + \frac{1}{C_{2n}}(1 - g_n(\varphi)) \right) \quad 0 \quad 0 \quad 0 \right] \quad (3.50)$$

Where $g_n(\varphi)$ is the absolute value of $f_n(\varphi)$. The ISF has a strong second harmonic component. It was the same for the N only architecture.

Second Harmonic Tank (p) To determine now the noise of the second harmonic tank at the pMOS side we define, similarly as before, the function $f_p(\varphi)$ (3.51) to divide the oscillation period between the *ON/OFF* states and the switching transition of the pMOS transistors.

$$f_p(\varphi) = \frac{A_1 \sin(\varphi)}{2(A_{2p} \cos(2\varphi) - V_{dc})} \quad (3.51)$$

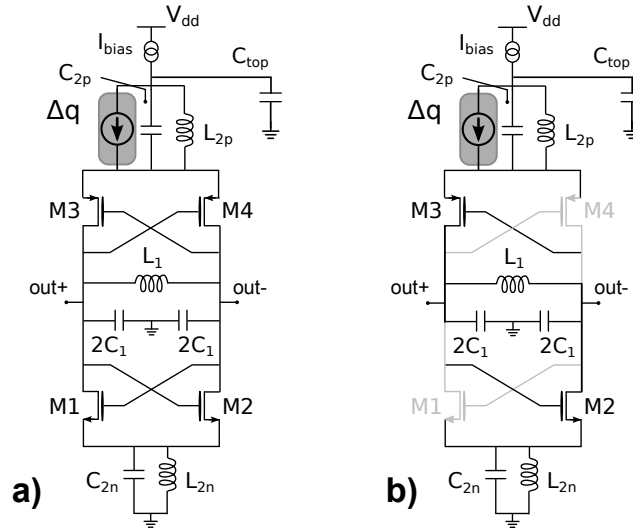


Figure 3.24: Noise charge referred to the second harmonic tank (p)

In general it is different from the one of the nMOS pair. Because of different parasitics capacitors, due to the transistors, and a little, but unavoidable unbalancing design, the voltage amplitudes as well as the capacitance values are different, having therefore $|A_{2n}| \neq |A_{2p}|$ and $C_{2n} \neq C_{2p}$. In (3.51) V_{dc} is again the DC voltage at the output. Assuming now that the transistor M_2 and M_3 are *ON*, referring to Fig. 3.24 and assuming the transistors are working as good switches we can write the voltage perturbation across the capacitors (3.52), with very similar considerations already made for the N counterpart.

$$\Delta V_1 = \frac{\Delta q}{2C_1 + C_{2p}} \quad \Delta V_{2,n} = 0 \quad \Delta V_{2,p} = \frac{\Delta q}{2C_1 + C_{2p}} \quad (3.52)$$

On the opposite situation M_1 and M_4 will be *ON* (3.53).

$$\Delta V_1 = -\frac{\Delta q}{2C_1 + C_{2p}} \quad \Delta V_{2,n} = 0 \quad \Delta V_{2,p} = \frac{\Delta q}{2C_1 + C_{2p}} \quad (3.53)$$

At last during the switching transition the only effect will be on $\Delta V_{2,n}$ (3.54).

$$\Delta V_1 = 0 \quad \Delta V_{2,n} = 0 \quad \Delta V_{2,p} = \frac{\Delta q}{C_{2p}} \quad (3.54)$$

When the transistors are completely *ON*, similarly in this case, the perturbations ΔV_1 and $\Delta V_{2,p}$ are equal in module, thus from these considerations we can write

the perturbation vector for a charge injected at the source of the pMOS (3.55).

$$\Delta\vec{X} = \begin{bmatrix} -\frac{f_p(\varphi)\Delta q}{2C_1 + C_{2p}} & 0 & 0 & 0 & \sqrt{\frac{C_{2p}}{C_1}} \left(\frac{g_p(\varphi)\Delta q}{2C_1 + C_{2p}} + \frac{1}{C_{2p}}(1 - g_p(\varphi)) \right) & 0 \end{bmatrix} \quad (3.55)$$

Also in this situation, since this is the dual situation as the N counterpart, there is a strong component at the second harmonic as expected.

Second Harmonic tank noise considerations The problem of this analysis is that it doesn't give to the designer a straightforward design procedure since the expression in this way can be evaluated numerically and it is not possible to obtain a closed form formula without simplifying the problem. For this reason let us simplify considering only the major component proportional to $\sin(2\varphi)$. In this condition it is possible to write $\Gamma_{2,n/p}$ as follows in (3.56) (in which for their similarities is either considered the n $\Gamma_{2,n}$ or the p part $\Gamma_{2,p}$).

$$\Gamma_{2,n/p} \approx \frac{q_{max} \sin(2\varphi)}{A_1 \left(1 + 4 \frac{C_{2n}}{C_1} \frac{A_{2n}^2}{A_1^2} + 4 \frac{C_{2p}}{C_1} \frac{A_{2p}^2}{A_1^2} \right)} \left(\frac{1}{2(2C_1 + C_{2,n/p})} + \frac{1}{C_1} \frac{A_{2,n/p}}{A_1} \right) \quad (3.56)$$

Only in case of good switching and as a consequence only for reasonably high voltage swings it is possible to well approximate the noise of second harmonic tank with (3.57).

$$\Gamma_{2,n/p} \approx \frac{q_{max}}{C_1 A_1 \left(1 + 4 \frac{C_{2n}}{C_1} \frac{A_{2n}^2}{A_1^2} + 4 \frac{C_{2p}}{C_1} \frac{A_{2p}^2}{A_1^2} \right)} \left(2\sqrt{2} \frac{A_{2,n/p}}{A_1} \sin(2\varphi) \right) \quad (3.57)$$

It can be immediately recognize the simplicity of (3.57) and it will be used for the derivation of a closed expression. As already mentioned it works and it well describes the noise of the second harmonic tail resonators only in case of good switching and as a consequence it underestimates dramatically the noise if there's almost no oscillation across the second harmonic tank. Using (3.57) can be obtained the phase noise contribution regarding the second harmonic tank at the nMOS source (3.58) and the one at pMOS source (3.59).

$$L_{T_{2,n}}(\Delta\omega) = 10 \log \left(\frac{4k_B T 2\omega_0 C_{2n}}{2\Delta\omega^2 Q_{2n}} \frac{4A_{2n}^2}{A_1^4 C_1^2 \left(1 + 4 \frac{C_{2n}}{C_1} \frac{A_{2n}^2}{A_1^2} + 4 \frac{C_{2p}}{C_1} \frac{A_{2p}^2}{A_1^2} \right)^2} \right) \quad (3.58)$$

$$L_{T_2,p}(\Delta\omega) = 10 \log \left(\frac{4k_B T 2\omega_0 C_{2p}}{2\Delta\omega^2 Q_{2p}} \frac{4A_{2p}^2}{A_1^4 C_1^2 \left(1 + 4\frac{C_{2n}}{C_1} \frac{A_{2n}^2}{A_1^2} + 4\frac{C_{2p}}{C_1} \frac{A_{2p}^2}{A_1^2}\right)^2} \right) \quad (3.59)$$

3.2.4.3 Active devices

Now we want to evaluate the noise of the active devices. In the following we will consider to injected noise charges and that the transistor noise is proportional to the device conductance.

$$\overline{i_{nMOS}^2} = 4k_B T \gamma g_0(\omega_0 t) = 4k_B T \gamma \frac{\partial I_{out}(\omega_0 t)}{\partial V_{in}(\omega_0 t)} \quad (3.60)$$

Where $\gamma = \gamma_n$ ($\gamma = \gamma_p$) is the channel noise factor for the nMOS (pMOS) transistors. Moreover since the noise described by (3.60) is cyclostationary, its associated ISF must be replaced by an effective ISF, or equivalently, the numerator in the general phase noise equation (3.5) is replaced with the mean square value of the product of the ISF with the noise current density, i.e. by (3.61).

$$\Gamma_{M,eff,rms}^2 \overline{i_{nMOS}^2} \equiv \frac{1}{2\pi} \int_0^{2\pi} \Gamma_M^2(\varphi) \overline{i_{nMOS}^2}(\varphi) d\varphi \quad (3.61)$$

Where neither $\Gamma_{M,eff,rms}^2$ nor $\overline{i_{nMOS}^2}$ are uniquely defined, but their products is. We consider the oscillation across the tanks defined in (3.22), and we represent the current by its Fourier expansion (3.22).

$$\begin{aligned} V_{tank} &= A_1 \sin(\omega_0 t) \\ V_{tank2,n} &= A_{2n} \cos(2\omega_0 t) \\ V_{tank2,p} &= -A_{2p} \cos(2\omega_0 t) \\ I_{out}(\omega_0 t) &= \sum_{k=0}^{\infty} I_{k,out} \sin(k\omega_0 t + \phi_k) \end{aligned} \quad (3.62)$$

Now substituting (3.60) in (3.62) we can write (3.63).

$$\begin{aligned}
g_{ds}(\omega_0 t) &= \frac{\partial I_{out}(\omega_0 t)}{\partial V_{in}(\omega_0 t)} \\
&= \frac{\partial I_{out}(\omega_0 t)/\partial t}{\partial V_{in}(\omega_0 t)/\partial t} \\
&= \frac{\sum_{k=0}^{\infty} k I_{k,out} \cos(k\omega_0 t + \phi_k)}{\frac{A_1}{2} \cos(\omega_0 t) + 2A_2 \sin(2\omega_0 t)}
\end{aligned} \tag{3.63}$$

In which the voltages of the MOS that is taken into account must be considered (in (3.63) generically is indicated A_2 , but it is clear that it is either $A_{2,n}$ or $A_{2,p}$, whenever an N or P transistor is analyzed). Now to determine the effect on the equivalent conductance in a pn structure we rely on [59]. It is possible to write the followings.

$$\Gamma_{M_1}(\varphi) = \Gamma(\varphi) \frac{g_{M2}}{g_{M1} + g_{M2}} \tag{3.64}$$

$$\Gamma_{M_2}(\varphi) = \Gamma(\varphi) \frac{g_{M1}}{g_{M1} + g_{M2}} \tag{3.65}$$

$$\Gamma_{M_3}(\varphi) = \Gamma(\varphi) \frac{g_{M4}}{g_{M3} + g_{M4}} \tag{3.66}$$

$$\Gamma_{M_4}(\varphi) = \Gamma(\varphi) \frac{g_{M3}}{g_{M3} + g_{M4}} \tag{3.67}$$

In which with $\Gamma(\varphi)$ is considered the actual ISF and the transconductance or conductance equivalent for each transistor. This yield to the result that if every MOS is symmetric and n-channel transistor are made electrically equivalent to the p-channel transistors then each MOS contributes for half the conductance/trasconductance. This result is in fact the peculiarity of p-n structures in general.

Transistors ISF (nMOS) In the following we will consider to injected noise charges across the nMOS transistor and that the transistor noise is proportional to the device conductance as previously shown. Let us consider the noise of M_2 . As it is shown in Fig. 3.25 the noise can be decomposed in a component that injects at the source and one that injects at the drain, that again can be decomposed in a differential and a common mode component. The differential part of the generator affects only ΔV_1 and since its value is half of the charge we have $\Delta V_1 = \Delta q/2C_1$. Now to analyze the effect and the interaction of the charge injected at the source and the common mode component injected at the main tank let us start considering

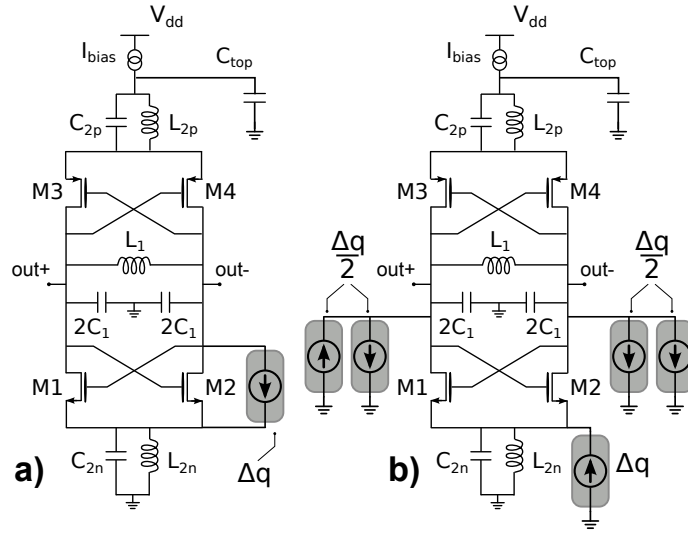


Figure 3.25: a) Noise charge referred to M_2 b) The decomposition of the generator for the analysis

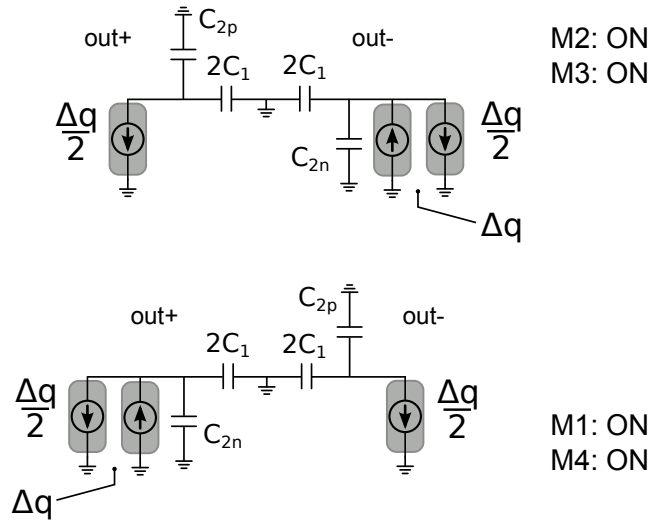


Figure 3.26: Interaction between noise charge generators (nMOS)

M_2 and M_3 ON.

$$\Delta V_1 = -\frac{\Delta q}{2C_1 + C_{2p}} - \frac{\Delta q}{2C_1 + C_{2n}} \quad \Delta V_{2,n} = \frac{\Delta q}{2C_1 + C_{2n}} \quad \Delta V_{2,p} = -\frac{\Delta q}{2C_1 + C_{2p}} \quad (3.68)$$

On the opposite situation M_1 and M_4 will be ON (3.69).

$$\Delta V_1 = \frac{\Delta q}{2C_1 + C_{2p}} + \frac{\Delta q}{2C_1 + C_{2n}} \quad \Delta V_{2,n} = \frac{\Delta q}{2C_1 + C_{2n}} \quad \Delta V_{2,p} = -\frac{\Delta q}{2C_1 + C_{2p}} \quad (3.69)$$

While during the switching transitions the only effect is on $C_{2,n}$ since the common mode components cancel each other.

$$\Delta V_1 = 0 \quad \Delta V_{2,n} = \frac{\Delta q}{C_{2n}} \quad \Delta V_{2,p} = 0 \quad (3.70)$$

The result of this analysis leads to similar considerations that were made for the N only architecture. The transistor ISF can be approximated with (3.71) making a small error during the transitions.

$$\Gamma_{M,n} = \frac{q_{max}}{C_1 A_1^2 \left(1 + 4 \frac{C_{2n}}{C_1} \frac{A_{2n}^2}{A_1^2} + 4 \frac{C_{2p}}{C_1} \frac{A_{2p}^2}{A_1^2}\right)} \left(\frac{A_1}{2} \cos(\varphi) - 2A_{2n} \sin(2\varphi) \right) + \Gamma_{M,n,err} \quad (3.71)$$

Neglecting $\Gamma_{M,n,err}$ and considering that the equivalent conductance is half if symmetry is maintained the phase noise of the nMOS transistor can be written as (3.72).

$$L_{M,n}(\Delta\omega) = 10 \log \left(\frac{1}{T} \int_0^T \frac{4k_B T \gamma_n}{2q_{max}^2 \Delta\omega^2} \Gamma_M^2(\omega_0 t) \frac{\sum_{k=0}^{\infty} k I_{k,out} \cos(k\omega_0 t + \phi_k)}{\frac{A_1}{2} \cos(\omega_0 t) + 2A_{2n} \sin(2\omega_0 t)} dt \right) \quad (3.72)$$

In general to evaluate (3.72) each current harmonic should be considered. However, since the denominator has 2 components: 1 at the fundamental and 1 at twice the frequency, and taking into account that we want to neglect $\Gamma_{M,n,err}$ and as a consequence that Γ_M in the expression (3.71) has the same components $A_1/2 \cos(\varphi) + 2A_{2n} \sin(2\varphi)$, it's now natural to consider also for the current the components at ω_0 , with the same phase as the signal, and the component at $2\omega_0$ with a phase shift of $\pi/4$. Moreover in (3.73) $I_1 = A_1(\omega_0 C_1/Q_1)$ and $I_{2n} = A_{2n}(2\omega_0 C_{2n}/Q_{2n})$ and for notation simplicity $\varphi = \omega_0 t$.

$$L_m(\Delta\omega) = 10 \log \left(\frac{1}{2\pi} \int_0^{2\pi} \frac{4k_B T \gamma I_1}{2\Delta\omega^2 A_1} \frac{1}{A_1^2 C_1^2 \left(1 + 4 \frac{C_{2n}}{C_1} \frac{A_{2n}^2}{A_1^2} + 4 \frac{C_{2p}}{C_1} \frac{A_{2p}^2}{A_1^2}\right)^2} \left(\frac{1}{2} \cos(\varphi) + 2 \frac{A_{2n}}{A_1} \sin(2\varphi) \right) \left(\cos(\varphi) + 2 \frac{I_{2n}}{I_1} \sin(2\varphi) \right) d\varphi \right) \quad (3.73)$$

Solving (3.73) we can write the phase noise due to the nMOS transistors (3.74).

$$L_m(\Delta\omega) = 10 \log \left(\frac{4k_B T \gamma_n I_1}{2\Delta\omega^2 A_1} \frac{\left(\frac{1}{4} + \frac{4A_{2n}^2 C_{2n} Q_1}{A_1^2 C_1 Q_{2n}}\right)}{A_1^2 C_1^2 \left(1 + 4 \frac{C_{2n}}{C_1} \frac{A_{2n}^2}{A_1^2} + 4 \frac{C_{2p}}{C_1} \frac{A_{2p}^2}{A_1^2}\right)^2} \right) \quad (3.74)$$

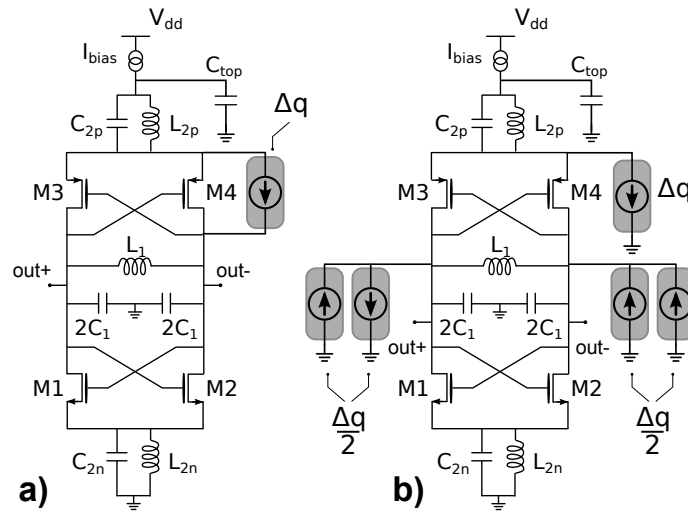


Figure 3.27: a) Noise charge referred to M_4 b) The decomposition of the generator for the analysis

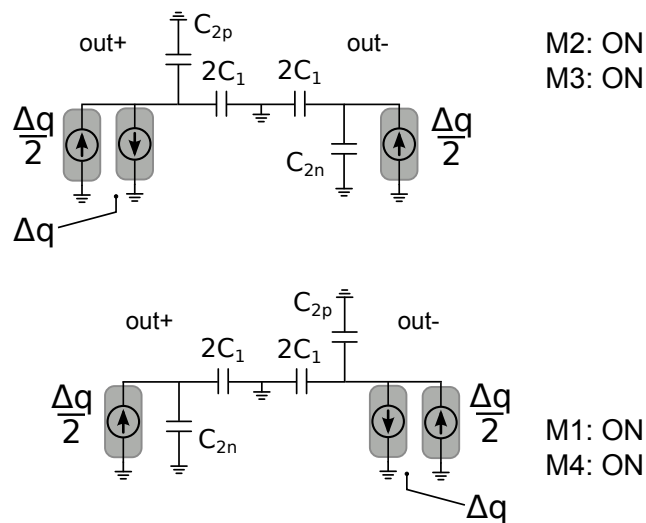


Figure 3.28: Interaction between noise charge generators (pMOS)

Where the ratio I_1/A_1 is equal to the equivalent resistance of the main tank and thus it represents its noise. Moreover, this means that the transistors noise is proportional to the one of the main tank by γ_n and a factor that depends on the design of the oscillator.

Transistors ISF (pMOS) The analysis can be made with in the same way as before, but considering now the noise of a pMOS. For example let us consider M_4 in Fig. 3.27. Again the noise generator can be decomposed in a component that injects at the source and one that injects at the drain, that again can be

decomposed in a differential and a common mode component. The differential part of the generator affects only ΔV_1 and since its value is again half of the charge we have $\Delta V_1 = -\Delta q/2C_1$. The only difference now is related to the sign and its due to the sign chosen for the noise generator. Now to analyze the effect and the interaction of the charge injected at the source of the pMOS and the common mode component injected at the main tank let us start considering M_2 and M_3 ON.

$$\Delta V_1 = -\frac{\Delta q}{2C_1 + C_{2p}} - \frac{\Delta q}{2C_1 + C_{2n}} \quad \Delta V_{2,n} = \frac{\Delta q}{2C_1 + C_{2n}} \quad \Delta V_{2,p} = -\frac{\Delta q}{2C_1 + C_{2p}} \quad (3.75)$$

On the opposite situation M_1 and M_4 will be ON (3.76).

$$\Delta V_1 = \frac{\Delta q}{2C_1 + C_{2p}} + \frac{\Delta q}{2C_1 + C_{2n}} \quad \Delta V_{2,n} = \frac{\Delta q}{2C_1 + C_{2n}} \quad \Delta V_{2,p} = -\frac{\Delta q}{2C_1 + C_{2p}} \quad (3.76)$$

While during the switching transitions the only effect is on $C_{2,n}$ since the common mode components cancel each other.

$$\Delta V_1 = 0 \quad \Delta V_{2,n} = 0 \quad \Delta V_{2,p} = -\frac{\Delta q}{C_{2p}} \quad (3.77)$$

The transistor ISF can be approximated with (3.78) making a small error during the transitions.

$$\Gamma_{M,p} = \frac{q_{max}}{C_1 A_1^2 \left(1 + 4 \frac{C_{2n}}{C_1} \frac{A_{2n}^2}{A_1^2} + 4 \frac{C_{2p}}{C_1} \frac{A_{2p}^2}{A_1^2}\right)} \left(-\frac{A_1}{2} \cos(\varphi) - 2A_{2,p} \sin(2\varphi)\right) + \Gamma_{M,p,err} \quad (3.78)$$

The same way it was done for nMOS transistors, neglecting $\Gamma_{M,p,err}$ and considering that the equivalent conductance is half if symmetry is maintained the phase noise of the pMOS transistor can be written as (3.79).

$$L_{M,p}(\Delta\omega) = 10 \log \left(\frac{1}{T} \int_0^T \frac{4k_B T \gamma_p}{2q_{max}^2 \Delta\omega^2} \Gamma_M^2(\omega_0 t) \frac{\sum_{k=0}^{\infty} k I_{k,out} \cos(k\omega_0 t + \phi_k)}{\frac{A_1}{2} \cos(\omega_0 t) + 2A_{2p} \sin(2\omega_0 t)} dt \right) \quad (3.79)$$

In general also in this case to evaluate (3.79) each current harmonic should be considered. However, doing the same observation that the denominator has 2 components: 1 at the fundamental and 1 at twice the frequency, and taking into account that we want to neglect $\Gamma_{M,p,err}$ and as a consequence that Γ_M in the expression (3.78) has the same components $A_1/2 \cos(\varphi) + 2A_{2p} \sin(2\varphi)$, it's now natural to consider also for the current the components at ω_0 , with the same phase

as the signal, and the component at $2\omega_0$ with a phase shift of $\pi/4$. Moreover in (3.80) $I_1 = A_1(\omega_0 C_1/Q_1)$ and $I_{2p} = A_{2p}(2\omega_0 C_{2p}/Q_{2p})$ and for notation simplicity $\varphi = \omega_0 t$.

$$L_{M,p}(\Delta\omega) = 10 \log \left(\frac{1}{2\pi} \int_0^{2\pi} \frac{4k_B T \gamma I_1}{2\Delta\omega^2 A_1} \frac{1}{A_1^2 C_1^2 \left(1 + 4 \frac{C_{2n}}{C_1} \frac{A_{2n}^2}{A_1^2} + 4 \frac{C_{2p}}{C_1} \frac{A_{2p}^2}{A_1^2} \right)^2} \right. \\ \left. \left(\frac{1}{2} \cos(\varphi) + 2 \frac{A_{2p}}{A_1} \sin(2\varphi) \right) \left(\cos(\varphi) + 2 \frac{I_{2p}}{I_1} \sin(2\varphi) \right) d\varphi \right) \quad (3.80)$$

Solving (3.80) we can write the phase noise due to the nMOS transistors (3.81).

$$L_{M,p}(\Delta\omega) = 10 \log \left(\frac{4k_B T \gamma_p I_1}{2\Delta\omega^2 A_1} \frac{\left(\frac{1}{4} + \frac{4A_{2p}^2 C_{2p} Q_1}{A_1^2 C_1 Q_{2p}} \right)}{A_1^2 C_1^2 \left(1 + 4 \frac{C_{2n}}{C_1} \frac{A_{2n}^2}{A_1^2} + 4 \frac{C_{2p}}{C_1} \frac{A_{2p}^2}{A_1^2} \right)^2} \right) \quad (3.81)$$

Where the ratio I_1/A_1 is equal to the equivalent resistance of the main tank and thus it represents its noise. Moreover, this means that the transistors noise is proportional to the one of the main tank by γ_p and a factor that depends on the design of the oscillator.

3.2.5 Considerations of the $1/f^2$ phase noise (p-n)

In this section we want to derive a closed form for the phase noise of the differential pair oscillator and to underline the similarities between the N only and the p-n structure, giving in this way an easy overview that permits to analyze and thus design the p-n version. Let us now derive a closed form for the phase noise to compare it with a classic oscillators that don't load the tank and of course with a class B with tail filter single switching pair. In the previous sections every contribution to the phase noise has been computed by means of its Impulse Sensitivity Function and starting from (3.5) is possible to derive the expression of the phase noise caused by each white current noise source in LC oscillator. The phase noise formula of the major contributors are reported in (3.82), (3.83), (3.84) and (3.85), (3.86).

$$L_{T_1}(\Delta\omega) = 10 \log \left(\frac{4k_B T \omega_0 C_1}{2\Delta\omega^2 Q_1} \frac{1/2}{A_1^2 C_1^2 \left(1 + 4 \frac{C_{2n}}{C_1} \frac{A_{2n}^2}{A_1^2} + 4 \frac{C_{2p}}{C_1} \frac{A_{2p}^2}{A_1^2} \right)^2} \right) \quad (3.82)$$

$$L_{T_{2n}}(\Delta\omega) = 10 \log \left(\frac{4k_B T 2\omega_0 C_{2n}}{2\Delta\omega^2 Q_{2n}} \frac{4A_{2n}^2/A_1^2}{A_1^2 C_1^2 \left(1 + 4\frac{C_{2n}}{C_1} \frac{A_{2n}^2}{A_1^2} + 4\frac{C_{2p}}{C_1} \frac{A_{2p}^2}{A_1^2}\right)^2} \right) \quad (3.83)$$

$$L_{T_{2p}}(\Delta\omega) = 10 \log \left(\frac{4k_B T 2\omega_0 C_{2p}}{2\Delta\omega^2 Q_{2p}} \frac{4A_{2p}^2/A_1^2}{A_1^2 C_1^2 \left(1 + 4\frac{C_{2n}}{C_1} \frac{A_{2n}^2}{A_1^2} + 4\frac{C_{2p}}{C_1} \frac{A_{2p}^2}{A_1^2}\right)^2} \right) \quad (3.84)$$

$$L_{m,n}(\Delta\omega) = 10 \log \left(\frac{4k_B T \gamma_p \omega_0 C_1}{2\Delta\omega^2 Q_1} \frac{\left(\frac{1}{4} + \frac{4A_{2n}^2 C_{2n} Q_1}{A_1^2 C_1 Q_{2n}}\right)}{A_1^2 C_1^2 \left(1 + 4\frac{C_{2n}}{C_1} \frac{A_{2n}^2}{A_1^2} + 4\frac{C_{2p}}{C_1} \frac{A_{2p}^2}{A_1^2}\right)^2} \right) \quad (3.85)$$

$$L_{m,p}(\Delta\omega) = 10 \log \left(\frac{4k_B T \gamma_n \omega_0 C_1}{2\Delta\omega^2 Q_1} \frac{\left(\frac{1}{4} + \frac{4A_{2p}^2 C_{2p} Q_1}{A_1^2 C_1 Q_{2p}}\right)}{A_1^2 C_1^2 \left(1 + 4\frac{C_{2n}}{C_1} \frac{A_{2n}^2}{A_1^2} + 4\frac{C_{2p}}{C_1} \frac{A_{2p}^2}{A_1^2}\right)^2} \right) \quad (3.86)$$

Summing each contributor and considering $P_{sig} = A_1^2 \omega_0 C_1 / (2Q_1)$ it is possible to write a closed expression for the phase noise of the Class B with tail filter oscillator. Now to further simplify the phase noise expression let us consider (3.83), (3.84) and (3.85), (3.86). There is a clear symmetry between the noise contributor related to the nMOS (both for the second harmonic LC resonator as well as the noise of nMOS transistors) and to the pMOS (the same as before, for both the second harmonic LC resonator and the pMOS transistors). In general there isn't any actual reason for which the designer should prefer to reduce particularly the noise related to either the N part or the P part. Instead, in general, it's desirable to keep both the noise low enough. As a consequence, even if it is true that there are always some little imbalances, without loss of generality it is possible to assume equivalent the design of the N part and the P part (same capacitance, at least as first approximation, and same voltage amplitude).

$$L_{tot}(\Delta\omega) = 10 \log \left(\frac{k_B T}{2P_{sig}} \left(\frac{\omega_0}{\Delta\omega Q_1} \right)^2 \frac{\left(1 + \frac{\gamma_n + \gamma_p}{2} \cdot \left(1 + 16 \frac{A_2^2 C_2 Q_1}{A_1^2 C_1 Q_2}\right) + 16 \frac{A_2^2 C_2 Q_1}{A_1^2 C_1 Q_2}\right)}{\left(1 + 8 \frac{C_2 A_2^2}{C_1 A_1^2}\right)^2} \right) \quad (3.87)$$

Like it was for (3.36), (3.87) suggests as a general rule that the quality factor of both the second harmonic tank should be maximized. In this way three effects would be achieved. First, the absolute noise is reduced. Second it increases the impedance seen during the switching avoiding the loading effect. This translates into a reducing of the factor that multiplies $\gamma_{n,p}$. Third, it helps increasing the efficiency. The second element that should be taken into account in the design

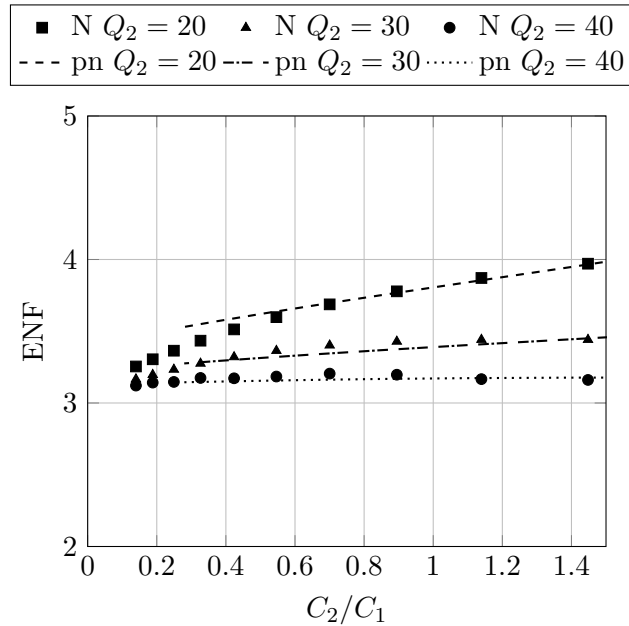


Figure 3.29: Excess noise factor of N only (markers) and pn (lines)

is about C_2 . It might seem that since C_2 appears squared at the denominator and instead it is linear at the numerator, it should be increased. However, this observation doesn't take into account the fact that it is multiplied by A_2 , which is, in general, inversely proportional to C_2 . This means that, for a given Q_2 , if C_2 increases, A_2 decreases, leading to a higher phase noise. This yields to the fact that C_2 should be in general reduced, even if also the simulations have shown that the optimum is not for $C_2 = 0$. For relatively small values of C_2 can be seen an optimum of C_2 which depends also on the quality factor Q_2 . Moreover, because the phase noise due to the second harmonic tanks is usually limited to about 5% of the total in usual design, it will be now neglected. Noticing that the factor which multiplies the MOS contributor is just twice the one of the negligible second harmonic tank noise and that the denominator is only slightly higher than 1, (3.36) can be written in a more handy way (3.88).

$$L_{tot}(\Delta\omega) \approx 10 \log \left(\frac{k_B T}{2P_{sig}} \left(\frac{\omega_0}{\Delta\omega Q_1} \right)^2 \left(1 + \frac{\gamma_n + \gamma_p}{2} \right) \right) \quad (3.88)$$

The result in (3.88) leads to the important result obtained by Andreani and Fard [59] that the phase noise becomes proportional to $(1 + \frac{\gamma_n + \gamma_p}{2})$ in a classic class B differential pair oscillator, neglecting the noise of the current generator, but maintaining in that case the transistor to work in saturation region. It is important to notice that once again the main difference is the efficiency of the two oscillators.

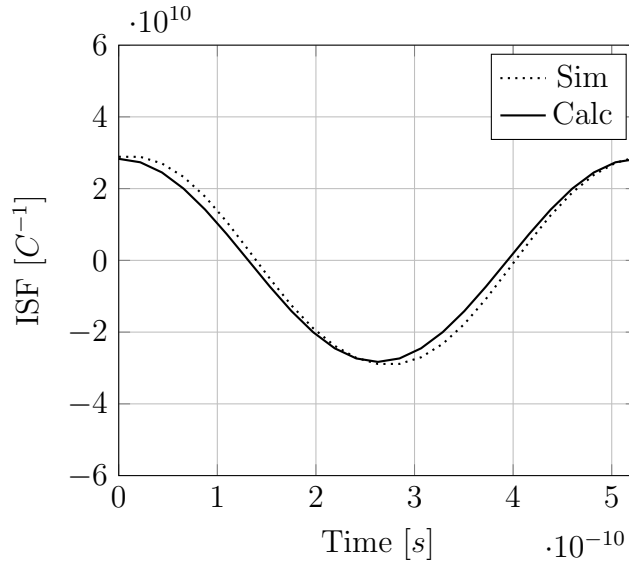


Figure 3.30: Main Tank ISF simulated and evaluated

With respect to a classic class B whose power efficiency is limited to less than 50%, using a tail filter it is possible to reach efficiencies of about 90% in simulation. In practice trade offs set by the tuning range, thus the limitations about parasitics, limit the maximum efficiency achievable which is still around 75-85%.

About the comparison between the single pair oscillator and the differential pair oscillator, an important observation was already made in Section 3.2.4. In fact if $|A_{2n}| = |A_{2p}| = |A_{2,N-only}|$, $|A_{1,N-only}| = |A_1|$ and $C_{2n} = C_{2p} = 1/2C_{2,N-only}$ consequently if the same amplitudes are achieved and half the capacitance is used at the transistors sources, not only the normalization factor becomes the same as the N only case, but also the noise contributors. Let us consider for this reason the Fig. 3.29 in which is reported a simulation of the Class B with tail filter both N only and p-n. The p-n has been polarized to twice the supply voltage with half the current to be able to achieve almost the same voltage swings. The capacitor $C_{2,n}$ and $C_{2,p}$ are half with respect to the N only case and of course every quality factor is equal between the two cases. Fig. 3.29 shows in fact that the simulations confirm what also the analysis suggested regarding the analogy between the two structures. There is, indeed, a good agreement between the two ENF and so the same considerations made for the N only can be done for the p-n.

In the following the evaluation previously made is verified with simulations. The analysis assumes the knowledge of the steady state and so we suppose to know the voltage amplitudes as well as the circuits parameters. In this particular case the oscillator in Fig. 3.20 has been simulated using a quality factor of the main

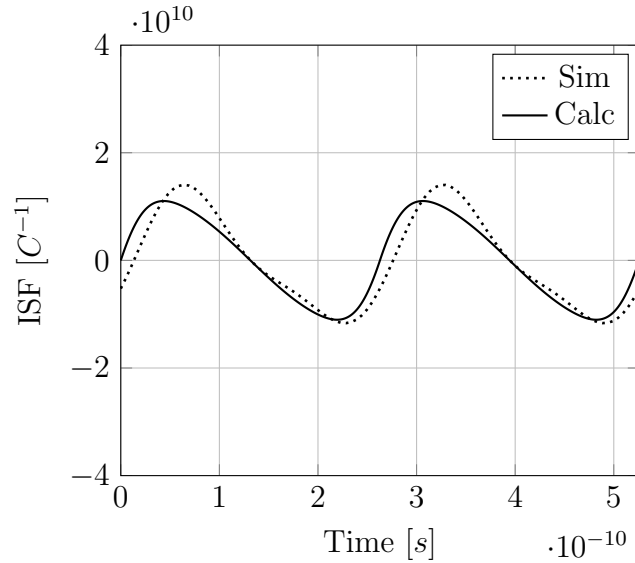


Figure 3.31: Second Harmonic Tank (n) ISF simulated and evaluated

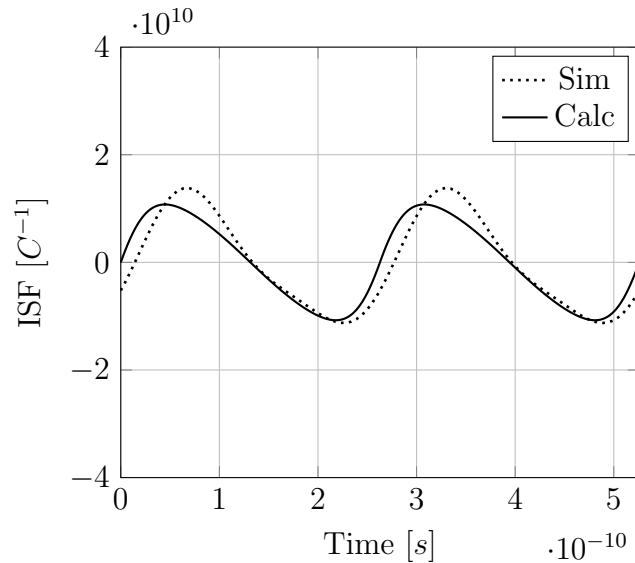


Figure 3.32: Second Harmonic Tank (p) ISF simulated and evaluated

tank $Q_1 = 20$, $Q_{2,n/p} = 20$ for second harmonic tank. The inductors have a value of $L_1 = 600pH$ and the oscillation frequency is set to about $2GHz$ (slightly lower due to parasitic capacitance) and the offset frequency considered is $10MHz$.

To have now a comparison between the impulse sensitivity function evaluated and the simulated one, we consider the method proposed by Pepe *et al.* [68]. In this efficient way is possible to obtain with a faster simulation the ISF of a noise source. For the p-n architecture in particular is reported the ISF of the main tank Fig. 3.30, the ISF of the second harmonic LC tanks, both n-side and p-side, Fig. 3.31, Fig. 3.32 and the ISF of the transistors Fig. 3.33, Fig. 3.34. The impulse sensitivity

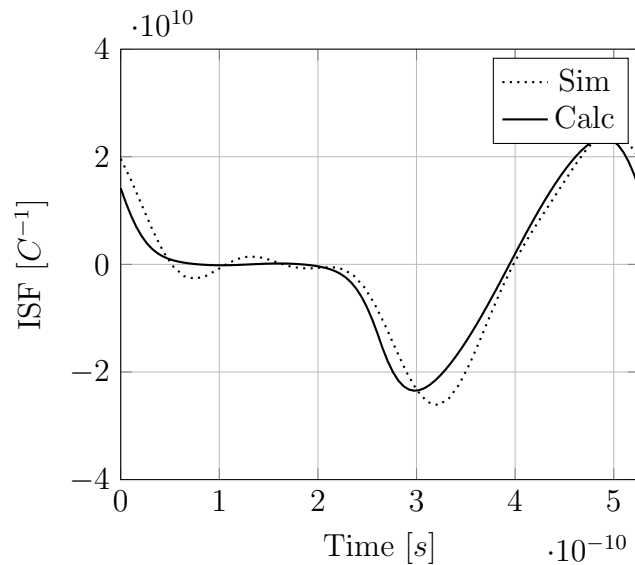


Figure 3.33: Active devices (nMOS, M_2) ISF simulated and evaluated

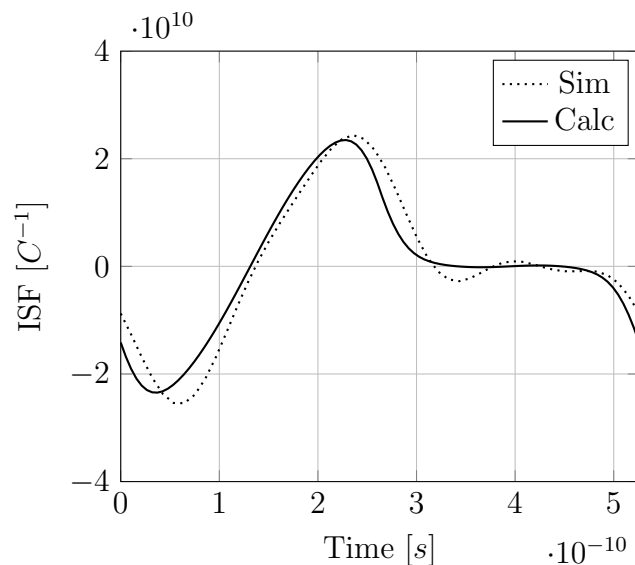


Figure 3.34: Active devices (pMOS, M_4) ISF simulated and evaluated

functions related to the transistors report only two examples of nMOS and pMOS that switch with opposite phase. The ISF of the remaining transistor follows the same behavior of the ones explicitly reported.

3.3 Class F

As it has been seen another way to improve efficiency is by acting on the resonator [7]. The goal is to create an output waveform with sharper transitions (ideally a

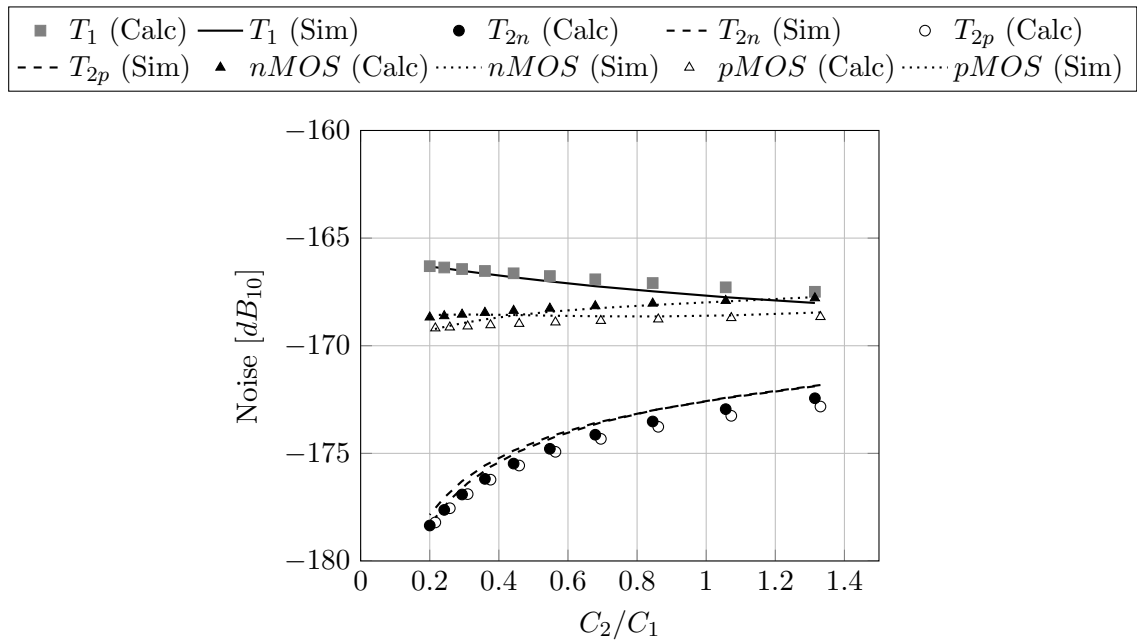


Figure 3.35: Output Noises of the different sources: simulated and calculated

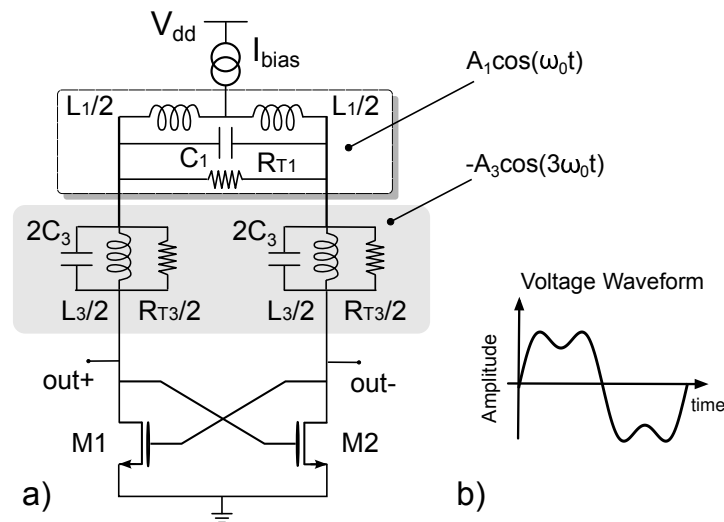


Figure 3.36: Class-F oscillator: a) circuit schematic and b) typical voltage waveform.

square wave) so that the active devices dissipate power for a smaller percentage of time. The same concept should give a better ENF (FoM) since efficiency and ENF (FoM) are directly related. In addition the new resonator has a different ISF compared to a classic single sinusoidal oscillator, with potentially an even larger effect on the ENF. For the analysis a possible implementation of a class-F oscillator (shown in Fig. 3.36a) that uses two series-connected LC tanks is considered. It is worth to notice that the analysis and the consequent normalization applies to

any oscillator whose resonator consists of more energy restoring elements. The two series LC tanks resonate respectively at the fundamental frequency (ω_0) and at the third harmonic. Assuming a square wave current and sufficiently high Q, the voltage across the first tank is a sinusoid at ω_0 and the voltage across the second tank a sinusoid at $3\omega_0$, with opposite phase. If the tank impedances at $3\omega_0$ and at ω_0 are comparable the voltage resembles the one of Fig. 3.36b. At the switching instants the waveform has a higher slope than a sinusoid with the same peak amplitude, potentially improving phase noise. This oscillator is analyzed using the ISF approach explained in the following. The phase noise can be expressed as (3.89).

$$L_{tot}(\Delta\omega) = 10 \log \left(\frac{k_B T}{2P_{sig}} \left(\frac{\omega_0}{\Delta\omega Q_{\omega_0}} \right)^2 f_{res} (1 + \gamma_{mos}) \right) \quad (3.89)$$

Where, P_{sig} is the signal power, Q_{ω_0} is the Q of the tank at ω_0 , and f_{res} is the resonator noise factor, which is a function of the ratio between the resonator impedances and the quality factors of the two resonators. Assuming transistor current noise is γ_{mos} times the derivative of the drain current with respect to the gate voltage, when the active devices are working in saturation region, the transistors phase noise is γ_{mos} times the tank phase noise i.e. the result derived in [35, 38] for harmonic oscillators is true also for class-F. To minimize ENF we need to minimize f_{res} and to maximize efficiency. It will be shown that f_{res} decreases as $Q_{3\omega_0}$ is increased. Moreover, if $Q_{3\omega_0}$ is greater than $5/3Q_{\omega_0}$, f_{res} is smaller than 1 and is proportional to C_3 . The minimum C_3 is when the impedances at $3\omega_0$ and at ω_0 are equal (to prevent oscillation at $3\omega_0$). If $Q_{3\omega_0}$ is too small f_{res} becomes larger than 1. To verify the analysis, two class-F and a class-B oscillators have been simulated for the same operating conditions. In one class-F $Q_{3\omega_0}$ is equal to Q_{ω_0} , while in the other $Q_{3\omega_0}$ is equal to $3Q_{\omega_0}$. In both cases the resonator impedance at ω_0 and at $3\omega_0$ is nearly equal.

Fig. 3.37 reports the simulated and calculated phase noise as a function of the DC power dissipation. As expected, increasing $Q_{3\omega_0}$ gives a better phase noise. When the Q_{ω_0} and $Q_{3\omega_0}$ are equal class-F and the class-B oscillators show the same phase noise since conversion efficiency and resonator noise compensate each other.

For the class-F oscillator of Fig. 3.36 the load is a fourth order system made of two LC tanks, resonating at ω_0 and $3\omega_0$. The ISF for each noise source is calculated

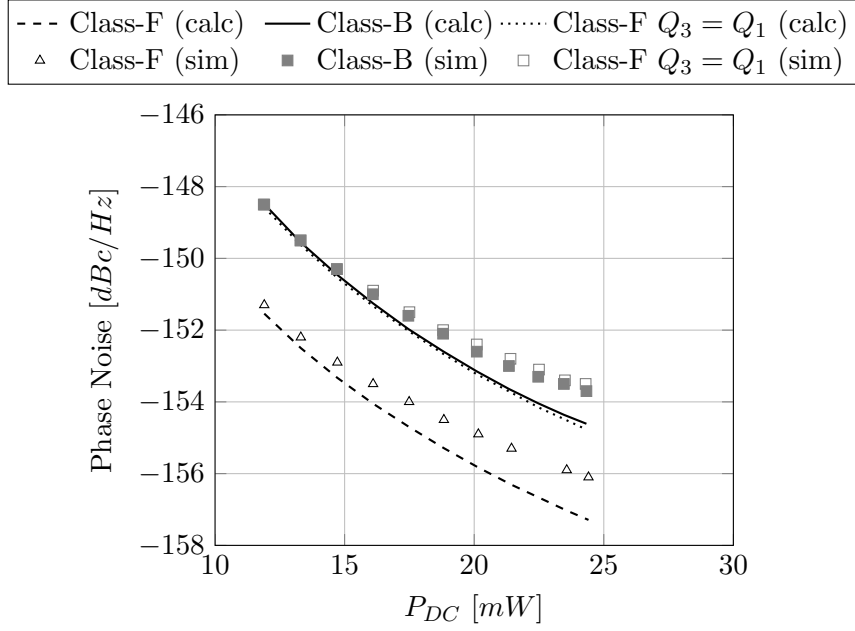


Figure 3.37: Comparison between Class-F and Class-B oscillators phase noise. Dots represent simulated data, lines are calculated

starting from the state vector \vec{X} (3.90).

$$\vec{X} = [V_{C_1} \quad \sqrt{\frac{L_1}{C_1}} I_{L_1} \quad \sqrt{\frac{C_3}{C_1}} V_{C_3} \quad \sqrt{\frac{L_3}{C_1}} I_{L_3}] \quad (3.90)$$

The steady-state oscillation (3.91) is approximated by a sinusoid at ω_0 across the main tank and a sinusoid at $3\omega_0$ across the second tank, (opposite in phase).

$$\begin{aligned} \vec{X}_0 = & [A_1 \cos(\omega_0 t) \quad A_1 \sin(\omega_0 t) \\ & - A_3 \sqrt{\frac{C_3}{C_1}} \cos(3\omega_0 t) \quad - A_3 \sqrt{\frac{C_3}{C_1}} \sin(3\omega_0 t)] \end{aligned} \quad (3.91)$$

In this analysis let us start once again from the steady state. Eventually, the system can be represented as the steady-state vector \vec{X}_0 , plus a random perturbation vector ΔX . Neglecting the component of ΔX orthogonal to the trajectory, the phase perturbation $\Delta\phi$ can be derived from the state variables derivatives. So the ISF in terms of state-space vectors can be expressed as (3.92).

$$\Gamma_i = \omega_0 \frac{q_{max}}{\Delta q} \frac{\Delta \vec{X}_i \cdot \dot{\vec{X}}}{|\dot{\vec{X}}|^2} \quad (3.92)$$

3.3.1 Main tank

The main noise sources are the tank losses and the transistors noise. The main tank is composed by the series of two LC tank resonators. If a charge is injected across the capacitor C_1 , $\Delta X_1 = \Delta q/C_1$ and the corresponding phase error is obtained multiplying for the first element of the derivative of the steady state vector normalized by its module squared (3.93).

$$\Delta\phi_1 = \omega_0 \frac{\Delta q}{C_1} \frac{\dot{X}_1}{|\dot{X}|^2} \quad (3.93)$$

Now let us consider that a charge is injected across the capacitor C_3 . The same evaluation can be done (3.94).

$$\Delta X_3 = \frac{\Delta q}{C_3} \sqrt{\frac{C_3}{C_1}} \quad \Delta\phi_3 = \omega_0 \frac{\Delta q}{C_3} \sqrt{\frac{C_3}{C_1}} \frac{\dot{X}_3}{|\dot{X}|^2} \quad (3.94)$$

Since the expression of the phase error can be equated, for both the noise charges, to the ISF (3.95) to evaluate the ISF itself (3.96).

$$\Delta\phi_1 = \frac{\Gamma_1(\omega_0\tau)}{q_{max}} \Delta q \quad \Delta\phi_3 = \frac{\Gamma_3(\omega_0\tau)}{q_{max}} \Delta q \quad (3.95)$$

$$\Gamma_1(\omega_0 t) = -\frac{q_{max}}{A_1 C_1} \frac{\sin(\omega_0 t)}{(1 + 9 \frac{C_3}{C_1} \frac{A_3^2}{A_1^2})} \quad \Gamma_3(\omega_0 t) = -\frac{q_{max}}{A_1 C_1} \frac{3 \frac{A_3}{A_1} \sin(3\omega_0 t)}{(1 + 9 \frac{C_3}{C_1} \frac{A_3^2}{A_1^2})} \quad (3.96)$$

Considering that the noise density of the LC tank resonating at ω_0 is $\overline{i_{n,1}^2}/\Delta f = 4k_B T \omega_0 C_1 / Q_{\omega_0}$ and $\overline{i_{n,1}^2}/\Delta f = 4k_B T 3\omega_0 C_3 / Q_{3\omega_0}$ for the LC tank resonating at $3\omega_0$ summing up the contributions it possible to write the phase noise as (3.97).

$$L_T(\Delta\omega) = 10 \log \left(\frac{k_B T}{2P_{sig}} \left(\frac{\omega_0}{\Delta\omega Q_{\omega_0}} \right)^2 f_{res} \right) \quad (3.97)$$

Where P_{sig} is the power dissipated by the resonator and the *tank noise factor* is expressed in (3.98).

$$f_{res} = \frac{\left(1 + 9 \frac{C_3}{C_1} \frac{A_3^2}{A_1^2} \frac{3Q_{\omega_0}}{Q_{3\omega_0}} \right) \left(1 + \frac{3Q_{\omega_0}}{Q_{3\omega_0}} \frac{C_3}{C_1} \frac{A_3^2}{A_1^2} \right)}{\left(1 + 9 \frac{C_3}{C_1} \frac{A_3^2}{A_1^2} \right)} \quad (3.98)$$

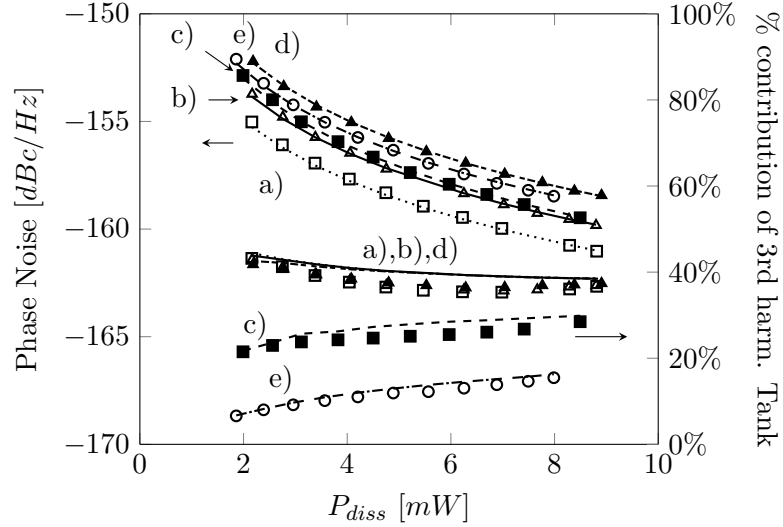


Figure 3.38: Class-F oscillators total phase noise of the resonator (left scale) and percentage of the third harmonic tank (right scale). Dots are simulations, lines are calculations: a) $Q_3=3Q_1$, $C_3=C_1$; b) $Q_3=2Q_1$, $C_3=2/3C_1$; c) $Q_3=2Q_1$, $C_3=C_1$; d) $Q_3=Q_1$, $C_3=1/3C_1$; e) $Q_3=Q_1$, $C_3=C_1$

When f_{res} is equal to 1 the resonator phase noise in a class-F oscillator is the same as that of tank in a class-B oscillator. To derive useful design insights (3.98) is simplified as follows. The ratio between the amplitude at the third harmonic (A_3) and at the fundamental (A_1) can be expressed in terms of the ratio between the impedance at the two resonance frequencies (z_3) as $A_3/A_1 = \beta z_3/3$, where β depends on the current waveforms and is equal to 1 for a square-wave. Using this approximation in (3.98) f_{res} becomes (3.99).

$$f_{res} = \frac{(1 + \beta^2 z_3) \left(1 + \frac{\beta^2}{9} z_3\right)}{\left(1 + \beta^2 z_3 \frac{Q_{3\omega_0}}{3Q_{\omega_0}}\right)} \quad (3.99)$$

To optimize phase noise f_{res} must be minimized. When z_3 is increased the amplitude of the third harmonic increases and a waveform with a steeper slope is obtained but the noise added by the third harmonic tank increases. For $Q_{3\omega_0}$ larger than $5/3Q_{\omega_0}$ f_{res} is smaller than 1 and decreases as z_3 is increased. For $Q_{3\omega_0}$ lower than $5/3Q_{\omega_0}$ f_{res} increases with z_3 . The oscillator in Fig. 3.36 has been simulated under the same operating conditions used for the class-B oscillators and the results are reported in Fig. 3.38. The simulated phase noise of the tank as well as the percentage due to the third harmonic tank match well with calculations. As predicted by (3.98), for C_3 and C_1 such that the impedance at the two resonance frequencies is the same, the percentage of noise of the third harmonic tank is nearly constant, independent

Q . When $Q_{3\omega_0}$ is equal to $2Q_{\omega_0}$ increasing z_3 improves the phase noise, while when $Q_{3\omega_0}$ is equal to Q_{ω_0} phase noise degrades for higher z_3 .

3.3.2 Active Devices

The ISF of the active devices (Γ_{mos}) is calculated using (3.92), but with a charge pulse applied across the whole tank. Γ_{mos} is equal to $\Gamma_1 + \Gamma_3$. The thermal noise of the transistors is a time-varying function equal to $4k_B T \gamma_{mos} g_m(t)$, considering that the transistor are working in saturation. The transconductance can be approximated considering the derivative of the current with respect to the voltage (3.100).

$$\begin{aligned} g_m(\omega_0 t) &= \frac{\partial I_{out}(\omega_0 t)}{\partial V_{in}(\omega_0 t)} \\ &= \frac{\partial I_{out}(\omega_0 t)/\partial t}{\partial V_{in}(\omega_0 t)/\partial t} \\ &= \frac{\sum_{k=0}^{\infty} k I_{k,out} \sin(k\omega_0 t + \phi_k)}{A_1 \sin(\omega_0 t) - 3A_3 \sin(3\omega_0 t)} \end{aligned} \quad (3.100)$$

Where I_k are the Fourier coefficients of the current waveform. Using (3.100) and (3.96) to compute Γ_{mos} , yields the transistors phase noise (3.101).

$$L_{mos}(\Delta\omega) = 10 \log \left(\frac{k_B T}{2P_{sig}} \left(\frac{\omega_0}{\Delta\omega Q_{\omega_0}} \right)^2 f_{res} \gamma_{mos} \right) \quad (3.101)$$

Where f_{res} is given by (3.98) or (3.99). This result is similar to the general result derived by Bank for sinusoidal oscillators i.e. the noise of the transistors is γ_{mos} times the noise of the tank, irrespective of the device details. However, in class F oscillator, the device size and bias influence the amplitude ratio between the third and the fundamental harmonic through the coefficient β . Based on (3.101) and (3.97) the phase noise expression of the class F oscillator is found, as reported in (3.89).

Chapter 4

Efficient p-n class B oscillator with transformer based tail filtering

A complementary p-n class-B oscillator with two magnetically coupled second harmonic tail resonators is presented. For the same oscillation amplitude (constrained by reliability considerations) and the same tank, the p-n oscillator achieves 3-4dB better Figure of Merit (FoM) than an n-only reference one. The transformer based tail filtering allows to save area occupation, respect to a classic implementation. After frequency division by 2, the p-n oscillator has a measured phase noise that ranges from -150.8 to -151.5 dBc/Hz at 10MHz offset from the carrier when the frequency of oscillation is varied from 3.64 to 4.15GHz. With a power consumption of 6.3mW, a peak FoM of 195.6 dBc/Hz is achieved.

4.1 Introduction

In LC oscillators reducing the power consumption while preserving their phase noise is a key goal especially for mobile applications. This can be achieved acting on the oscillator topology and/or on the tank quality factor (Q). Oscillator topology affects the conversion of circuit noise sources into phase noise changing the impulse sensitivity function (ISF) [6]. Moreover, it affects the power vs phase noise trade-off through the maximum achievable power conversion efficiency (η_P), i.e. the

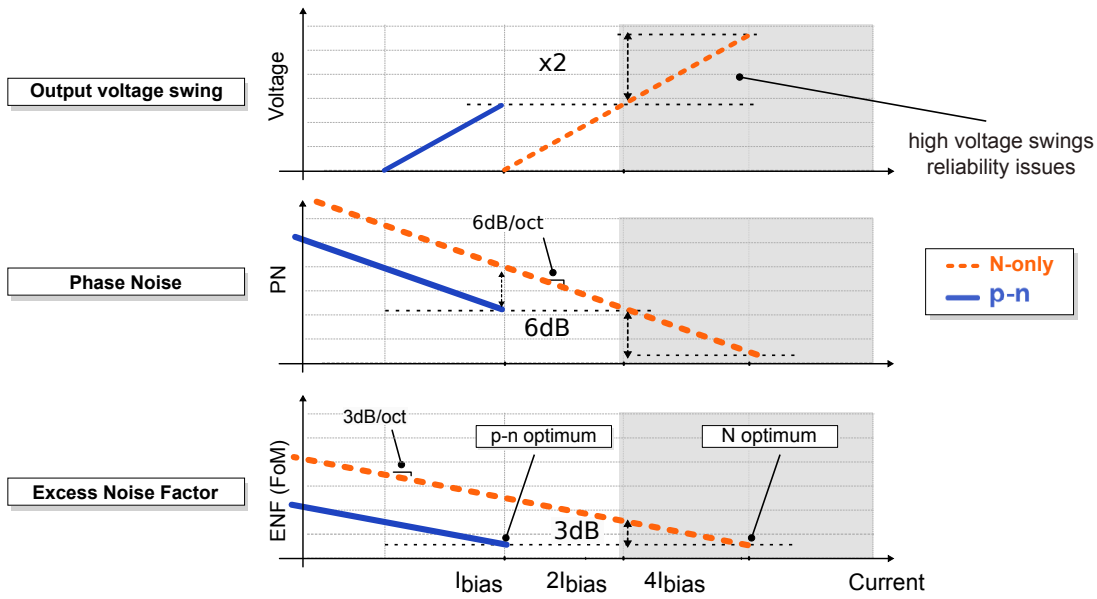


Figure 4.1: Characteristic behavior of N-only and p-n oscillators

conversion of DC power (P_{DC}) into resonator RF power (P_{RF}), which directly affects the phase noise [7]. The use of voltage-biased topologies [8–10] eliminates a source of phase noise (i.e. the current generator) and improves power efficiency, but increases frequency pushing. Large voltage swing (relative to the supply voltage) is desirable to achieve high power efficiency and to reduce phase sensitivity to device noise, as described by the ISF. However, as the active devices are driven by large signals, they can enter the triode region, thereby loading the tank, potentially degrading phase noise. This trade-off can be partially broken by adopting a low supply voltage, such that the active devices do not enter into triode even as the signal swing approaches (or exceeds) the supply rails. In practice, the use of a low supply voltage (e.g. 0.4V in [8]) makes the performances very sensitive to supply voltage variations and, when the oscillator is embedded in a complete transceiver, it necessitates a dedicated switch-mode voltage regulator to preserve power efficiency, thereby increasing cost.

Other solutions include class-D oscillators [9], where the transistors are operated in deep triode to achieve good phase noise thanks to the low r_{ON} and the very fast switching, and clip-and-restore [10], where loading effects are compensated adopting step-up transformers to boost the gate voltage and reduce phase sensitivity to device noise. However, on-chip transformers typically have lower quality factors

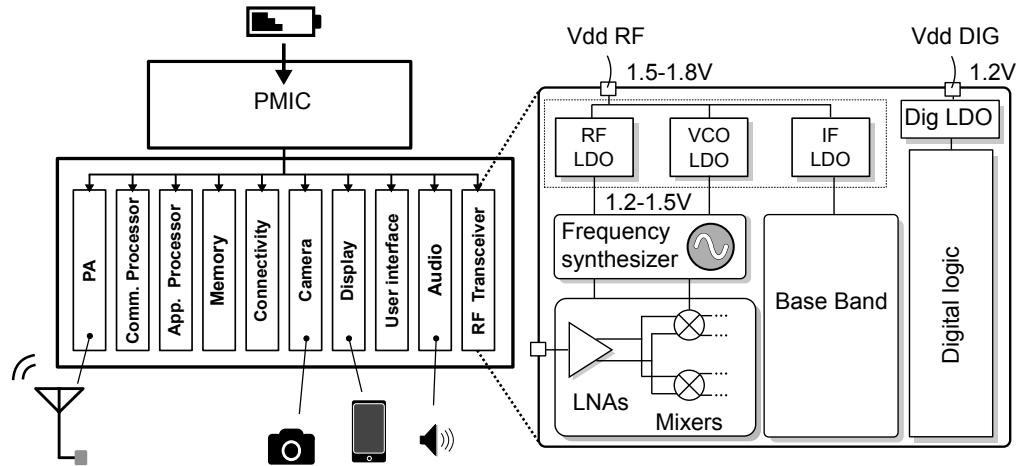


Figure 4.2: Conceptual block diagram of a complete mobile system

than simple inductors [11]¹, moreover, in both cases a low supply is required for reliability. Higher order resonators have also been proposed (class-F oscillators [13]) in order to increase the maximum slope of the output signal for a given peak-to-peak voltage swing. However, an accurate analysis [7] reveals that this approach is beneficial only when the Q of the resonator is higher at $3f_{OSC}$ than at f_{OSC} , which is typically not the case.

For a standard NMOS Class-B oscillator, if an additional LC tank (resonating at $2\omega_0$) is inserted at the source of the active devices [14], the switching transistors can enter the triode region without loading the tank since they see a high impedance in series with them. This allows to preserve the ISF while increasing power efficiency. High η_P and low phase noise however correspond to excessive voltage swings (ideally up to π times the supply voltage for 100% η_P). A possible solution is to lower supply voltages in order to achieve reliable swings. However, the design of the oscillator should be considered within the design of the system and in general the oscillator does not impose a particular supply voltage within the system since it is a part of a more complex and complete architecture (Fig. 4.2). In most of practical cases the supply voltage adopted in the analog circuitry is still higher than 1V [3, 15–22]. In all these cases an N-only oscillator is actually used in a sub-optimal working condition (Fig. 4.1) since it has to be limited to avoid reliability issues never being able to reach its optimum. Adopting a complementary (push-pull) topology, the peak efficiency is reached at lower (theoretically half) voltage swing compared with an N-type-only one, avoiding reliability concerns and being able to

¹This is only partially compensated by the fact that transformer-based resonators display a steeper phase response with respect to a simple LC-tank for the same quality factor [12].

reach the optimum ENF or equivalently FoM. For this reason we present a high efficiency complementary Class-B oscillator with dual LC tail filter, which can use efficiently the supply current and achieve a low phase noise.

4.2 Excess Noise Factor in LC-Tank Oscillators

To benchmark the performance of an oscillator we rely on the widely used Figure of Merit (FoM) that normalizes phase noise to frequency of oscillation, offset frequency from the carrier and power consumption. Using the theory of Hajimiri and Lee [6] and assuming a nearly sinusoidal oscillation voltage, that the energy restoring element does not load the tank, 100% power efficiency, noiseless transistors and no other noise contribution, it can be shown that the FoM has a maximum called FoM_{MAX} that depends only on the Q of the tank as given below:

$$FoM_{MAX} = -10\text{Log} \left[\frac{kT}{2 \cdot 10^{-3} \cdot Q^2} \right] \quad (4.1)$$

FoM_{MAX} is a thermodynamic limit associated with the power dissipation of the unloaded tank. The Excess Noise Factor (ENF), defined [7] as the difference between FoM_{MAX} and the actual FoM, provides a figure of merit of the topology, independent from the tank Q. For a VCO with a direct coupling between tank and MOS gates, if the transistor current noise power spectral density is proportional to the derivative of the drain current with respect to the gate voltage and the active devices do not load the tank Mazzanti and Andreani [38] have shown that the transistors noise is γ_{MOS} times the tank noise, where γ_{MOS} is the excess noise of the MOS transistors. Using this result it can be shown that ENF is given by:

$$ENF = 10\text{Log} \left[\frac{(1 + \gamma_{MOS})}{\eta_P} \right] \quad (4.2)$$

This shows that for all the topologies falling under the hypotheses above and for a given tank, the only differentiator is power efficiency.

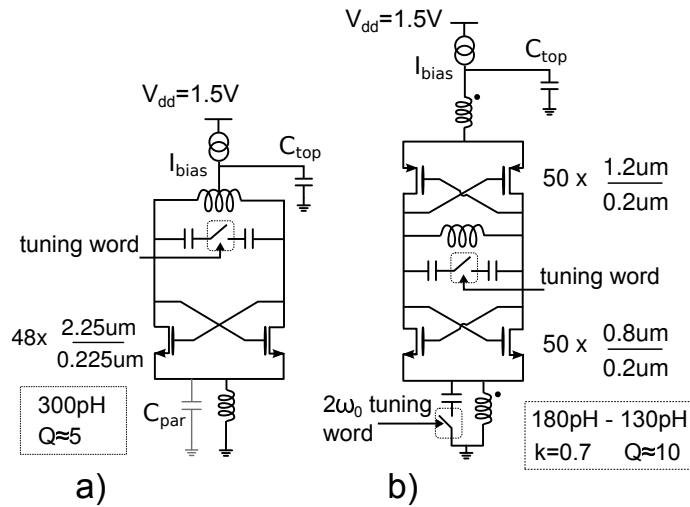


Figure 4.3: Class-B oscillators with $2\omega_0$ LC tail filters: N-only and p-n

4.3 Class-B with tail filter

Power efficiency is equal to the product of current efficiency (i.e. the ratio between the tank current at the fundamental frequency and the supply current), times voltage efficiency (i.e. the ratio between tank voltage and supply voltage). The key design goal of maximizing efficiency can be achieved acting on both current and voltage efficiencies. In class-C oscillators [38, 58], current efficiency is very high (up to 90%) but voltage efficiency need to be limited (to about 50%) to avoid loading the tank since the switching devices are connected to AC ground (resulting in a η_P between 45% and 55% [38, 58]). Standard class-B oscillators have lower current efficiency (ideally $2/\pi$) and voltage efficiency at maximum FoM similar to class-C (for the same reasons). The use of an additional LC tank at the source of the active devices (Fig. 4.3a) was originally proposed to reduce the current source noise [14] thanks to the filtering action of the large capacitance (C_{top}) in parallel with it. This topology has, however, two other important advantages.

First, the common source node can swing below ground, increasing the maximum achievable voltage swing. Since current efficiency remains nearly constant, η_P is also increased, ultimately reaching a value close to 90%. Second, the switching transistors can enter the triode region without loading the tank since they see a high impedance in series with them. Hence, the peak efficiency corresponds also to the peak FoM because noise remains constant even when the switching transistors are pushed deeply into linear region, as opposed to what happens for class-C. Table

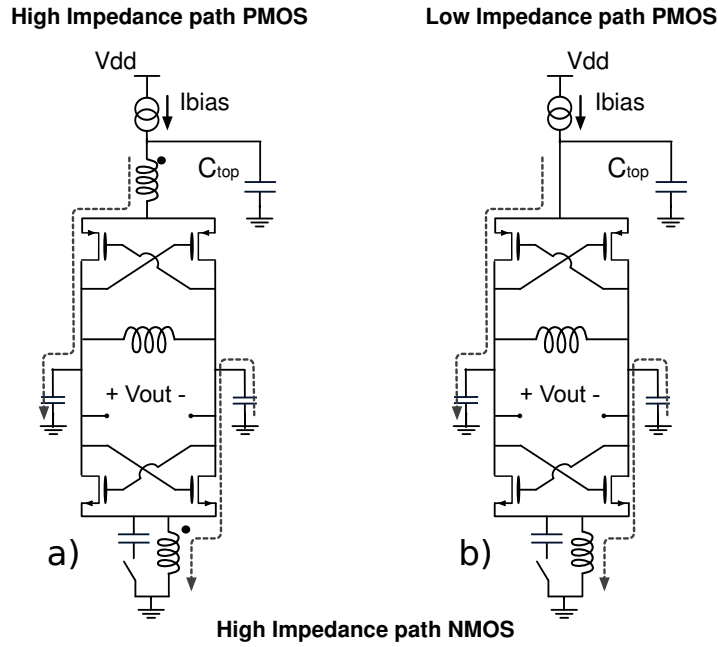


Figure 4.4: Complementary p-n class-B oscillator with a) dual and b) single $2\omega_0$ LC tanks at the tails

4.1, reported in Section 4.5, compares the measured performance of various VCOs with different topologies, including their ENF (computed using the data available in the referenced papers). The comparison shows that the class-B oscillator with tail filter in [14] is superior by more than 1dB compared to any reported VCO (assuming accurate Q estimation). The main problem of this topology is the fact that for the optimum FoM the peak voltage across the transistors is more than twice the supply voltage, which may create reliability issues unless very high voltage devices or an extremely low supply are used. For the oscillator in [14], implemented in a $0.35\mu\text{m}$ CMOS technology and biased from 2.5V, the peak FoM of 195.4dBc/Hz is reached with a η_P of 81% for a peak swing of 6.4V (computed from the values of tank Q, inductor and current provided in the paper) which is almost twice the maximum allowed by the technology. This issue can be overcome using the complementary p-n topology shown in Fig. 4.3b, which, having twice the current efficiency of the N-only one, achieves the peak power efficiency (or equivalently reaches the peak FoM) with half the voltage swing. In [49] a p-n version of the oscillator of reference [14] was presented which achieved a FoM of 183.8 dBc/Hz and a ENF of 11dB. However, the focus of that work was to reduce the tail current noise at low frequencies ($1/f$), not to reduce ENF. The simplest way to implement a complementary oscillator with tail filter is shown in Fig. 4.4b. In this implementation the source of the pMOS transistors is connected directly

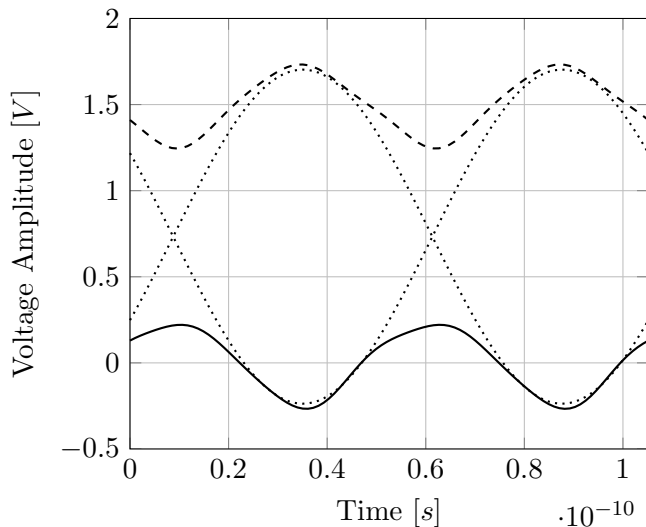


Figure 4.5: Simulated voltage waveforms

to the current source and to the large capacitor C_{top} . However, since the tank cannot be made perfectly-differential, the pMOS transistors noise would see a low impedance path to ground, thereby loading the tanks and increasing phase noise at large amplitudes. This is confirmed by simulations, showing that at the higher end of the tuning range, when the common mode portion of the tank dominates, the pMOS transistors contribute more than 40% of the phase noise, while the nMOS contribute only 23%. An additional tail tank placed on the p-side of the VCO², as shown in Fig. 4.4a, prevents the pMOS transistors from loading the tank when they go into triode. As a result their phase noise contribution is reduced to 21% of the total, while the nMOS stays the same (at 23%) resulting in a 1.8dB phase noise improvement. Simulation shows (Fig. 4.5) that, thanks to the dual LC tail filter, the common source of nMOS and pMOS transistors can swing significantly above and below their DC voltage. This results in an oscillation amplitude (and consequently a power efficiency) 30% larger. Under these conditions the oscillator achieves, in simulation a maximum η_P of 85% and an ENF close to 4.2dB. To reduce area overhead, the tail inductances were magnetically coupled and laid out inside each other. The two coupled resonators have the same resonance frequency and can be tuned using a single capacitor bank. No attempt to control the second (higher frequency) resonance present in such a transformer was attempted [69].

Second harmonic tail filter is used in some recent implementation (Fanori and Andreani, ESSCIRC 2014) to reduce flicker noise upconversion since it helps in reducing the tail capacitance modulation and the Groszkowski effect [70]. What is

²A similar architecture was presented in [69] but not integrated in silicon.

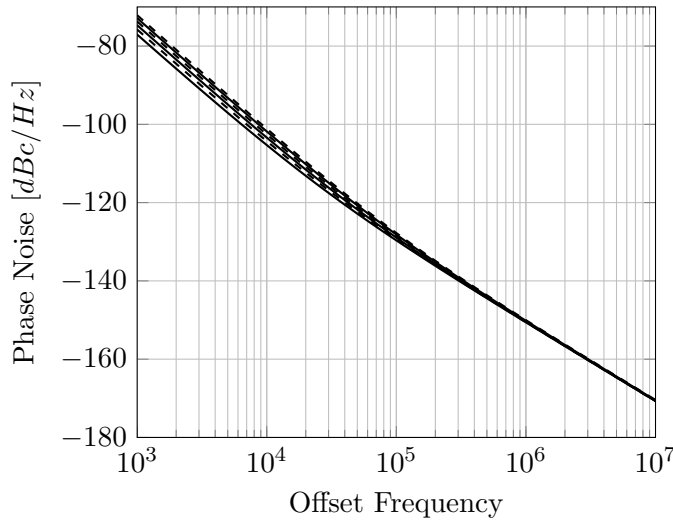


Figure 4.6: Phase Noise simulation mistuning the tail filter

interesting to notice is flicker noise upconversion sensitivity with tail filter tuning. As shown in Fig. 4.6 with a mistuning of the second harmonic resonator at the tail the flicker noise has much higher sensitivity and variation compared to the thermal noise. This underlines the importance of tuning the second harmonic tank.

4.4 Magnetically coupled resonator

We would like now to explain the effects of adding a magnetically coupled tail filter. The necessity of two resonators is due to the fact that without a perfectly differential LC main tank the noise of the active devices may find a low impedance path affecting too much the phase noise performance pushing the transistors in triode region. A direct and maybe more intuitive comparison can be done with the help of Fig. 4.7. Folding the pMOS side makes the comparison with the N-only counterpart more straightforward. It directly suggests the necessity of another resonator. The reader may argue if the use of the transformer could change the ISF thereby affecting the noise to phase noise conversion of the main noise sources. According to the classical small signal analysis the designer can have the impression of some noise recirculating effect that might or it might not help in noise to phase noise conversion. However, the study of phase noise in electrical oscillator have already demonstrated to be in general a different and often more difficult task than traditional noise analysis and that it may lead to wrong results.

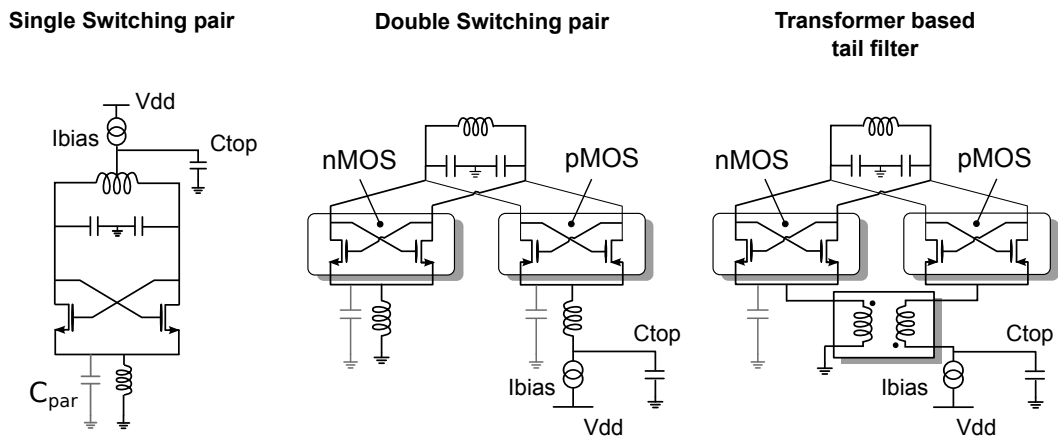


Figure 4.7: From N only structure to complementary p-n class-B oscillator with magnetically coupled LC tanks at the tails

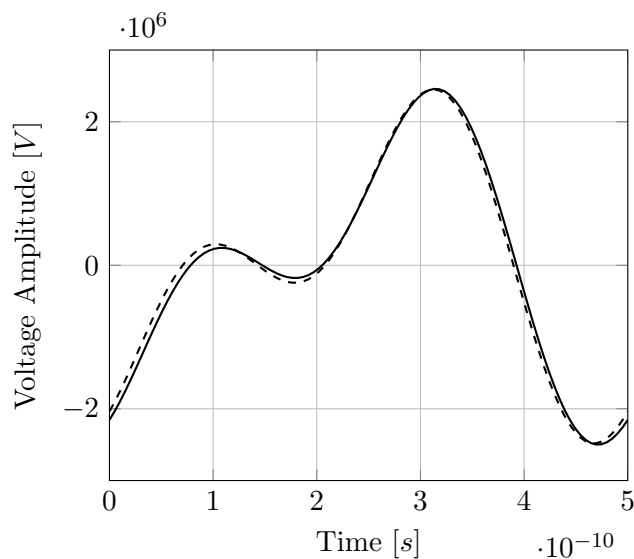


Figure 4.8: Simulated ISFs with and without transformer coupling

Simply let us consider the Impulse Sensitivity Function theory. When a noise impulse charge is applied, only the voltage across the capacitor is changed and no effect is present on the current flowing through the inductor [6]. For this reason it is possible to conclude that, at least as first order analysis, there is no difference in the impulse sensitivity by using a magnetically coupled resonators or two separate LC tanks. The true difference relies in the limits that such decision implies, like a typically lower quality factor with respect to a single inductor. To demonstrate the absence of any major effect on the ISF let us consider the simulated ISFs in Fig. 4.8. The simulation is made considering a double switching pair oscillator (p-n architecture) with and without the magnetically coupled LC tail filters. Everything else is maintained equal in both cases: $L_1 = 600pH$,

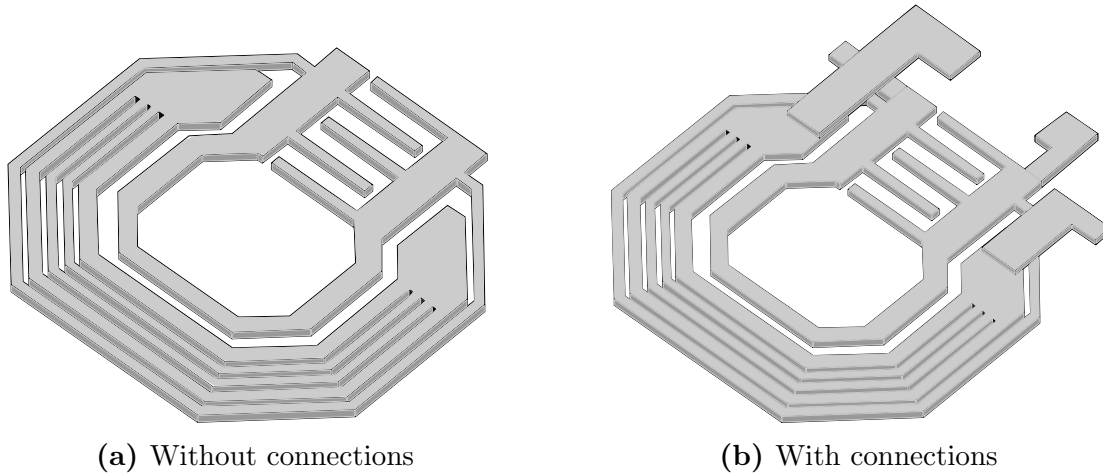


Figure 4.9: Layout of the magnetically coupled tail filter

$L_{2,p/n} = 400pH$, $Q_1 = Q_{2,p/n} = 20$. We have already demonstrated that for a high quality factor the effect for different inductance and capacitance value is overall limited to less than $1dB$, therefore a slightly lower quality factor due the limitation imposed by the magnetic coupling is only a minor impact, or at least can be maintained low by design. For simplicity only the first two harmonics of the ISF are shown in Fig. 4.8.

Another important advantage in using magnetically coupled tail filter is related to tuning capacitors array. Maximizing the coupling factor, tuning the desired resonance on one side of the transformer also on the other side it will be tuned. It is clear that coupling factor is key to have this and the design of the transformer was focused on achieving the maximum coupling factor using one inductor inside the other one (Fig. 4.9). The coupling factor obtained is about 0.7 which is in practice among the maximum possible.

4.5 Oscillators Implementation

The difficulty to extract the tank Q , together with the high sensitivity of phase noise to Q , limits the ability to accurately assess the potential of a new topology. Because of this we have built a test chip that allows to compare the proposed topology with a reference oscillator, both working in the same operating conditions. The implemented chip prototype includes the class-B complementary p-n oscillator (with magnetically coupled tail filters), together with a class-B N-only oscillator with a single tail filter (used as reference) and was fabricated in a $55nm$ standard

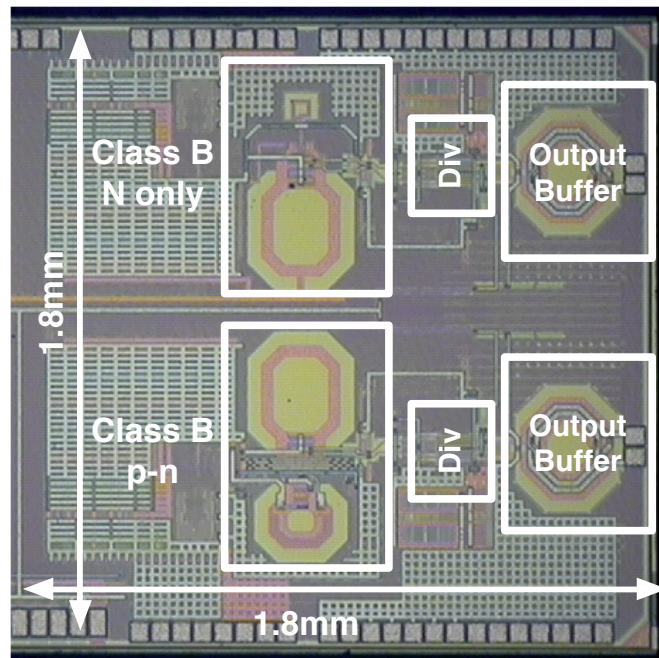


Figure 4.10: Chip photo

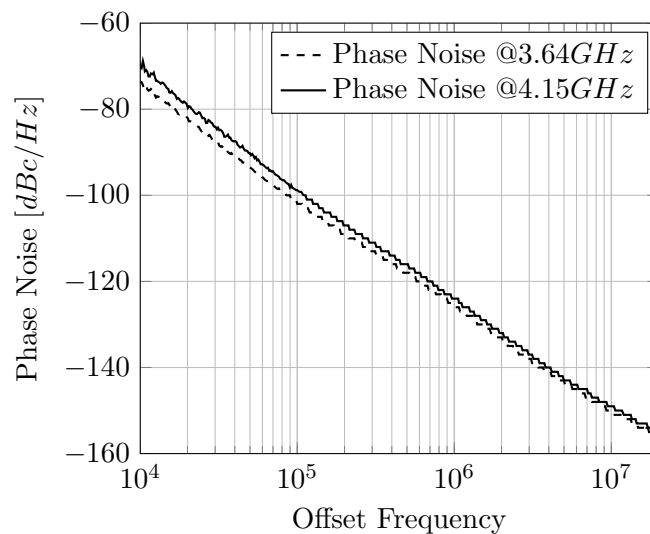


Figure 4.11: Phase Noise measurements (after freq divider by 2) at the minimum and maximum frequency of oscillation (p-n)

CMOS technology with only one ultra-thick metal layer. Circuit schematics are reported in Fig. 4.3. The oscillators use thick oxide devices (1.8V maximum voltage) and are biased from a 1.5V internal supply derived from the external 1.8V supply through an on-chip band-gap referenced low-voltage-drop regulator. Both use identical tanks and can be tuned from about 7.4 GHz to 8.4GHz (before frequency division by 2) with a 5 bits MOM capacitor bank. For the tail tanks the main design goal is to maximize its impedance at $2\omega_0$. This can be achieved using

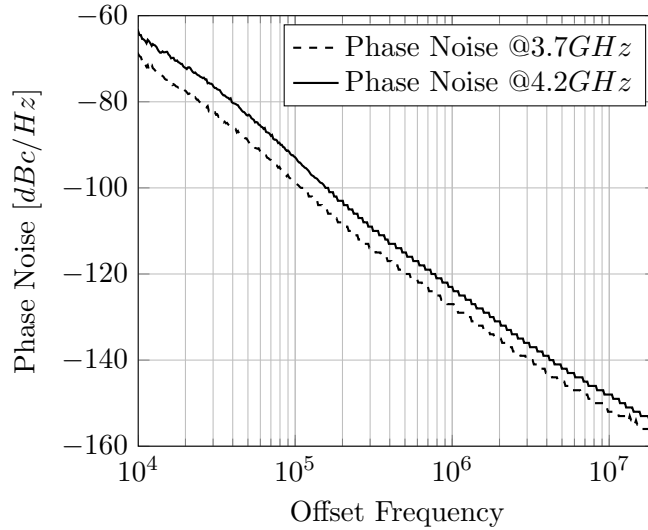


Figure 4.12: Phase Noise measurements (after freq divider by 2) at the minimum and maximum frequency of oscillation (N only)

a high Q tank and/or a large inductor. A small inductor with high Q is preferable because it allows to use very large switching devices (with very low r_{ON} but large parasitic capacitance). This allows to improve power efficiency and gives about 1dB phase noise improvement (from simulations), although at the cost of an extra capacitor array for the tuning of the $2\omega_0$ tank. The coupled tanks (with inductance values of 180pH and 130pH and a coupling factor of 0.7) have a quality factor of about 10. A single 3-bit capacitor bank at the NMOS switching transistors source (controlled independently from the main tank) is used for tuning them. For the N-only oscillator the single tail tank has a quality factor of about 6 and uses an inductor of 300pH. A die photograph of the oscillators is shown in Fig. 4.10.

Figures 4.12 and 4.11 shows the measured phase noise at the minimum and maximum frequencies for both oscillators. The $1/f^3$ noise corner is between 200kHz and 400kHz for the p-n oscillator and between 400kHz and 600kHz for the N only while the $1/f^2$ noise exceeds the 2G TX specification at 20MHz frequency offset by more than 7dB for the p-n oscillator and by 8 dB for the N-only, giving sufficient margin for other non-idealities. Fig. 4.13 shows the phase noise of both oscillators at the minimum frequency as a function of power consumption. The pn-oscillator has 0-1 dB lower phase noise of the N-only one with half the power consumption (i.e. the same output voltage for the same tank), hence the pn-oscillator has 3-4 dB higher FoM. The best achievable FoM is 195.6dBc/Hz for the p-n oscillator and 192.3 dBc/Hz for the N-only, limited by reliability considerations,

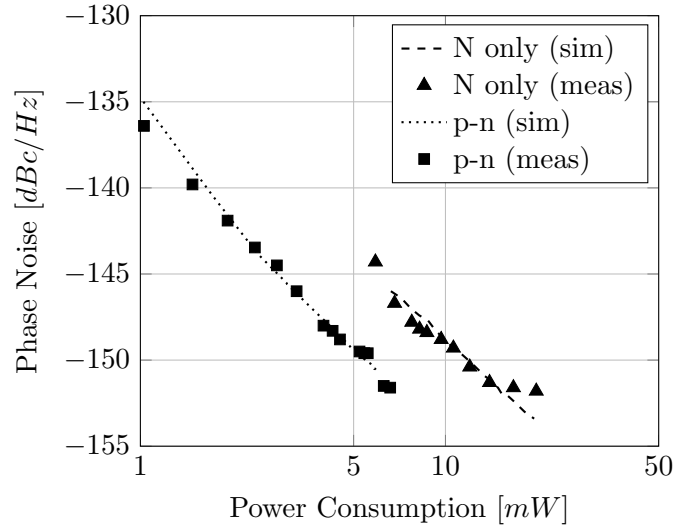


Figure 4.13: Measured (dots) phase noise after freq. divider by 2 and simulated (lines) phase noise with 6dB reduction as a function of power dissipation of p-n and N only oscillators

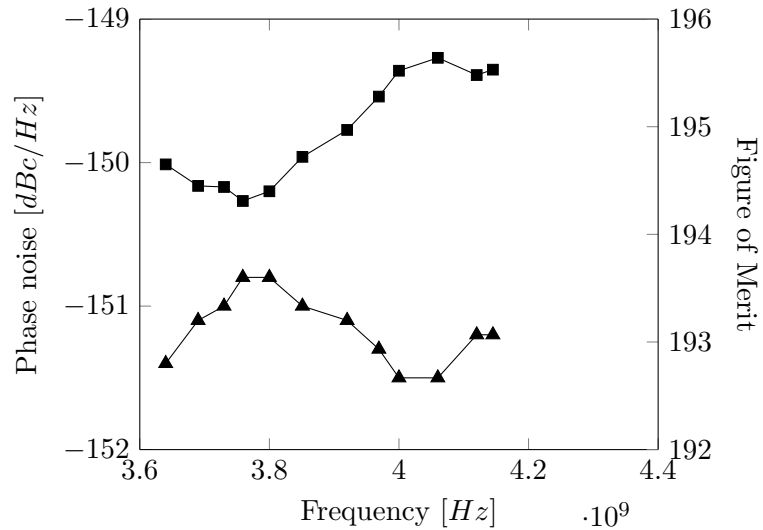


Figure 4.14: Measured Phase Noise and FoM over tuning range (p-n)

and it varies about 1.3 dB and 1.8 dB respectively across the tuning range (Fig. 4.15 and Fig. 4.14).

Table 4.1 compares the two prototype oscillators with the state of the art. With the exception of [8], the average FoM over the tuning range of the p-n oscillator is the highest reported. However the oscillator in [8] has an unpractical low supply and its FoM drops by 1dB for a 25mV supply voltage variation. For a further comparison the ENF was computed. The Q of the two prototype oscillators was estimated measuring both the minimum supply current needed to startup oscillations and the maximum absorbed current for a given supply voltage. Fitting the measured

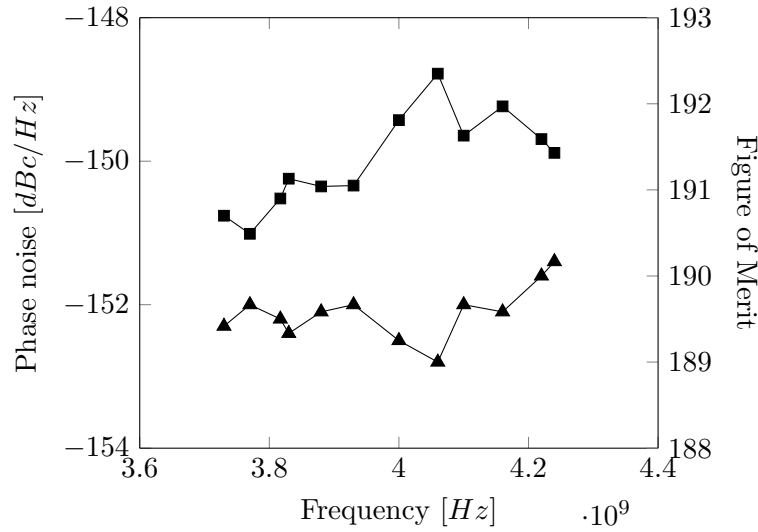


Figure 4.15: Measured Phase Noise and FoM over tuning range (N only)

Table 4.1: Comparison table

Ref	Topology	Tech	$V_{dd} - V_{pk}$ diff	f_{osc} [GHz]	FoM [dBc/Hz]	FoM_T [dBc/Hz]	ENF (Q)
[58]	class C PN	0.18um CMOS	1.8V 0.9V	6.1 - 7.5	189 - 191	196	5.8 (10)
[38]	Class C N-only	0.13um CMOS	1V 1.24V	4.5 - 5	193.5-196	196.4	5.4 (17)
[14]	Class B N-only	0.35um CMOS	2.5V 6.4V	1.2	195.4	-	4.3 (14)
[9]	Class-D	65nm CMOS	0.4V 1.28V	2.5 - 3.3	189 - 190	199	6.8 (10)
[8]	Colpitts	0.13um CMOS	0.48V 1.5V	4.9	196.2	184.2	5.8 (18)
[13]	Class-F	65nm CMOS	1.2V 2V	5.9 - 7.6	192.2	200.2	8.7 (16)
This Work	Class B N-only	55nm CMOS	1.5V 2.1V	7.4 - 8.4	190.5 - 192.3	194.5	8 (15)
This Work	Class B PN	55nm CMOS	1.5V 1.6V	7.4 - 8.4	194.3 - 195.6	197.8	4.7 (15)

number with simulation gives in both cases an estimated Q between 14 and 15. With the exception of the N-only oscillator in [14] (that however far exceeds technology voltage limitations), the presented pn-oscillator has the lowest reported ENF. The p-n oscillator also has a high FoM_T of $197.8dBc/Hz$, which is among the best of the high FoM and low ENF oscillators reported in the literature.

4.6 Conclusion

Since in most practical cases, down to $1V$ supply voltage push pull p-n structures are the most efficient choice, in this chapter has been proposed a complementary class-B oscillator with transformer based tail filtering. The solution permits to save area and introduce tuning capabilities using the transformer. The oscillator exhibits a high efficiency at a regulated voltage supply of $1.5V$ and has 3-4dB better FoM than a reference N-only oscillator, which is limited by reliability considerations. The fabricated 55nm CMOS oscillator displays one of the best FoM and ENF avoiding reliability concerns.

Bibliography

- [1] E. Hegazi and A. Abidi, “A 17 mW transmitter and frequency synthesizer for 900 MHz GSM fully integrated in 0.35 μ m CMOS,” in *Symposium on VLSI Circuits Digest of Technical Papers, 2002*, 2002, pp. 234–237.
- [2] R. Staszewski, J. Wallberg, S. Rezeq, C.-M. Hung, O. Eliezer, S. Vemulapalli, C. Fernando, K. Maggio, R. Staszewski, N. Barton, M.-C. Lee, P. Cruise, M. Entezari, K. Muhammad, and D. Leipold, “All-digital PLL and transmitter for mobile phones,” *IEEE Journal of Solid-State Circuits*, vol. 40, no. 12, pp. 2469–2482, Dec. 2005.
- [3] L. Vercesi, L. Fanori, F. De Bernardinis, A. Liscidini, and R. Castello, “A dither-less all digital PLL for cellular transmitters,” *IEEE Journal of Solid-State Circuits*, vol. 47, no. 8, pp. 1908–1920, Aug. 2012.
- [4] H. Darabi, P. Chang, H. Jensen, A. Zolfaghari, P. Lettieri, J. Leete, B. Mohammadi, J. Chiu, Q. Li, S.-L. Chen, Z. Zhou, M. Vadipour, C. Chen, Y. Chang, A. Mirzaei, A. Yazdi, M. Nariman, A. Hadji-Abdolhamid, E. Chang, B. Zhao, K. Juan, P. Suri, C. Guan, L. Serrano, J. Leung, J. Shin, J. Kim, H. Tran, P. Kilcoyne, H. Vinh, E. Raith, M. Koscal, A. Hukkoo, C. Hayek, V. Rakhshani, C. Wilcoxson, M. Rofougaran, and A. Rofougaran, “A quad-band GSM/GPRS/EDGE SoC in 65 nm CMOS,” *IEEE Journal of Solid-State Circuits*, vol. 46, no. 4, pp. 870–882, Apr. 2011.
- [5] J. Borremans, G. Mandal, V. Giannini, B. Debaillie, M. Ingels, T. Sano, B. Verbruggen, and J. Craninckx, “A 40 nm CMOS 0.4–6 GHz receiver resilient to out-of-band blockers,” *IEEE Journal of Solid-State Circuits*, vol. 46, no. 7, pp. 1659–1671, Jul. 2011.
- [6] A. Hajimiri and T. Lee, “A general theory of phase noise in electrical oscillators,” *IEEE Journal of Solid-State Circuits*, vol. 33, no. 2, pp. 179–194, 1998.

-
- [7] M. Garampazzi, S. Dal Toso, A. Liscidini, D. Manstretta, P. Mendez, L. Romanò, and R. Castello, “An intuitive analysis of phase noise fundamental limits suitable for benchmarking LC oscillators,” *IEEE Journal of Solid-State Circuits*, vol. 49, no. 3, pp. 635 – 645, 2014.
- [8] T. Brown, F. Farhabakhshian, A. Guha Roy, T. Fiez, and K. Mayaram, “A 475 mV, 4.9 GHz enhanced swing differential colpitts VCO with phase noise of -136 dBc/Hz at a 3 MHz offset frequency,” *IEEE Journal of Solid-State Circuits*, vol. 46, no. 8, pp. 1782–1795, 2011.
- [9] L. Fanori and P. Andreani, “A 2.5-to-3.3GHz CMOS class-D VCO,” in *Solid-State Circuits Conference Digest of Technical Papers (ISSCC), 2013 IEEE International*, 2013, pp. 346–347.
- [10] M. Babaie, A. Visweswaran, Z. He, and R. Staszewski, “Ultra-low phase noise 7.2 - 8.7 GHz clip-and-restore oscillator with 191 dBc/Hz FoM,” in *2013 IEEE Radio Frequency Integrated Circuits Symposium (RFIC)*, Jun. 2013, pp. 43–46.
- [11] H. Krishnaswamy and H. Hashemi, “Inductor and transformer-based integrated RF oscillators: A comparative study,” in *IEEE Custom Integrated Circuits Conference, 2006. CICC '06*, Sep. 2006, pp. 381–384.
- [12] A. El-Gouhary and N. Neihart, “An analysis of phase noise in transformer-based dual-tank oscillators,” *IEEE Transactions on Circuits and Systems I: Regular Papers*, vol. Early Access Online, 2014.
- [13] M. Babaie and R. Staszewski, “A class-F CMOS oscillator,” *IEEE Journal of Solid-State Circuits*, vol. 48, no. 12, pp. 3120–3133, Dec. 2013.
- [14] E. Hegazi, H. Sjoland, and A. Abidi, “A filtering technique to lower LC oscillator phase noise,” *IEEE Journal of Solid-State Circuits*, vol. 36, no. 12, pp. 1921 –1930, Dec. 2001.
- [15] T. Choke, H. Zhang, S. Tan, W. Yang, Y. Tan, S. Karri, Y. Sun, D. Li, Z. Lee, T. Gao, W. Shu, and O. Shana’a, “A multiband mobile analog TV tuner SoC with 78-dB harmonic rejection and GSM blocker detection in 65-nm CMOS,” *IEEE Journal of Solid-State Circuits*, vol. 48, no. 5, pp. 1174–1187, May 2013.
- [16] M. Hammes, C. Kranz, D. Seippel, J. Kissing, and A. Leyk, “Evolution on SoC integration: GSM baseband-radio in 0.13um CMOS extended by fully

- integrated power management unit,” *IEEE Journal of Solid-State Circuits*, vol. 43, no. 1, pp. 236–245, Jan. 2008.
- [17] Y. Huang, W. Li, S. Hu, R. Xie, X. Li, J. Fu, Y. Sun, Y. Pan, H. Chen, C. Jiang, J. Liu, Q. Chen, D. Qiu, Y. Qin, Z. Hong, and X. Zeng, “A high-linearity WCDMA/GSM reconfigurable transceiver in 0.13 μ m CMOS,” *IEEE Transactions on Microwave Theory and Techniques*, vol. 61, no. 1, pp. 204–217, Jan. 2013.
- [18] M. Jeong, B. Kim, Y. Cho, Y. Kim, S. Kim, H. Yoo, J. Lee, J. K. Lee, K. S. Jung, J. Lee, J. Lee, H. Yang, G. Taylor, and B.-E. Kim, “A 65nm CMOS low-power small-size multistandard, multiband mobile broadcasting receiver SoC,” in *Solid-State Circuits Conference Digest of Technical Papers (ISSCC), 2010 IEEE International*, Feb. 2010, pp. 460–461.
- [19] S. Liao, Y.-S. Chang, C.-H. Wu, H.-C. Tsai, H.-H. Chen, M. Chen, C.-W. Hsueh, J.-B. Lin, D.-K. Juang, S.-A. Yang, C.-T. Liu, T.-P. Lee, J.-R. Chen, C.-H. Shih, B. Hong, H.-R. Hsu, C.-Y. Wang, M.-S. Lin, W.-H. Tseng, C.-H. Yang, L. Lee, T.-J. Jheng, W.-W. Yang, M.-Y. Chao, and J.-S. Pan, “A 70-Mb/s 100.5-dBm sensitivity 65-nm LP MIMO chipset for WiMAX portable router,” *IEEE Journal of Solid-State Circuits*, vol. 47, no. 1, pp. 61–74, Jan. 2012.
- [20] S. Plevridis, K. Vavelidis, N. Haralabidis, T. Georgantas, S. Bouras, C. Kapnistis, E. Kytonaki, Y. Kokolakis, T. Chalvatzis, S. Kavadias, H. Peyravi, N. Kanakaris, C. Kokozidis, S. Liolis, K. Tsilipanos, A. Kyranas, C. Xesternos, P. Betzios, I. Bouras, and M. Rofougaran, “A 65nm 3G femtocell multiband transceiver,” in *2014 IEEE Radio Frequency Integrated Circuits Symposium*, Jun. 2014, pp. 137–140.
- [21] J. Strange, H.-H. Chang, P. Muller, W. Ali-Ahmad, C. Beghein, F. Ben Abdeljelil, W.-C. Lee, C. Chiu, T. Y. Sin, T.-H. Lin, D. Ivory, H.-T. Shih, C. Beale, D. Nalbantis, I. Lu, C.-W. Fan, S.-H. Lin, H.-H. Chen, C.-H. Sun, L.-S. Lai, J.-R. Chen, and S.-J. Huang, “A HSPA-WCDMA/EDGE 40nm modem SoC with embedded RF transceiver supporting RX diversity,” in *2014 IEEE Radio Frequency Integrated Circuits Symposium*, Jun. 2014, pp. 133–136.
- [22] T. Tsukizawa, N. Shirakata, T. Morita, K. Tanaka, J. Sato, Y. Morishita, M. Kanemaru, R. Kitamura, T. Shima, T. Nakatani, K. Miyanaga, T. Urushihara, H. Yoshikawa, T. Sakamoto, H. Motozuka, Y. Shirakawa, N. Yosoku,

- A. Yamamoto, R. Shiozaki, and N. Saito, "A fully integrated 60GHz CMOS transceiver chipset based on WiGig/IEEE802.11ad with built-in self calibration for mobile applications," in *Solid-State Circuits Conference Digest of Technical Papers (ISSCC), 2013 IEEE International*, Feb. 2013, pp. 230–231.
- [23] W. P. Robins, *Phase Noise in signal sources*. Peter Peregrinus Ltd. on behalf of the Institution of Electrical Engineers, 1982.
- [24] T. Lee and A. Hajimiri, "Oscillator phase noise: a tutorial," *Solid-State Circuits, IEEE Journal of*, vol. 35, no. 3, pp. 326–336, Mar. 2000.
- [25] D. Leeson, "A simple model of feedback oscillator noise spectrum," *Proceedings of the IEEE*, vol. 54, no. 2, pp. 329–330, 1966.
- [26] A. Demir, "Phase noise in oscillators: DAEs and colored noise sources," in *1998 IEEE/ACM International Conference on Computer-Aided Design, 1998. ICCAD 98. Digest of Technical Papers*, Nov. 1998, pp. 170–177.
- [27] A. Demir, A. Mehrotra, and J. Roychowdhury, "Phase noise in oscillators: a unifying theory and numerical methods for characterization," *IEEE Transactions on Circuits and Systems I: Fundamental Theory and Applications*, vol. 47, no. 5, pp. 655–674, 2000.
- [28] K. Kundert, "Introduction to RF simulation and its application," *IEEE Journal of Solid-State Circuits*, vol. 34, no. 9, pp. 1298–1319, Sep. 1999.
- [29] F. Kaertner, "Determination of the correlation spectrum of oscillators with low noise," *IEEE Transactions on Microwave Theory and Techniques*, vol. 37, no. 1, pp. 90–101, 1989.
- [30] P. Andreani and X. Wang, "On the phase-noise and phase-error performances of multiphase LC CMOS VCOs," *IEEE Journal of Solid-State Circuits*, vol. 39, no. 11, pp. 1883–1893, 2004.
- [31] J. Rael and A. Abidi, "Physical processes of phase noise in differential LC oscillators," in *Custom Integrated Circuits Conference, 2000. CICC. Proceedings of the IEEE 2000*, 2000, pp. 569–572.
- [32] P. Andreani, X. Wang, L. Vandi, and A. Fard, "A study of phase noise in colpitts and LC-tank CMOS oscillators," *Solid-State Circuits, IEEE Journal of*, vol. 40, no. 5, pp. 1107–1118, May 2005.

- [33] D. Murphy, J. Rael, and A. Abidi, "Phase noise in LC oscillators: A phasor-based analysis of a general result and of loaded," *IEEE Transactions on Circuits and Systems I: Regular Papers*, vol. 57, no. 6, pp. 1187–1203, 2010.
- [34] P. Kinget, *Integrated GHz Voltage Controlled Oscillators*. Kluwer Academic Publishers, 1999, pp. 353–381.
- [35] J. Bank, "A harmonic-oscillator design methodology based on describing functions," Ph.D. dissertation, Chalmers University of Technology, Sweden, 2006.
- [36] J. van der Tang and D. Kasperkovitz, "Oscillator design efficiency: a new figure of merit for oscillator benchmarking," in *The 2000 IEEE International Symposium on Circuits and Systems, 2000. Proceedings. ISCAS 2000 Geneva*, vol. 2, 2000, pp. 533–536 vol.2.
- [37] A. Zanchi, A. Bonfanti, S. Levantino, C. Samori, and A. Lacaita, "Automatic amplitude control loop for a 2-V, 2.5-GHz LC-tank VCO," in *Custom Integrated Circuits, 2001, IEEE Conference on.*, 2001, pp. 209–212.
- [38] A. Mazzanti and P. Andreani, "Class-C harmonic CMOS VCOs, with a general result on phase noise," *IEEE Journal of Solid-State Circuits*, vol. 43, no. 12, pp. 2716–2729, 2008.
- [39] L. Fanori and P. Andreani, "Highly efficient class-C CMOS VCOs, including a comparison with class-B VCOs," *IEEE Journal of Solid-State Circuits*, vol. 48, no. 7, pp. 1730–1740, 2013.
- [40] T. H. Lee, *The design of CMOS radio-frequency Integrated circuits*. Cambridge University Press, 1998.
- [41] A. Visweswaran, R. Staszewski, and J. Long, "A clip-and-restore technique for phase desensitization in a 1.2V 65nm CMOS oscillator for cellular mobile and base stations," in *Solid-State Circuits Conference Digest of Technical Papers (ISSCC), 2012 IEEE International*, 2012, pp. 350–352.
- [42] L. Fanori and P. Andreani, "Class-D CMOS oscillators," *IEEE Journal of Solid-State Circuits*, vol. 48, no. 12, pp. 3105–3119, Dec. 2013.
- [43] H. Wang, "A 9.8 GHz back-gate tuned VCO in 0.35um CMOS," in *Solid-State Circuits Conference, 1999. Digest of Technical Papers. ISSCC. 1999 IEEE International*, 1999, pp. 406–407.

- [44] A. Hajimiri and T. Lee, "Design issues in CMOS differential LC oscillators," *IEEE Journal of Solid-State Circuits*, vol. 34, no. 5, pp. 717–724, 1999.
- [45] B. De Muer, M. Borremans, M. Steyaert, and G. Li Puma, "A 2-GHz low-phase-noise integrated LC-VCO set with flicker-noise upconversion minimization," *IEEE Journal of Solid-State Circuits*, vol. 35, no. 7, pp. 1034–1038, 2000.
- [46] C. Samori, A. Lacaita, A. Zanchi, S. Levantino, and G. Cali, "Phase noise degradation at high oscillation amplitudes in LC-tuned VCO's," *IEEE Journal of Solid-State Circuits*, vol. 35, no. 1, pp. 96–99, 2000.
- [47] F. Svelto, S. Deantoni, and R. Castello, "A 1 mA, -120.5 dBc/Hz at 600 kHz from 1.9 GHz fully tuneable LC CMOS VCO," in *Custom Integrated Circuits Conference, 2000. CICC. Proceedings of the IEEE 2000*, 2000, pp. 577–580.
- [48] D. Ham and A. Hajimiri, "Concepts and methods in optimization of integrated LC VCOs," *IEEE Journal of Solid-State Circuits*, vol. 36, no. 6, pp. 896–909, 2001.
- [49] P. Andreani and H. Sjoland, "Tail current noise suppression in RF CMOS VCOs," *IEEE Journal of Solid-State Circuits*, vol. 37, no. 3, pp. 342–348, 2002.
- [50] N. H. W. Fong, J. O. Plouchart, N. Zamdmer, D. Liu, L. Wagner, C. Plett, and N. Tarr, "Design of wide-band CMOS VCO for multiband wireless LAN applications," *IEEE Journal of Solid-State Circuits*, vol. 38, no. 8, pp. 1333–1342, 2003.
- [51] G. De Astis, D. Cordeau, J.-M. Paillot, and L. Dascalescu, "A 5 GHz fully integrated full PMOS low phase noise LC VCO," in *IEEE Compound Semiconductor Integrated Circuit Symposium, 2004*, Oct. 2004, pp. 151 – 154.
- [52] H. Kim, S. Ryu, Y. Chung, J. Choi, and B. Kim, "A low phase-noise CMOS VCO with harmonic tuned LC tank," *IEEE Transactions on Microwave Theory and Techniques*, vol. 54, no. 7, pp. 2917–2924, 2006.
- [53] H.-H. Hsieh and L.-H. Lu, "A high-performance CMOS voltage-controlled oscillator for ultra-low-voltage operations," *IEEE Transactions on Microwave Theory and Techniques*, vol. 55, no. 3, pp. 467–473, 2007.

- [54] S. Toso, A. Bevilacqua, M. Tiebout, N. Da Dalt, A. Gerosa, and A. Neviani, "A 0.06 mm 11 mW local oscillator for the GSM standard in 65 nm CMOS," *IEEE Journal of Solid-State Circuits*, vol. 45, no. 7, pp. 1295–1304, 2010.
- [55] P. Andreani, K. Kozmin, P. Sandrup, M. Nilsson, and T. Mattsson, "A TX VCO for WCDMA/EDGE in 90 nm RF CMOS," *Solid-State Circuits, IEEE Journal of*, vol. 46, no. 7, pp. 1618–1626, Jul. 2011.
- [56] A. Liscidini, L. Fanori, P. Andreani, and R. Castello, "A 36mW/9mW power-scalable DCO in 55nm CMOS for GSM/WCDMA frequency synthesizers," in *Solid-State Circuits Conference Digest of Technical Papers (ISSCC), 2012 IEEE International*, 2012, pp. 348–350.
- [57] G. Li, L. Liu, Y. Tang, and E. Afshari, "A low-phase-noise wide-tuning-range oscillator based on resonant mode switching," *IEEE Journal of Solid-State Circuits*, vol. 47, no. 6, pp. 1295–1308, 2012.
- [58] A. Mazzanti and P. Andreani, "A Push-Pull class-C CMOS VCO," *IEEE Journal of Solid-State Circuits*, vol. 48, no. 3, pp. 724–732, 2013.
- [59] P. Andreani and A. Fard, "More on the phase noise performance of CMOS differential-pair LC-Tank oscillators," *IEEE Journal of Solid-State Circuits*, vol. 41, no. 12, pp. 2703–2712, 2006.
- [60] B. Soltanian and P. Kinget, "Tail current-shaping to improve phase noise in LC voltage-controlled oscillators," *IEEE Journal of Solid-State Circuits*, vol. 41, no. 8, pp. 1792–1802, Aug. 2006.
- [61] K. Okada, Y. Nomiya, R. Murakami, and A. Matsuzawa, "A 0.114-mW dual-conduction class-C CMOS VCO with 0.2-V power supply," in *2009 Symposium on VLSI Circuits*, 2009, pp. 228–229.
- [62] L. Fanori, A. Liscidini, and P. Andreani, "A 6.7-to-9.2GHz 55nm CMOS hybrid class-B/class-C cellular TX VCO," in *Solid-State Circuits Conference Digest of Technical Papers (ISSCC), 2012 IEEE International*, Feb. 2012, pp. 354–356.
- [63] S. Rong and H. Luong, "A 0.05-to-10GHz 19-to-22GHz and 38-to-44GHz SDR frequency synthesizer in 0.13um CMOS," in *Solid-State Circuits Conference Digest of Technical Papers (ISSCC), 2011 IEEE International*, 2011, pp. 464–466.

- [64] A. Bevilacqua, F. Pavan, C. Sandner, A. Gerosa, and A. Neviani, "A 3.4-7 GHz transformer-based dual-mode wideband VCO," in *Solid-State Circuits Conference, 2006. ESSCIRC 2006. Proceedings of the 32nd European*, 2006, pp. 440–443.
- [65] J. Borremans, A. Bevilacqua, S. Bronckers, M. Dehan, M. Kuijk, P. Wambacq, and J. Craninckx, "A compact wideband front-end using a single-inductor dual-band VCO in 90 nm digital CMOS," *IEEE Journal of Solid-State Circuits*, vol. 43, no. 12, pp. 2693–2705, 2008.
- [66] A. Goel and H. Hashemi, "Frequency switching in dual-resonance oscillators," *IEEE Journal of Solid-State Circuits*, vol. 42, no. 3, pp. 571–582, 2007.
- [67] A. Pirola, A. Liscidini, and R. Castello, "Current-mode, WCDMA channel filter with in-band noise shaping," *IEEE Journal of Solid-State Circuits*, vol. 45, no. 9, pp. 1770–1780, Sept 2010.
- [68] F. Pepe, A. Bonfanti, S. Levantino, P. Maffezzoni, C. Samori, and A. Lacaita, "An efficient linear-time variant simulation technique of oscillator phase sensitivity function," in *2012 International Conference on Synthesis, Modeling, Analysis and Simulation Methods and Applications to Circuit Design (SMACD)*, Sep. 2012, pp. 17–20.
- [69] Q. Jin, K. Yang, C. Zhou, D. Yang, L. Zhang, Y. Wang, Z. Yu, and W. Geng, "A transformer-based filtering technique to lower LC-oscillator phase noise," in *2012 IEEE International Symposium on Circuits and Systems (ISCAS)*, 2012, pp. 1383–1386.
- [70] J. Groszkowski, "The interdependence of frequency variation and harmonic content, and the problem of constant-frequency oscillators," in *2012 International Conference on Synthesis, Modeling, Analysis and Simulation Methods and Applications to Circuit Design (SMACD)*, vol. 21, Sep. 1933, pp. 958–981.